Watershed Classification in the Great Lakes Basin: Implications for Water Quality and Agricultural Management Practices

by

Amina Hassan

A thesis

presented to the University of Waterloo

in fulfilment of the

thesis requirement for the degree of

Master of Science

in

Geography (Water)

Waterloo, Ontario, Canada, 2024

Author's Declaration

I hereby declare that I am the sole author of this thesis. This is a true copy of the thesis, including any required final revisions, as accepted by my examiners.

I understand that my thesis may be made electronically available to the public.

Abstract

In recent years, the Great Lakes have faced a resurgence of cyanobacterial harmful algae blooms (cHAB), primarily attributed to non-point sources, notably agricultural activities. While significant efforts have been directed toward implementing conservation practices to mitigate nutrient losses, existing literature often examines the efficacy of best management practices (BMPs) and spatiotemporal drivers of nutrient loss separately, neglecting their interconnectedness. Recent studies suggest that conservation practices' effectiveness may vary spatially, necessitating targeted interventions to avoid trade-offs. This study aims to delineate distinct ecoregions based on known spatiotemporal drivers of nutrient loss and analyze their implications for water quality across different land use-land cover (LULC) types. Using Google Earth Engine (GEE), two Cascade K-means clustering analyses were conducted separately on climate and geophysical variables, resulting in three distinct ecoregions for each domain. These findings were integrated with data from the Provincial Water Quality Monitoring Network (PWQMN) and HYDAT stations to assess patterns in water quality degradation and nutrient loss mechanisms across ecoregions. Additionally, statistically downscaled climate change datasets from Environment and Climate Change Canada (ECCC) were utilized to determine shifts in climate conditions across established climate ecoregions. Furthermore, climatic ecoregions displayed a latitude-dependent pattern in water quality degradation. Under projected climate changes, the coolest regions are anticipated to resemble current conditions in the warmest regions, leading to a northward shift in agricultural suitability. These findings underscore the necessity of adopting a context-dependent approach to agricultural management practices, especially in light of projected climate shifts. A one-size-fits-all approach to BMP recommendations and implementation falls short, highlighting the importance of tailored strategies to address the unique challenges posed by each ecoregion.

Acknowledgements

I want to express my sincere gratitude to Dr. Merrin Macrae, who has been an invaluable resource to me throughout my academic career. As an undergraduate, she provided me with the opportunity to establish a strong foundation in her lab and offered the space and encouragement for me to grow as a researcher. Thank you for your steadfast support, encouragement, and belief in my abilities, even during moments of self-doubt. Your guidance has been instrumental in shaping this research project, and I am truly grateful for your mentorship every step of the way.

Special thanks are also extended to Dr. Peter Deadman and Dr. Grant Gunn for their constructive criticism, valuable insights, and dedication to upholding the academic rigour of this work. I sincerely appreciate the time and effort you invested in working with me throughout my degree, helping me develop essential research skills.

To my colleagues and lab mates, thank you for your camaraderie, stimulating discussions, and shared experiences that have enriched my academic journey. I am incredibly grateful to Dr. Jania Plach and Dr. Will Pluer for their steadfast support during my transition from undergraduate to graduate studies.

My heartfelt appreciation goes to my friends for their constant encouragement, understanding, and occasional distractions that provided much-needed breaks during intense periods of research. Special thanks to Pedro Serrano, Anika Chiang, Kathy Wilson, Mike Wilson, Ben Vang, and Elissa France for your invaluable support during the challenging moments of my academic journey.

Finally, I am indebted to my family for their boundless love, encouragement, and unwavering belief in my abilities. Asiya, Yusuf, Hassan, and Fatima, your support has been my source of strength and motivation throughout this academic endeavour. I cannot adequately express my gratitude to my parents, Fauzia and Ahmed. Their sacrifices, guidance, and firm belief in my potential have been the driving force behind my academic pursuits. My mother inspired me to pursue a graduate degree, while my father motivated me to push myself academically and personally. This thesis stands as a testament to their unwavering support and unconditional love.

Table of Contents

List of Figures

List of Abbreviations

Chapter 1
Problem Statement

The Laurentian Great Lakes, also known as the Great Lakes of North America, comprise a network of five lakes: Lakes Superior, Michigan, Huron, Erie, and Ontario; the Great Lakes outflow eastward into the St. Lawrence River, which empties into the Atlantic Ocean. These lakes hold approximately 20 percent of the Earth's freshwater, rendering them highly vital to the survival of the surrounding communities (Steffen et al., 2014). Since the beginning of the British and French colonies and throughout the industrial age, the water quality of the Great Lakes has steadily declined due to pollution from both urban and rural regions (Choquette et al., 2019). Due to the unique geographical positioning of the Great Lakes, which crosses the border between Canada and the United States, both countries have embarked on collaborative initiatives to improve and restore the water quality of the lakes (GLWQA NAS, 2019; Bunch, 2022).

The Great Lakes have encountered new challenges over the course of several decades, including a re-eutrophication of Lake Erie (Watson et al., 2016), prompting the establishment of research, proposals, and initiatives aimed at mitigating water quality concerns (Steffen et al., 2014; Choquette et al., 2019; Macrae et al., 2021). In the 1910s, the improper disposal of untreated sewage was identified as the primary cause of water quality degradation, which led to typhoid epidemics in communities dependent on the Lakes for drinking water (Bunch, 2022). In the 1940s and 50s, a transboundary study found that sewage, chemical, and industrial sources of pollution, coupled with ship waste and channel bed excavation, were the primary contributors to contamination in the Great Lakes (Bunch, 2022). Finally, in the 1960s, the primary sources of pollution ranged from chemical inputs to nutrient contamination, but by the following decade, industrial and ship waste exhibited a decline (Bunch, 2022) in response to the identification of phosphorus (P) as the limiting nutrient by Schindler (1977).

Currently, governing bodies have taken extensive measures to repair past damage and have made great strides in restoring the overall health of the Great Lakes (Choquette et al., 2019). Past efforts were directed toward managing point sources of pollution in the form of wastewater and industrial contamination from specific locations along the shores of the Lakes (Dolan and Chapra, 2012; Maccoux et al., 2016). By regulating these specific sources throughout the 20th century, harmful algae blooms were drastically reduced, and water health was vastly enhanced (Steffen et al., 2014). However, since the 90s, the Great Lakes have experienced a reemergence of algae blooms and a

deterioration in water quality, and experts have denoted non-point sources, mainly agricultural sources, as the primary source of this resurgence (Dolan and Chapra, 2012; Maccoux et al., 2016; Choquette et al., 2019; Macrae et al., 2021). Managing non-point sources is significantly more complex than controlling point sources, and researchers have been tasked with understanding the various driving mechanisms of these sources and recommending solutions to governing bodies (Kleinman et al., 2011).

Although substantial work has been done on conservation practices in agricultural settings, recent work (Kast et al., 2021; Macrae et al., 2021) has suggested that the efficacy of conservation practices may vary spatially and that targeted conservation practices are needed to avoid trade-offs (Kleinman et al., 2022). Jarvis et al. (2017) found that despite largescale conversation practice implementations within Lake Erie watersheds to mitigate P loss through a specific mode, they inadvertently led to higher rates of P entering waterways through other pathways. Since Lake Erie has been the most heavily impacted of the Great Lakes, much of the focus has been on the Lake Erie watershed, particularly the Maumee and Sandusky watersheds, which dominate P loads to the lake. However, recent work suggests that pollution from other areas, such as Muskegon Lake, Michigan, may be relevant (Mancuso et al., 2021). Moreover, in accordance with the State of Great Lakes report (2022) conducted in collaboration with the Governments of Canada and the United States of America, other Great Lakes, such as Lake Huron and Lake Ontario, are also showing signs of eutrophication. Thus, guidance on conservation practice efficacy throughout the Great Lakes region is needed. Moreover, given the anticipated effects of climate change on the Great Lakes region (Byun et al., 2019; Demaria et al., 2016), which may change agricultural practices and streamflow, insight is needed on suitable conservation practices for regions in the future.

In light of the ambiguity surrounding the context-dependency of conservation practice recommendations, watershed classification emerges as a valuable tool to synthesize and contextualize our understanding of spatial phenomena, particularly regarding P loss dynamics (Macrae et al., 2021; Kleinman et al., 2022; Reid et al., 2018). By integrating spatial analysis techniques with a comprehensive understanding of P loss dynamics, watershed classification can inform the optimization of conservation practices and the development of tailored recommendations that account for both current conditions and anticipated future shifts (Hastie et al., 2001; McDonnell & Woods, 2004). This thesis aims to address this need by fulfilling three objectives: (1) defining broad zones in agricultural landscapes across the Great Lakes Basin based on climate and landscape drivers of P loss

under contemporary climate conditions, (2) determining whether water quality differs for various land uses across these zones, and (3) assessing implications of changing climate on the regional classifications developed in (1) and infer water quality trajectories in the future. Through these objectives, this research aims to enhance our understanding of the complex interactions between P loss drivers, encompassing landscape dynamics and climate variability, and their impact on water quality within agricultural landscapes across the Great Lakes Basin amid shifting climatic conditions.

Chapter 2
Literature Review

2.1 Phosphorus Dynamics in Ecosystems

2.1.1 Brief Overview of Phosphorus in Soil and Water

P is a naturally occurring element that limits the growth of both terrestrial and aquatic plants and animals (Schindler, 1977). Excess P loss, predominantly from agricultural landscapes, can and has caused downstream freshwater systems to become increasingly eutrophic as aquatic plants continue to feed on the abundance of P (Jarvie et al., 2013). Schindler et al. (2008) completed a 37-year study of eutrophic lakes and found that P is the main nutrient of concern in terms of improving water quality. Understanding how P cycles through various forms in terrestrial ecosystems and aquatic environments are vital in effectively managing P loss vulnerability (Schindler et al., 2008). In contrast to other biogeochemical processes (e.g., carbon and nitrogen), P cycles are considerably slower and can last for days, months, years, or even decades, and fluxes between pools do not include a gaseous form (Holtan et al., 1988). The rates, fluxes, and pools within P cycles are sensitive to human activity and can vary substantially across ecosystems (i.e., terrestrial vs. aquatic) and scales (i.e., watershed vs. local) (Schipanski & Bennett, 2021).

Within the P cycle, P is transformed into various forms or pools that affect its access to living organisms and can influence water quality (Sharpley et al., 1991). Total P (TP), including organic and inorganic forms of P, is present in aquatic and terrestrial ecosystems (Holtan et al., 1988). Organic P refers to P bound to tissues and molecules of living and nonliving organisms, whereas inorganic P denotes P that does not exist in organic matter (Holtan et al., 1988). All organic and inorganic forms of TP are divided into two main fractions: dissolved P and particulate P (PP) (Holtan et al., 1988). Dissolved or soluble P (SP) is the form of P that passes through a 0.45μm filter, and this pool can be further subdivided into two groups, soluble reactive P (SRP) and soluble unreactive P (SUP), based on whether they react (or do not react) to particular reagents (Sharpley et al., 1991). SRP is associated with P found present in inorganic matter, with the predominant component being orthophosphate, which is the most accessible form of P for absorption by plants (Holtan et al., 1988). In contrast, SUP, which consists of primarily organic P, tends to have longer residence periods in aquatic environments than SRP, thereby increasing the likelihood of affecting nutrient levels in vulnerable waterbodies

(Holtan et al., 1988). The sum of SRP and SUP is termed total dissolved P (TDP) (Holtan et al., 1988).

PP can be determined as the difference between TP and TDP (Holtan et al., 1988). Unlike SP, PP exhibits limited accessibility for absorption by terrestrial and aquatic plants (Condron & Newman, 2011). PP is a solid form bonded to sediment particles, constituting between 70 and 90 percent of agricultural runoff during high-flow events (Sharpley et al., 1991). As mentioned, PP may exist in an organic form held in microbial, plant residuals, or humus that can become bioavailable upon decomposition (Cavalcante et al., 2018). On the other hand, inorganic forms of PP are either adsorbed/surface bonded to mineral surfaces (e.g., iron and aluminum oxides, clays, etc.) or absorbed/chemically bonded to secondary compounds (e.g., calcium, magnesium, etc.) within sediments (Dittrich et al., 2013). Depending on the fraction of PP, these composites can break down, and the P released can become bioavailable under varying conditions within the water column, contributing to internal P loading (Condron & Newman, 2011).

Detection limits in lab analysis arbitrarily define P forms and their associated pools, and they are typically associated with specific chemical and filtration methods developed by prior research (Condron & Newman, 2011). As stated earlier, SP encompasses all P elements that pass through a 0.45 μm filter; however, PP, in the form of P-bound nanoparticles, can pass through the filter to pass through (River & Richardson, 2019). The risks of overestimating the SP pools can misrepresent the bioavailability of P within aquatic ecosystems (River and Richardson, 2019). Research has established that colloidal P is responsible for the largest percentage of P loss from agricultural landscapes, linked to increased internal P loading levels (Liu et al., 2014).

2.1.2 Sources and Pathways of Phosphorus from Terrestrial Landscapes to Water Bodies

P loads are introduced into aquatic systems through a multitude of transport pathways originating from diverse sources (McDowell et al., 2001; Dinnes, 2004). The source and transport pathways that dictate the composition of P forms in these water bodies have a major influence on the overall impact of P on these ecosystems (Pasek et al., 2014). P sources entering waterways are derived from terrestrial landscapes, including cropland, pastures, urban settlements, and natural environments (e.g., forests and upstream waterbodies) (Dines, 2004). P transported via biogeochemical pathways from its source to its sink (i.e., streams, rivers, and lakes) can undergo transformations or be mobilized within

and between terrestrial and aquatic ecosystems (McDowell et al., 2001). Physical, chemical, or biological transport to aquatic ecosystems is contingent upon the P form (Pasek et al., 2014).

P sources originating from terrestrial landscapes are categorized as either point or non-point sources (Sharpley et al., 2001). Point sources of P loss are traceable inputs from areas such as sewage treatment facilities or industrial plants (Bennett et al., 2001). Because it is easily identifiable, P inputs from various point sources have been significantly reduced through targeted efforts by government bodies and other organizations (Bennett et al., 2001). For instance, waste treatment plants have removed as much as 95% of P from wastewater in urban regions entering nearby waterbodies (Bennett et al., 2001). In contrast, non-point sources are more challenging to identify due to their inability to be traced back to a specific location and their limited recognition as upstream sources, such as agricultural fields or residential areas (Kleinman et al., 2015). Consequently, managing P inputs from these regions is considerably more complex and requires more effort to mitigate P loss risks (Reid et al., 2018). Most non-point or diffused sources of P originate from agricultural landscapes and are then transported to adjacent water bodies at a rate of approximately 15 million tons annually (Kleinman et al., 2011). As a consequence, P concentrations in these aquatic environments remain excessively high, having tripled in waterways since preindustrial levels (Bennett et al., 2001).

The supply of P is either applied, acting as a transient source or accumulates as legacy P, which consists of long-term reserves (McDowell et al., 2001). However, legacy soil P refers to the surplus nutrients that endure in the soil profile without being assimilated by plants or depleted through erosion (Kleinman et al., 2011). The accumulation of legacy soil P in the soil profile over extended periods of time due to excessive P application in arable lands presents a significant threat of P loss via transport pathways (Keatley et al., 2011). Johnston and Poulton (1976) discovered that it took 73 years for excess soil P levels to decrease by more than 50 mg kg^{-1} after manure-based P application was discontinued (Mcdowell et al., 2001). In aquatic ecosystems, legacy soil P, which is present along water bodies' beds, contributes to internal P loading through resuspension (Baker et al., 2019; Da-Peng & Yong, 2010). As an illustration, P-bound bed sediment accounts for 20 to 42 percent of the persistent quantities of SRP within Lake Erie's western basin (Baker et al., 2019).

Water movement within and across terrestrial and aquatic ecosystems regulates the transport of P (Dinnes, 2004). Locally, soil P moves vertically and horizontally within the soil profile; however, at

the regional scale, soil P traverses landscapes via two main pathways: overland flow and subsurface flow both above and below the water table (Sharpley et al., 2001). Overland flow, also known as surface runoff, is the most important P pathway and occurs when water fails to infiltrate the ground and flows across the surface, eroding applied P into adjacent waterways (Pärn et al., 2012; Reid et al., 2018). Consequently, non-point sources of PP account for 70 to 90 percent of agricultural runoff during high-flow events (Sharpley et al., 1991). Several studies have highlighted the importance of accounting for P loss through surface runoff because of the tendency of applied P to remain concentrated in topsoil layers and to be tightly bound to soil elements (Wang et al., 2010; Jarvie et al., 2017; Watson et al., 2016).

Conversely, subsurface flow occurs when soil layers reach a specific saturation level, allowing water to flow horizontally and empty into adjacent waterways (Dinnes, 2004). When applied, P occupies lower soil layers (also known as leaching) in agricultural regions and can contribute to P loss through subsurface flow (Sloan et al., 2016). Among the most significant contributors to subsurface flow is the installation of tile drains by farmers to lower the water table artificially (Smith et al., 2015). Tile drainage is primarily used in regions with poor drainage, where the root zones of crops remain exceedingly saturated with no air pockets (Smith et al., 2015). Waterlogging hinders the ability of crops to extract water and nutrients from the soil; therefore, farmers install pipes under the surface to drain excess water from their fields (Sloan et al., 2016). Consequently, tile drains in these drained arable regions significantly contribute to P loss through subsurface flow (King et al., 2015). Researchers have observed that in regions with hydrologically connective tile drainage systems, P loss through overland flow is significantly diminished, and subsurface flow emerges as the predominant mode of P transportation (King et al., 2015). Introducing tile drains in areas with insufficient drainage systems enables more P sources to infiltrate aquatic ecosystems, exacerbating the difficulty of preventing P loss (Reid et al., 2018).

2.1.3 Influences of the Nitrogen Cycle on Phosphorus Dynamics

Across the many biogeochemical processes that occur within the soil matrix and water columns, the nitrogen (N) cycle has one of the largest impacts on P dynamics within these ecosystems and along transport pathways (Dodds & Whiles, 2020). N cycling can impact the availability, mobility, and transformations of P within these systems (Zheng et al., 2020). For instance, both P and N act as limiting factors in plant growth, and an imbalance in the availability of these nutrients can pose a risk

of P loss (Li et al., 2023). Moreover, the extent to which these elements impact the P cycle varies based on the particular nutrient processes and the configurations of these nutrients within the ecosystem (Zheng et al., 2020). This knowledge will facilitate the establishment of more precise management targets for mitigating P loss from agricultural landscapes (Zheng et al., 2020).

The interactions between N and P add to the complexity of nutrient dynamics in terrestrial and aquatic environments since macronutrients are essential to plant growth and development (Dodds & Whiles, 2020). Within the N cycles, the presence and transformation of N can influence the availability and mobility of P (Zheng et al., 2020). For instance, multiple soluble nutrients are released into the systems during the mineralization of organic matter (Gao et al., 2014). Microbes can mineralize organic N compounds, which results in the availability of SP for plant uptake or transportation to adjacent water bodies (Gao et al., 2014). Organic N compounds can potentially enhance the solubility and mobility of P by either competing for sorption sites or forming complex compounds with P (Grunes, 1959). Likewise, ammonium released via mineralization can also increase the bioavailability of P by sorbing to accessible sites on soil colloids or being abundantly present, leading to a surge in P desorption (Grunes, 1959). Furthermore, nitrification processes, which involve the conversion of ammonium into nitrates, reduce pH levels and facilitate the desorption of P from calcium compounds (Li et al., 2023). Conversely, at elevated pH levels, ammonium can reduce the bioavailability of P through the formation of complex compounds (Li et al., 2023).

2.2 Spatiotemporal Factors Impacting Phosphorus Availability and Mobility

2.2.1 Seasonal Variability in Phosphorus Loss Pathways

Climatic conditions play a pivotal role in shaping P dynamics within and across ecosystems by governing the horizontal and vertical movement of water (Rattan et al., 2019). The dynamics of P are influenced by the complex interaction between temperature fluctuations and precipitation rates, including factors such as amount, form/changes, and timing (Reid et al., 2018; Macrae et al., 2021). However, the seasonal variability dictates the timing, magnitude, and pathways of P loss from source to sink (Reid, 2011). This becomes particularly crucial in regions with cold climates, where annual precipitation and temperature fluctuations determine critical runoff periods (Plach et al., 2019).

Precipitation is pivotal in governing hydrological processes that influence P transport within and across ecosystems (Plach et al., 2019). In conjunction with geomorphological and topographic

variables, climate drivers regulate runoff movement and distribution, with climatic conditions directly amplifying their impact on P loss (Reid et al., 2018). In light of the diverse forms of precipitation, such as rainfall, snowfall, hail, and sleet, it becomes crucial to recognize their distinct effects on P dynamics (Liu et al., 2013). Precipitation patterns exhibit seasonal and regional variation, with rainfall and snowfall typically predominating (Liu et al., 2013). Rainfall is the predominant mode of transport for P in warmer climates, whereas snowmelt assumes this role in colder temperatures (Reid et al., 2018). These precipitation forms influence the speed and mode of P transport and are intricately linked to timing and intensity (Liu et al., 2013).

Precipitation directly impacts soil moisture, which dictates the mode of the P transport pathway (i.e., surface runoff vs. subsurface discharge, including tile drain rates) (Reid et al., 2018). Due to the rapid saturation of surface soils, infiltration rates are greatly reduced when precipitation intensity peaks, particularly during storm events; runoff volumes entering adjacent waterways are exacerbated by excess precipitation inputs (Reid et al., 2018; Rittenburg et al., 2015). In contrast to infiltration rates imposed by soil type, changes to crop type or soil management practices have no impact on the consequences of excess runoff resulting from saturated environments (Reid et al., 2018). Increased water flow across agricultural landscapes causes erosion of topsoil layers, typically P-enriched soils and aids the delivery of soluble and PP (Fouli et al., 2013). Moreover, an increase in precipitation inputs is associated with a corresponding surge in discharge in areas equipped with artificial drainage systems (King et al., 2015). Smith et al. (2015) found that tile discharge peaks coincided with surface runoff peak flows due to preferential flows facilitating the hydrological connectivity between surface and subsurface soils. Research has indicated that elevated flow events, which are caused by increased precipitation amounts, lead to the greatest P loss through subsurface discharge (King et al., 2015; Smith et al., 2015).

In addition to precipitation form and intensity, the timing of storm events emerges as the most influential factor in P transport (Reid, 2011). The greatest risk of P loss occurs when storm events follow P applications, such as fertilizer or manure (Kleinman et al., 2011). P application to the surface during fall and winter seasons significantly contributes to P loss during snowmelt events (King et al., 2017). Conversely, freshly applied P may be transported via tile drains during the growing season (May to September) as a result of low soil moisture, displaced as runoff or rapidly leached into subsurface soils during summer rain events (Smith et al., 2015). While summer runoff poses a risk, it

is generally lower than winter runoff because soil moisture capacity is reduced during the cooler months (Reid et al., 2018; Macrae et al., 2021).

In regions with a cold climate, snowfall and snow cover are crucial factors in P mobilization and transport (Liu et al., 2013). Regions with increased snowpack development have greater spring snowmelt contributions in the form of P-enriched surface (i.e., frozen or saturated ground) and subsurface (i.e., unfrozen ground) discharge (Reid et al., 2018; Macrae et al., 2021). In areas with prolonged snow cover, the ground is insulated from the harsh surface winter conditions, and the soil temperature remains moderately higher, preventing the ground from freezing and allowing moisture to permeate the soil layers (Liu et al., 2013). Conversely, researchers have discovered that intermittent or brief snow cover causes the frozen ground to impede infiltration rates, and P-enriched topsoil can be eroded once the temperature rises (Reid et al., 2018; Macrae et al., 2021). Additionally, precipitation-induced runoff further amplifies the risk of P loss in these soils by decreasing P uptake (Reid et al., 2018). Rain events that coincide with snowmelt further induce P transport from agricultural surfaces, particularly if they occur earlier in the season (Reid et al., 2018; Liu et al., 2013).

The seasonal variation in cold climates introduces unique temporal patterns in P loss not commonly observed in other global regions (Rattan et al., 2019). Temperature fluctuations influence P mineralization rates and the fluxes of P between different pools (Pasek et al., 2014). Higher soil temperatures enhance plant P uptake, depleting P from soil layers. However, warmer temperatures also accelerate decomposition, increasing P availability (Reid, 2011). During the growing season, evapotranspiration reduces surface soil moisture, leading to increased infiltration rates during summer storm events (Reid, 2011). Warmer temperatures contribute to decreased runoff rates, with overland flow typically confined to edge-of-field regions (Reid, 2011). Concurrently, during the summer, low soil moisture increases the likelihood of P transport through preferential flow paths to tile drains (Pärn et al., 2012). This contributes to base tile drain flow carrying legacy P when plant uptake is equivalent to or lower than the applied P rates (Smith et al., 2015).

Temperature fluctuations within and between seasons drive freeze and thaw cycles, impacting both hydrological responses and soil processes associated with P loss (Kværnø & Øygarden, 2006). The transition between freezing and thawing alters soil particle size and influences P bonding forms (Fan et al., 2014). Decreased particle size enhances surface area, leading to higher rates and capacities of P

sorption within the soil profile (Kværnø & Øygarden, 2006). However, Fan et al. (2014) note that the breakdown of soil particles can release surface-bound P, thereby becoming accessible for plant uptake. Mid-season snowmelts can rapidly transport bioavailable P to aquatic environments (Reid, 2011). As winter months experience temperature fluctuations, climate change-induced weather variability can exacerbate and increase this form of P delivery (Rattan et al., 2019). Additionally, freeze-thaw cycles create preferential flow pathways and macropores within the soil profile (Karahan & Erşahin, 2017). During cooler months, water molecules expand due to freezing (Kværnø & Øygarden, 2006), and as temperatures rise, the soil structure contracts, forming flow pathways (Kværnø & Øygarden, 2006). These preferential flow pathways govern the volume and velocity of downward P movement, redirecting runoff from the surface to subsurface lateral flows (Pärn et al., 2012).

Temperature serves as a crucial determinant for both the duration of growing and non-growing seasons, and the index used to measure this duration is called Growing Degree Days (GDD) (Reid, 2011; AAFC, 2015). Developed as a tool for farmers and experts, GDD accounts for the number of days per year when temperatures are optimal for plant growth (AAFC, 2015). GDD serves as an indicator for planning P application on fields and determining harvest windows for various crops (AAFC, 2015). A longer GDD signifies an extended growing season, providing more time for plant growth, increased P uptake, and potentially reducing the risk of P loss (Macrae et al., 2021). Furthermore, GDD, much like temperature, is latitude-dependent, and with ongoing climate change, higher latitudes are anticipated to experience longer GDD, with cold climate regions particularly affected (Macrae et al., 2021).

2.2.2 Landscape Drivers Affecting Phosphorus Movement and Mobilization

As discussed earlier, climatic conditions primarily impact the overall volume of water entering and moving through landscapes. Nevertheless, the local geophysical characteristics determine the mode of P transport (Rittenburg et al., 2015; Sharpley et al., 2015). Variability in the topography and geomorphology of the region, along with existing land use types and farming systems, significantly influences P loss from agricultural landscapes (Habibiandehkordi et al., 2020). Additionally, the hydrological connectivity of the landscape is a crucial factor to consider when assessing the risk of P loss (Sharpley et al., 2015). The interdependence of land use, hydrological processes, and nutrient

loading underscores the need to implement targeted management strategies in these areas (Macrae et al., 2021).

The topographical features of the landscape have a direct influence on the trajectory and speed of water flow (Pärn et al., 2012). In addition to elevation and slope, surface landforms dictate the proportion of precipitation that flows off the surface of agricultural fields. Due to the limited subsurface percolation rates, regions with lower elevations experience shallow water tables, which subsequently impact the rate and capacity of infiltration (Reid et al., 2018). There is typically a noticeable increase in the implementation of tile drains in these areas to address insufficient drainage rates (King et al., 2015). On the other hand, they exhibit cooler climates and higher rates of snowfall, both of which can substantially influence the increased release of P into adjacent downstream waterways during the spring as a result of snowmelt. (Habibiandehkordi et al., 2020). Additionally, regions with higher elevation changes are more prone to experience increased runoff flows because steeper slopes reduce infiltration, leading to the erosion of P-enriched surface soils (Fouli et al., 2013). The predominant form of P loss caused by erosion is PP. In Ontario watersheds, the proportion of this fraction accessible to algae can range from approximately 6 to 35 percent (DePinto et al., 1981).

Different surface landforms determine the configuration of the landscape, which, by extension, influences the topography (i.e., elevation and slope) and their impact on P loss rates (Wolfe et al., 2019). For instance, hummocky terrains are covered in a complex series of irregularly sized and shaped knolls and depressions with widely varying slopes (9-70%), creating micro-topographic features (Soil Landscapes of Canada Working Group, 2011). Depressions across the landscape can retain water and impede its passage across the surface to form wetlands or detention ponds (Wolfe et al., 2019). Inundation of soils along hydrological pathways linked to regions that are temporarily or permanently flooded has a multiplicative effect on P transport and redox conditions, which in turn alter forms of P bonding (Pärn et al., 2012). Temporarily flooded soils have the potential to provide sources of P by means of rewetting sediments (Pärn et al., 2012). This process alters redox conditions and induces an anaerobic state, re-releasing sorbed P (King et al., 2015; Pärn et al., 2012; Vymazal, 2007).

Additional landforms with flatter surfaces, such as undulating landscapes, create a wavelike pattern of gentle slopes (2-5%) (Soil Landscapes of Canada Working Group, 2011). Notwithstanding its

reduced gradient, this terrain introduces surface roughness into the landscapes, impacting the speed, direction, and rate of water movement (Soil Landscapes of Canada Working Group, 2011). Römkens et al. (2002) found that surface roughness was correlated with greater soil losses due to the concentrated flow paths transporting large volumes of runoff over a small area. The positive relationship between runoff and erosion rates is the key factor in determining the erodibility of surface soils because runoff volumes increase, so does velocity (Rittenburg et al., 2015). In addition, surface roughness also determines drainage network development within the landscape, where smoother terrain increases stream density but reduces overall stream order within the catchment (Römkens et al., 2002).

The variability in soil characteristics is another key landscape driver that affects both the P dynamics within agricultural landscapes and the risk of P transport to aquatic ecosystems (Plach et al. 2018b). A landscape's geological diversity (i.e., the parent material) of soils determines its physical and chemical properties, including their texture/type and composition (McDowell et al., 2001). This further affects the hydrological responses primarily associated with P transport and can potentially disrupt the prevailing redox conditions in the region (Pärn et al., 2012). For instance, regions characterized by fine-textured soils experience inadequate drainage, leading to a higher prevalence of tile drain installation, which is usually higher in these regions (Smith et al., 2015). Consequently, the predominant mode of P transport in these soils is through tile drains, where it is generally present as PP (Smith et al., 2015).

The soil type present in surface and subsurface sediments substantially impacts the movement and quantity of bioavailable P leaching into adjacent aquatic ecosystems (Smith et al., 2015). Soil type is one factor controlling both the vertical and horizontal movement of water above and below the surface (Pärn et al., 2012). As mentioned previously, overland flow occurs when input precipitation and snowmelt fail to percolate at the surface, and runoff erodes applied P into waterways (Sharpley et al., 2001). Nonetheless, the infiltration rate can vary significantly depending on the particulate size of the soil profile (Sloan et al., 2016). As an illustration, sands possess the highest drainage capacity, which facilitates the downward movement of P from the surface and is dominated by subsurface flows either through pre-existing tile drains or the lateral movement of subsurface flows (Smith et al., 2015).

Sandy soils have coarser particle sizes, facilitating preferential flow pathways for the movement of P both vertically and horizontally through the soil profile (Reid et al., 2018). On the other hand, soil profiles with substantial clay contents experience higher levels of runoff as the presence of finer sediment reduces surface infiltration rates (Eastman et al., 2010). Conversely, other studies have found that macropores in subsurface sediments can increase P leaching to subsurface tile drains controlled by clay content (Eastman et al., 2010; Karahan & Erşahin, 2017). Karahan and Erşahin (2017) observed a statistically significant and negative correlation between clay content and the hydrological conductivity of soils. These findings indicate that macropore size increases in tandem with the size of soil particles, thereby increasing the likelihood of P leaching in these landscapes (Karahan & Erşetsin, 2017).

Similarly, soil composition can influence the retention and transport of P throughout terrestrial ecosystems (McDowell et al., 2001). Once P is introduced into terrestrial soils, whether through weathering or intentional application in the case of croplands (i.e., fertilizer P or animal manure), it has the propensity to rapidly bind to soil particles and convert from a bioavailable state to PP (Schipanski & Bennett, 2021). Depending on the soil characteristics, the chemical process of adsorption or absorption rates are regulated by the number of positively charged slots that permit the P ions to occupy (Pasek et al., 2014). Thus, the soil composition regulates the bioavailability of PP and its impact on algae growth within aquatic ecosystems (McDowell et al., 2001).

Soils rich in iron and aluminum are more likely to absorb P that travels through them, which can then be mobilized once the particulate forms enter aquatic environments (Cavalcante et al., 2018). These P bonds can be released under anoxic conditions, making them bioavailable to algae within aquatic systems (Cavalcante et al., 2018). In contrast, soils rich in calcium and magnesium form chemical bonds with available P under more stringent conditions (Dittrich et al., 2013). Calcium fractions of PP dissolve in acidic environments and become available for plant uptake (Dittrich et al., 2013). Moreover, it is noteworthy that the organic matter in soil profiles derived from frozen plant residue is a significant source of dissolved P released when temperatures rise (Reid et al., 2018). For this reason, the soil characteristics of the extant surface and subsurface sediments substantially affect the movement and quantity of bioavailable P leaching into neighbouring aquatic ecosystems (Reid et al., 2018).

The capacity of tile drainage to transport both SP and PP depends on the soil type and composition (King et al., 2015). Tile drains provide hydrological connectivity in these regions and affect hydrological response rates of P loss (King et al., 2015). Transport limitations or lack of connectivity to a transport pathway render the risk of P loss minimal or negligible in regions with abundant sources of P (Plach et al., 2018a). However, transport limitations do not preclude the possibility that available P in a region could eventually become hydrologically connective (via the installation of a tile drain, for instance) (Plach et al., 2018a). The hydrological connectivity of the landscape, geophysical properties, and the flow of water from the source area to surface water bodies largely determines the effect of hydrological responses on P loss (Reid et al., 2018; Habibiandehkordi et al., 2020). The hydrological responses within watersheds and the existing soil and vegetation characteristics can considerably induce P loss from agricultural landscapes (Habibiandehkordi et al., 2020).

Additionally, prior investigations have estimated P loss based on proximity to surface water to determine the hydrological connectivity of a region (Habibiandehkordi et al., 2020). The assumption was that P loss occurs predominantly through overland flow from the edge-of-fields to adjacent edge-of-water (Reid et al., 2018). Reid (2011), however, argued that this reasoning is flawed because P transport associated with hydrological response is not restricted to surface runoff. As mentioned previously, in drained landscapes, tile drainage modifies P transport pathways, which not only reduces the volume of surface runoff but also alters the timing of peak runoff flows reaching water bodies (King et al., 2015; Reid et al., 2018; Sloan et al., 2016).

Land use plays a pivotal role in shaping the hydrological connectivity of a region, influencing both P sources and transport pathways, and the interaction of these factors increases the risk of P loss (Reid, 2011). Anthropogenic activities further exacerbate the P cycling rate, introducing mined P into regional and local cycles via fertilizers, animal feed, and detergents (Bennett et al., 2001). Notably, agricultural and urban areas emerge as the primary contributors to both point and non-point P sources (Kleinman et al., 2011). Scavia et al. (2016) found that despite constituting only 4 percent of the average flow to Lake Erie, the Maumee River basin delivers a striking 48 percent of TP, with 31 percent being SRP. Remarkably, 70 percent of this basin consists of agricultural landscapes, emphasizing the disproportionate impact of these regions on P loading (Wilson et al., 2019).

During the growing season, all landscapes adjacent to water bodies are more susceptible to receiving elevated P loads (Reid, 2011). However, preliminary observations conducted by Habibiandehkordi et al. (2020) indicated that using a standardized distance of a 150-meter radius from nearby waterways does not account for the natural variability present at the farm scale within Ontario and Manitoba tributaries. Due to the variability of P transport pathways, proximity to surface water is insufficient as a sole indicator of P loss (Reid et al., 2018; Macrae et al., 2021). Some agricultural regions have natural barriers that separate fields from surface waters (e.g., riparian zones) and effectively filter out P from contaminated sources (Reid et al., 2018). Vegetation eliminates P from surface runoff entering the system via the adsorption of SP or infiltration processes that induce P leaching into subsurface soil layers (Li et al., 2011). Vymazal (2007) found that inflow P concentrations entering these ecosystems were 40 to 60 percent higher than the outflow concentrations of P leaving these ecosystems.

2.2.3 Combined Influence of Land-Climate Drivers on Phosphorus Loss in the Great Lakes Watershed

Sources and transport of P within the Great Lakes can vary considerably between and within sub-basins. For instance, Lake Erie has been suffering from a recurrence of cyanobacterial harmful algae blooms (cHAB) since the 1990s, which has caused the lake to turn bright blue-green during the warmer months (Steffen et al., 2014). The primary source of excess P loss causing eutrophic conditions in Lake Erie is non-point sources from agricultural regions (Choquette et al., 2019; Macrae et al., 2021). Due to the abundance of favourable conditions for plant growth, the Lake Erie watershed is dominated by agricultural activity, and understanding and accounting for nutrient pollution leaving these regions and entering upstream waterways has proven to be a challenge for researchers attempting to recommend mitigation measures (Macrae et al., 2021). On the other hand, Lake Superior and Huron have the best water quality among the five lakes due to the absence of non-point sources (Bunch, 2022). Certain areas characterized by significant shoreline activity—such as Saginaw Bay, Michigan, and Silver Bay, Minnesota—have been subject to pollution restrictions since the 1960s (Bunch, 2022).

The five watersheds of the Great Lakes have diverse climatic conditions, which are dependent on latitude in certain regions (LaZerte & Albers, 2018; Macrae et al., 2021). Lake Superior basin is the coldest (highest latitude), Lake Erie is the warmest (lowest latitude), Lake Huron is the wettest (due

to lake effect), and the regions with the lowest annual average precipitation rates are the Lake Erie, Ontario and Superior (at lower elevation and in the absence of lake effect) (LaZerte & Albers, 2018). As stated previously, the fluctuations in precipitation and temperature rates have distinct effects on P loss (Reid, 2011). For instance, in Lake Huron, the lake effect induces high precipitation rates, causing the regions to have more snowfall and extended periods of snow cover (LaZerte & Albers, 2018). This suggests that snow cover preventing frozen ground and decreasing runoff rates may increase infiltration rates or contribute significantly to snowmelt runoff as a risk factor for P loss (Reid et al., 2018).

It is anticipated that future climate change consequences will further exacerbate the established climate conditions on P loss from agricultural regions within the Great Lakes Basin (Eimers et al., 2020). For instance, Wang et al. (2018) found a 25 to 108 percent increase in TP loss from two small catchments within the Great Lakes Basin due to intensification of extreme precipitation and temperature. In addition, future scenarios have projected that climate change effects may not impact the entire region of the Great Lakes Basin equally (Eimers et al., 2020). The Intergovernmental Panel on Climate Change (IPCC) has reported that the region will likely experience an increase in both the mean and extreme precipitation levels in the coming years (IPCC, 2023). However, the Lake Superior sub-basin is projected to have greater snowfall accumulation compared to the other watersheds (IPCC, 2023). Lucas et al. (2023) highlighted that future surges in extreme precipitation have the greatest influence on P loss from agricultural landscapes to waterbodies globally. Specifically, Ross et al. (2022) found that after analyzing water quality data from 11 sub-watersheds that drain into the lower Great Lake Basin. Ross et al. (2022) discovered that between 55 and 100 percent of storm events exhibit a positive correlation between TP levels and streamflow.

In a similar vein, climate models forecast with exceptional accuracy that regional temperatures will surpass the global average (IPCC, 2023). Annual temperatures increase, and days with extreme temperatures are more probable, particularly in the winter months (IPCC, 2023). These impacts are projected to affect the sub-watersheds differentially (IPCC, 2023). For instance, future rising temperatures in the Western Lake Erie basin are expected to offset the impacts of extreme precipitation on P loss within the region (Kalcic et al., 2019). Increases in evapotranspiration and decreased snowfall will lead to a decline in soil moisture levels, and P-enriched runoff is more likely to infiltrate deeper into the soil matrix (Lucas et al., 2023). On the other hand, rising temperatures in cooler sub-basins (i.e., Lake Huron) have a greater probability of generating sporadic snow cover,

which impedes infiltration rates and causes a reduction in soil temperature (frozen ground) (Eimers et al., 2020). Furthermore, freeze-thaw cycles are anticipated to intensify in duration and frequency, leading to various impacts on P loss dynamics, including a rise in tile drainage runoff (Lucas et al., 2023; Eimers et al., 2020).

P loss across the Great Lakes is influenced by various geophysical factors (MNRF, 2019b & 2019c; AAFC, 2018a & 2018b). Depending on the targeted region, soil texture, elevation, and land use type may all play a significant role in the risk of P loss (Rittenburg et al., 2015). For example, the soil texture in the southern areas of the Lake Ontario watershed bordering the United States is predominately fine, while it is mainly coarse in the northeastern region of the watershed (Soil Landscapes of Canada Working Group, 2011). This implies that P transport pathways may vary based on the location of P loss within the watershed (e.g., runoff vs subsurface flow or SP vs PP) (Reid et al., 2018). Another distinction among the sub-basins pertains to land use types, briefly mentioned in the preceding section (AAFC, 2018a). For instance, agricultural regions predominate in Lake Erie, where the Lake Superior watershed lacks the conditions necessary for farming systems to thrive (AAFC, 2018a). This distinction will lead to variable concentrations of P sources, which in turn will cause P loss from these sub-basins (Macrae et al., 2021). Climate and geomorphology continue to influence the prevalence of tile drainage in regions with high agricultural activity (Lake Erie vs. Lake Ontario), highlighting once more the disparity in P loss risk between the two regions (Reid et al., 2018; Macrae et al., 2021).

2.3 Conservation Practices for Reducing Phosphorus Loss

Best management practices (BMPs) are mechanisms implemented to mitigate the detrimental effects of pollution entering nearby surface waters (Li et al., 2011). In the case of agriculture, BMPs reduce overall nutrient loss by targeting both nutrient sources and transport pathways (Li et al., 2011). These BMPs may be structural or non-structural systems installed either in source areas (e.g., fields), along conveyance pathways (e.g., tile drains), or at edge-of-field regions before entering surface waters (e.g., stream banks) (King et al., 2015; Rittenburg et al., 2015). BMPs that are customized to target the field-specific factors contributing to P loss may be implemented (Macrae et al., 2021; Kleinman et al., 2022). For this reason, diverse BMPs have been developed and set up across various agricultural regions over the years (Macrae et al., 2021; Kleinman et al., 2022).

Despite the considerable rise in the number of watersheds implementing BMPs globally in recent decades, there remains a substantial lack of knowledge regarding their efficacy (Rittenburg et al., 2015). Natural and anthropogenic spatiotemporal variations within tributaries pose the greatest obstacle to assessing the efficacy of BMPs (Li et al., 2011). Decreased efficacy has also been associated with discrepancies between BMPs and established geophysical processes and installation in a region where source and transport variability fails to restrict P loss (Rittenburg et al., 2015; Kleinman et al., 2022). Macrae et al. (2021) identified three P management regions in the Lake Erie watershed that necessitated three distinct BMP approaches to prevent P loss. Negligible progress in P loss beyond initial levels and exacerbation of P loss beyond baseline levels would result from the implementation of the incorrect BMP in one or more of these distinct P management regions (Macrae et al., 2021; Kleinman et al., 2022). In order to optimize the placement of BMP, it is imperative to consider both geophysical and climate drivers (Li et al., 2011; Sharpley et al., 2009, 2015; Macrae et al., 2021).

The optimization of BMP is highly dependent on the primary P loss drivers and should concentrate on reducing P loss via P sources and transport pathways (Wilson et al., 2018). On the other hand, BMP adoption is linked to farmer behaviour, which can only be altered by adjusting the perception of BMP efficacy (Wilson et al., 2018). For instance, Macrae et al. (2021) identify a specific point of contention concerning the extent to which tilling fields decreased P loss risk in the Lake Erie watershed. The recommendation for non-till was first endorsed to limit soil erosion and the transport of PP (Macrae et al., 2021). However, as knowledge surrounding conservation practices advanced, it became evident that no-till fields increased SP loss to surface waters (Macrae et al., 2021). Consequently, the till versus non-till debate has raised more questions in the minds of farmers and obscured their understanding of the effectiveness of conservation practices in reducing P loss (Macrae et al., 2021). This, subsequently, leads to a decline in perceived efficacy among farmers and lowers adoption rates (Wilson et al., 2018).

The existing literature has primarily examined the efficacy of BMP and spatiotemporal drivers of P loss in isolation, with little emphasis on the connections between the two (Macrae et al., 2021; Habibiandehkordi et al., 2020; Wilson et al., 2018). Merely investigating the interplay between these variables is inadequate; a more substantial focus should be directed toward determining the specific factors that govern P loss across different landscapes and in different climatic conditions (Rittenburg et al., 2015). Distinctions of this nature may manifest across regions (e.g., Canadian Prairies, the

Northern Great Plains, and the Great Lakes region) and within a given region (e.g., across Ontario). In order to maximize the efficacy of BMP placement and optimization, all landscape processes, climate drivers, and land management practices must be considered (Rittenburg et al., 2015).

Subsequently, a watershed classification will help reduce ambiguity concerning the context-dependent benefits of BMPs (Macrae et al., 2021; Kleinman et al., 2022; Reid et al., 2018). Several studies have devoted their efforts to monitoring and analyzing the extent and scope of the contribution of P (Wilson et al., 2019). The watershed classification approaches are valuable in synthesizing the most current and up-to-date understanding of P loss (Wolfe et al., 2019). Furthermore, recommendations regarding the most effective BMP approaches can be made based on the emerging P management zones (Macrae et al., 2021; Wolfe et al., 2019). The evaluation of BMP optimization can be facilitated by a classification approach that considers P loss drivers and current source areas of P (Macrae et al., 2021). The patterns can then be used to target motivated BMP adopters with outreach and educational initiatives in an effort to boost their perception of the program's efficacy and, subsequently, its adoption rates (Wilson et al., 2018).

2.4 Classification Approaches Employed in Watershed Analysis

Spatial analysis experts leverage machine learning algorithms, including clustering and modelling techniques, to understand spatial patterns and relationships within geographic datasets. Machine learning algorithms are powerful tools for making human-like predictions and decisions based on large-scale geographic datasets (Hastie et al., 2001). Depending on the objectives, methodologies, and outputs, experts may employ either clustering or modelling approaches to classify complexities within and across watersheds. Clustering identifies spatial groupings to facilitate exploratory analysis by analyzing attributes (Lee, 1981). Meanwhile, modeling predicts and explains spatial phenomena by capturing the irrelationships between variables (Dinov, 2018). Such approaches empower analysts through supervised learning, where models are trained on labelled data, and unsupervised learning, which explores patterns within unlabeled data (Hastie et al., 2001).

For the purposes of exploring and classifying spatial distributions and phenomena, watershed analysis studies employ clustering analysis methods (Wolfe et al., 2019; Macrae et al., 2021; Knoben et al., 2018). Clustering analysis, which falls under the unsupervised learning umbrella, divides the data points into groups (or clusters) based on their degree of similarity (Lee, 1981). However, due to the availability of multiple clustering methods, studies have utilized hierarchical or partitioning

clustering techniques. Hierarchical clustering focuses on either a top-down approach (divisive clustering) or a bottom-down approach (agglomerative clustering) to produce a tree-like structure (dendrogram) that shows the relationships between clusters at different levels of granularity (Serra-Burriel & Ames, 2021). Alternatively, partitioning clustering divides the dataset into non-overlapping clusters based on a predefined number of partitions (K) (Lee, 1981).

Wolfe et al. (2019) used an agglomerative hierarchical clustering approach to establish watershed classifications, delineating sub-watershed boundaries based on varying hydrological attributes. The hierarchical clustering method provided flexibility, allowing the exploration of clusters at different levels of granularity through hierarchical links between each sub-watershed (Wolfe et al., 2019). However, the formation of hierarchical links imposed constraints on modifying cluster numbers or reassigning data points without reconstructing the entire hierarchy (Lee, 1981). Additionally, interpretation challenges arise when determining the final number of clusters, as it can be subjective and reliant on domain knowledge (Hastie et al., 2001). Hierarchical clustering algorithms can also be computationally demanding, especially in facilitating the identification of prominent patterns across sub-regions within the Canadian Prairie region, as they need to consider all pairwise distances between data points (Serra-Burriel & Ames, 2021). As a preprocessing step, a principal component analysis was applied to all the variables in the study to reduce dimensionality while preserving inherent variability (Serra-Burriel & Ames, 2021).

In contrast, Macrae et al. (2021) utilized a K-means clustering approach to delineate broad regions within the Lake Erie watershed based on shared conservation practice recommendations from similar P loss risks. In a K-means analysis, K is the value of the user-specified number of clusters and clusters are formed based on the distance (e.g., Euclidean distance) from the cluster mean (centre or centroid) (Dinov, 2018). If the actual number of clusters is unknown or ambiguous, it poses a challenge for the experts to perform the analysis (Dinov, 2018). To circumvent this limitation of partitioning clustering, the researchers utilized a variant of K-means clustering, called Cascade K-means, that iteratively applies the K-means algorithm at different levels of granularity (Macrae et al., 2021). Instead of producing a dendrogram, the Cascade K-mean results in a flat set of clusters at each level of detail, where each cluster may contain subclusters from lower levels. Similarly, Knoben et al. (2018) produced a quantitative hydrological climate classification with fuzzy C-means, another variant of K-means clustering. Unlike the K-means approach, fuzzy C-means create clusters with fuzzy boundaries, allowing data points to belong to more than one cluster (Bezdek et al., 1984). This

nonprescriptive approach accounts for the limitations imposed by the algorithm and introduces some flexibility in cluster formation (Bezdek et al., 1984).

In considering future directions, innovative clustering techniques, such as agglomerative hierarchical clustering of principal components and Cascade K-means, offer promising avenues for exploratory studies in watershed analysis (Hastie et al., 2001; McDonnell & Woods, 2004). Exploratory studies, conducted without predefined hypotheses, aim to uncover hidden patterns and relationships within complex geographic spatial data (McDonnell & Woods, 2004). On the one hand, hierarchical clustering produces visual dendrograms, highlighting natural groupings and hierarchical links within watershed datasets (Serra-Burriel & Ames, 2021). However, Cascade K-mean clustering enhances interpretability by efficiently handling large-scale datasets and, through iterative refinement, enables exploration of watershed data at various levels of detail (Serra-Burriel & Ames, 2021). Depending on the objectives of watershed studies, either methodological approach can be utilized to elucidate nuanced watershed characteristics and inform adaptive management strategies.

Chapter 3
Materials and Methods

3.1 Site Description

The scope of the current study is the province of Ontario and encompasses all the individual catchments of the Laurentian Great Lakes – St. Lawrence basin, except for the Lake Superior sub-watershed (Figure 3.1). A second, smaller study area was developed within the original study area to emphasize regions with active agricultural activity (Figure 3.1B). Due to the climate conditions in Northern Ontario, the Lake Superior sub-basin is not susceptible to P loss induced by farming activity. Therefore, this sub-basin was excluded as it does not adequately meet the objectives of the current study. The remaining Great Lakes, Lake Huron, Erie, and Ontario all have sub-basin boundaries that overlap with the study area (Figure 3.1). Furthermore, the Upper St. Lawrence River sub-basin was also included in the scope of the current study as it depicts the outflow dynamics of the Great Lakes draining into the Atlantic Ocean (Figure 3.1).

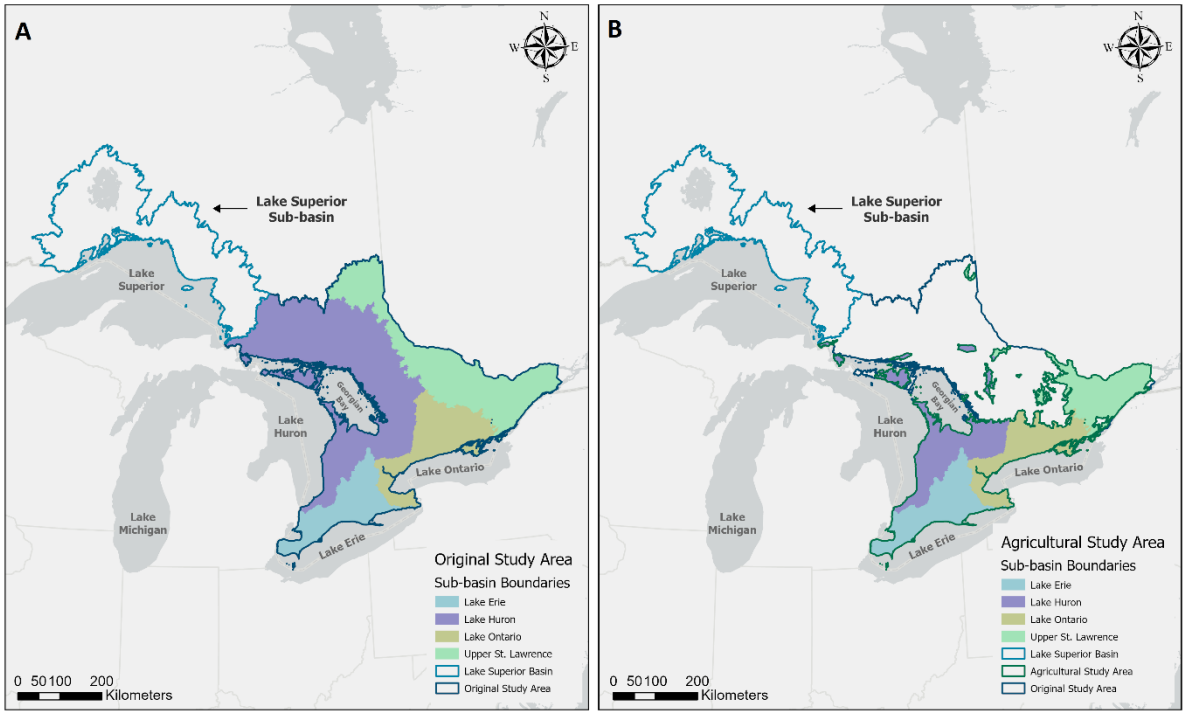

Figure 3.1. Map illustrating the Great Lakes – St. Lawrence basin extent in the province of Ontario, excluding the Lake Superior sub-basin: (A) original study area, the full extent of the sub-basins, and

(B) agricultural study area, the agricultural extent of the sub-basins (Data sources: Ontario Ministry of Natural Resources and Forestry & ESRI)

3.2 Data Inputs

The selected data inputs related to P loss dynamics for the current study include physiographic variables that account for region-specific features split into cause and effect. Of the P loss causes, two main categories represent the relationship between the physiographic parameters and their corresponding drivers: (1) climate drivers and (2) land drivers (Figure 3.2). A list of variables for each of these groups was selected based on established knowledge included in the literature review section of this paper. The climate driver category contains a major input group related to climate change impacts under various emission scenarios. Some of these parameters are similar to climate drivers and differ in terms of the time range. P loss effects are captured through data inputs that highlight macronutrient factors associated with water quality from various land use and land cover (LULC) types throughout the region. All the data inputs were restricted or modified to align with the scope of this study. For instance, detailed data were consolidated into broader categories or omitted entirely if they were not pertinent to a large geographical study area (see section 3.3 for further details). In addition, specific data inputs included in the clustering analysis (section 3.3.1) were highlighted in Figure 3.2. All data inputs are shown in the North American Datum 1983 (NAD83) / Ontario MNR Lambert projection, and the World Light Gray Base layer provided by Esri was used as the basemap.

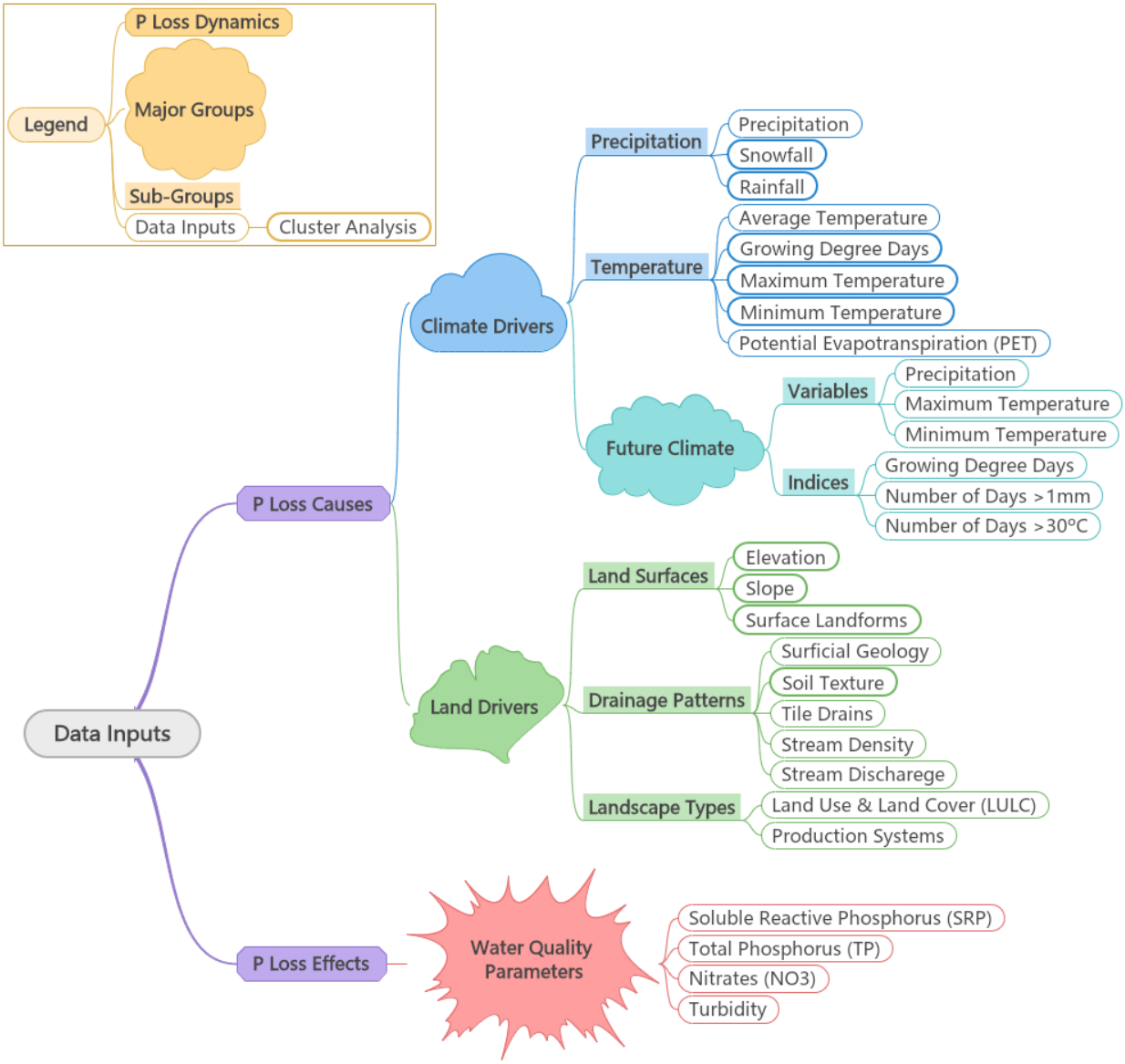

Figure 3.2. Conceptual diagram of the linkages between and groupings of different physiographic variables, including climate drivers, land drivers, nutrient factors, and future climate impacts.

3.2.1 Climate Drivers

Data inputs associated with climate drivers focus on the facets of P loss influenced by the two main aspects of climate conditions: precipitation and temperature (Figure 3.2). Principal precipitation parameters include total annual precipitation, rainfall, and snowfall (Figure 3.4). The Climate Normals dataset specifies total yearly precipitation as the sum of total annual rainfall and total annual

snowfall (LaZerte & Albers, 2018). The second group of climate driver indicators relates to temperature and consists of annual average temperature, annual maximum and minimum temperature, the number of growing degrees per day, and potential evapotranspiration (PET) (Figure 3.5). These values were computed using base temperatures for GDD, representing the minimum temperature required for plant growth in different species (AAFC, 2015). To exclude the minimum temperature required for bean growth, a base temperature of 10 degrees Celsius was selected (Macrae et al., 2021). In addition, the PET for each climate station was calculated using the Thornthwaite equation through the R package, SPEI (Beguería & Vicente-Serrano, 2023). The Thornthwaite equation uses air temperature and the latitude of each station to estimate PET. As highlighted in Figure 3.2, the total precipitation and average temperature datasets were omitted from the cluster analysis (see section 3.3 for additional discussion).

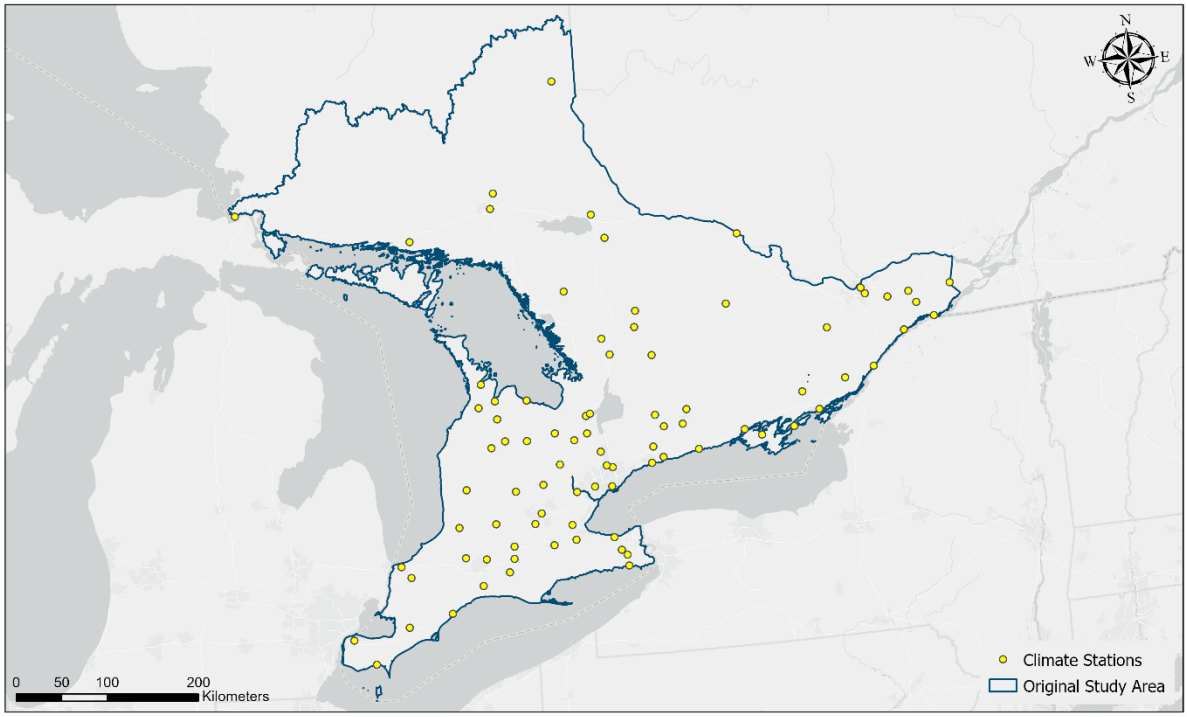

Figure 3.3. Map showing climate stations used to derive contemporary climate driver indicators from 1981 to 2010 within the current study area using Climate Normals (Data source: WeatherCAN).

The climate data inputs contained Canadian Climate Normals ranging from 1981 to 2010 and were extracted from an R package, WeatherCAN, initially compiled by the Ministry of Environment and Climate Change Canada (ECCC) (LaZerte & Albers, 2018). Climate Normals encapsulate a 30-year

window to eliminate short-term weather variability and provide representative averages and patterns by highlighting long-term climatic trends within a specific region. Both precipitation and temperature parameters were derived from various weather stations across the original study area, and regions with higher station concentrations overlapped with higher urban densities (Figure 3.3). The average climate parameters underscore the potential influences on P loss in general. However, components of the totals (i.e., minimum and maximum temperatures, rainfall and snowfall) were included to capture seasonal variation within the study (Figures 3.4 and 3.5).

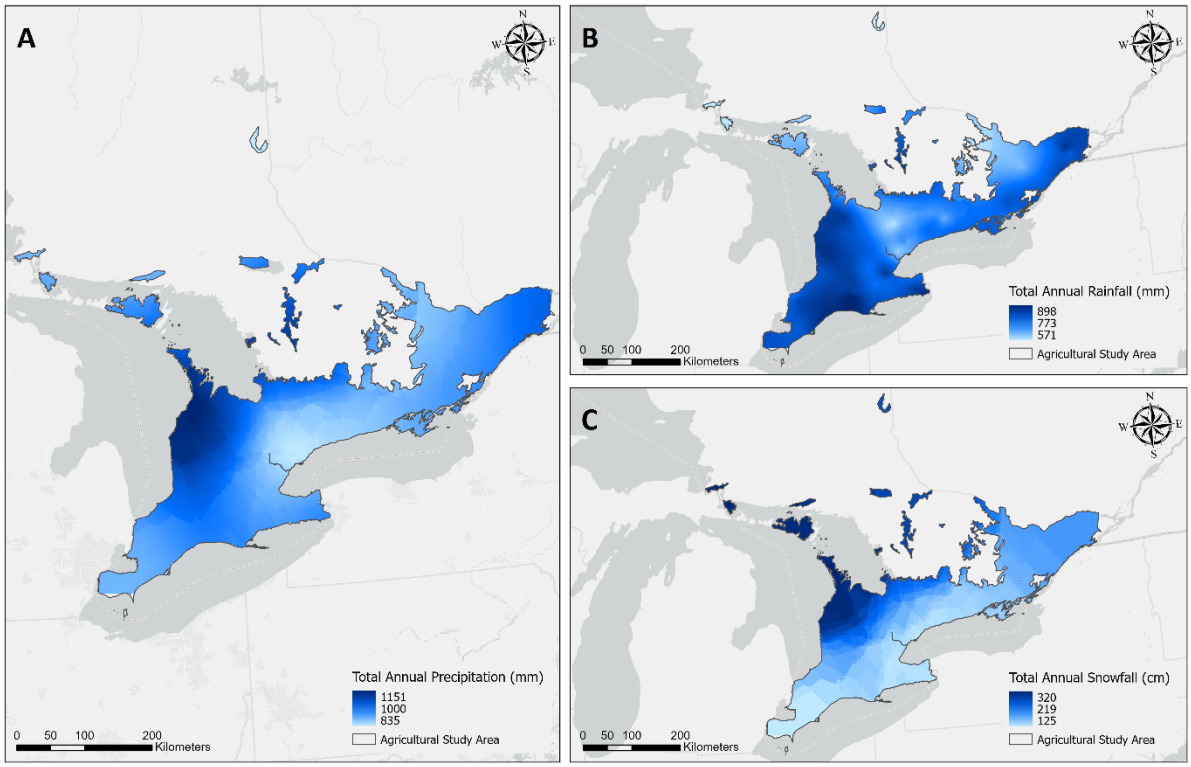

Figure 3.4. Map of contemporary climate conditions from 1981 to 2010 showing three precipitation-related climate driver indicators: (A) total annual precipitation, (B) total annual rainfall, and (C) total annual snowfall (Data source: WeatherCAN).

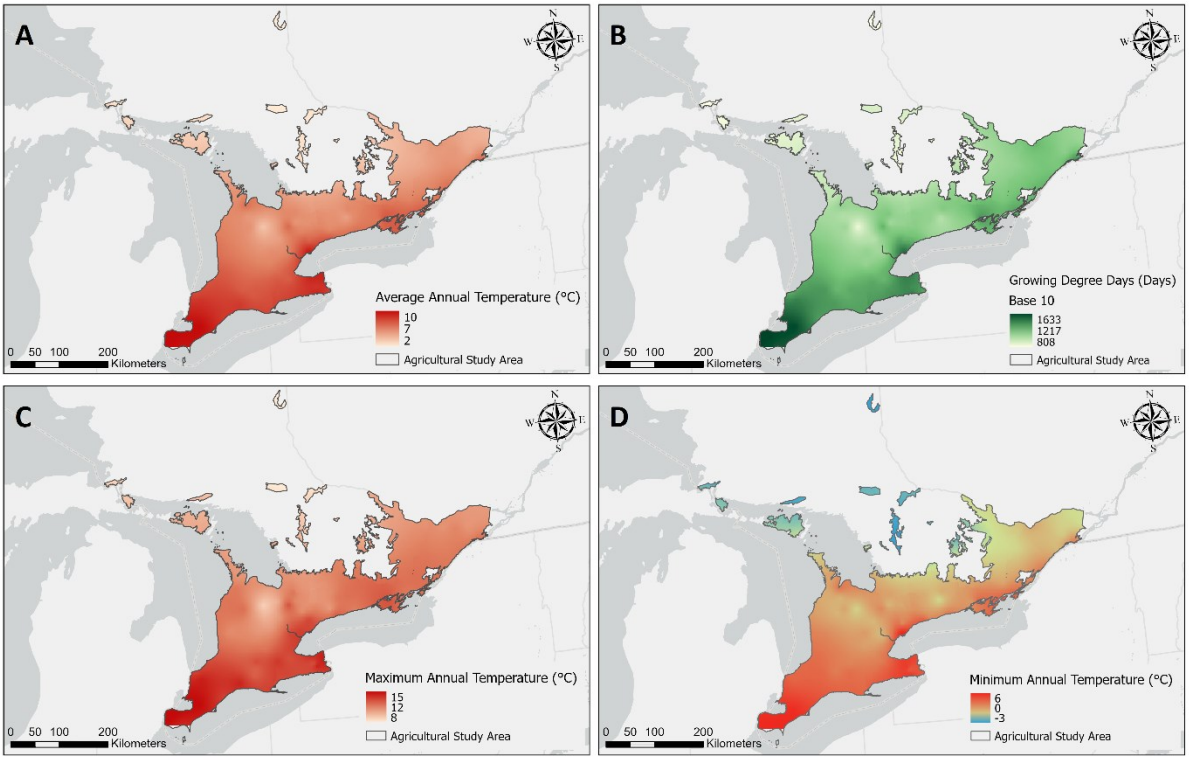

Figure 3.5. Map of contemporary climate conditions from 1981 to 2010 showing four temperature-related climate driver indicators: (A) total average annual mean temperature, (B) growing degree days, (C) total average annual maximum temperature, and (D) total average annual minimum temperature (Data source: WeatherCAN).

Figure 3.2 lists future climate conditions as a data input under climate drivers. While contemporary precipitation and temperature rates adequately capture the dynamic relationship between climate variables and P loss, future forecasts suggest that these dynamics are expected to change as global temperatures rise (IPCC, 2023). Future climate data, an ensemble of multi-model datasets from Coupled Model Intercomparison Project Phase 5 (CMIP5), were obtained directly from ECCC (2023). The dataset has been statistically downscaled to facilitate regional analysis from 1-degree (~116 km) grid resolution to 0.086 degrees (10 km). In addition, ECCC provides the user with two time periods, historical simulations spanning from 1951 to 2005 and future predictions from 2006 to the end of the century (2100) under three distinct emission scenarios (RCP 2.6, RCP 4.5, and RCP 8.5). Representative concentration pathway or RCP is used by climate scientists to predict future climate scenarios based on greenhouse gas concentrations in the atmosphere labelled by a radio

forcing value (i.e., 2.6 = 2.6 W/m^2) (ECCC, 2023). The IPCC uses these three emission scenarios to measure how greenhouse emissions are expected to impact climatic conditions (ECCC, 2023). For instance, RCP 2.6 is considered a low-emission scenario where global temperatures are predicted to remain below 2℃. In contrast, RCP 8.5, a high emission scenario, is considered a worse-case situation where temperatures are expected to soar past 2℃ (ECCC, 2023). The historical time range can be used to gain a more comprehensive understanding of how contemporary levels compare with future conditions and the potential influence these changes may have on P loss.

3.2.2 Land Drivers

The land data inputs were categorized into three main groups highlighting geophysical features that drive P loss: land surfaces, drainage patterns, and landscape types (Figure 3.3). The land surface variables describe the topographic features of the study area and include surface landforms, elevation, and slope (Figure 3.6). The data input for surface landforms was obtained from Soil Landscapes of Canada, published by Agriculture and Agri-Food Canada (AAFC) (Soil Landscapes of Canada Working Group, 2010). The local surface forms dataset categorizes mineral surface forms into eight distinct landform classes that characterize the physical surface terrain formed during the Late Pleistocene era (Soil Landscapes of Canada Working Group, 2010). Both elevation and slope data were derived from the Provincial Digital Elevation Model (PDEM), a three-dimensional model that extends across the entire province of Ontario at a 30-meter resolution (Figure 3.6) (Ministry of Natural Resources and Forestry [MNFR], 2019c). The Ministry of Natural Resources and Forestry (MNRF) developed PDEM using various data acquired from NASA's Shuttle Radar Topographic Mission (SRTM), Ontario Radar Digital Surface Model (ORDSM) and other LiDAR measurements, among others (MNFR, 2019c). The slope variable was calculated from the PDEM using the slope function in ESRI's ArcGIS software, which measures the percentage of change in each raster cell.

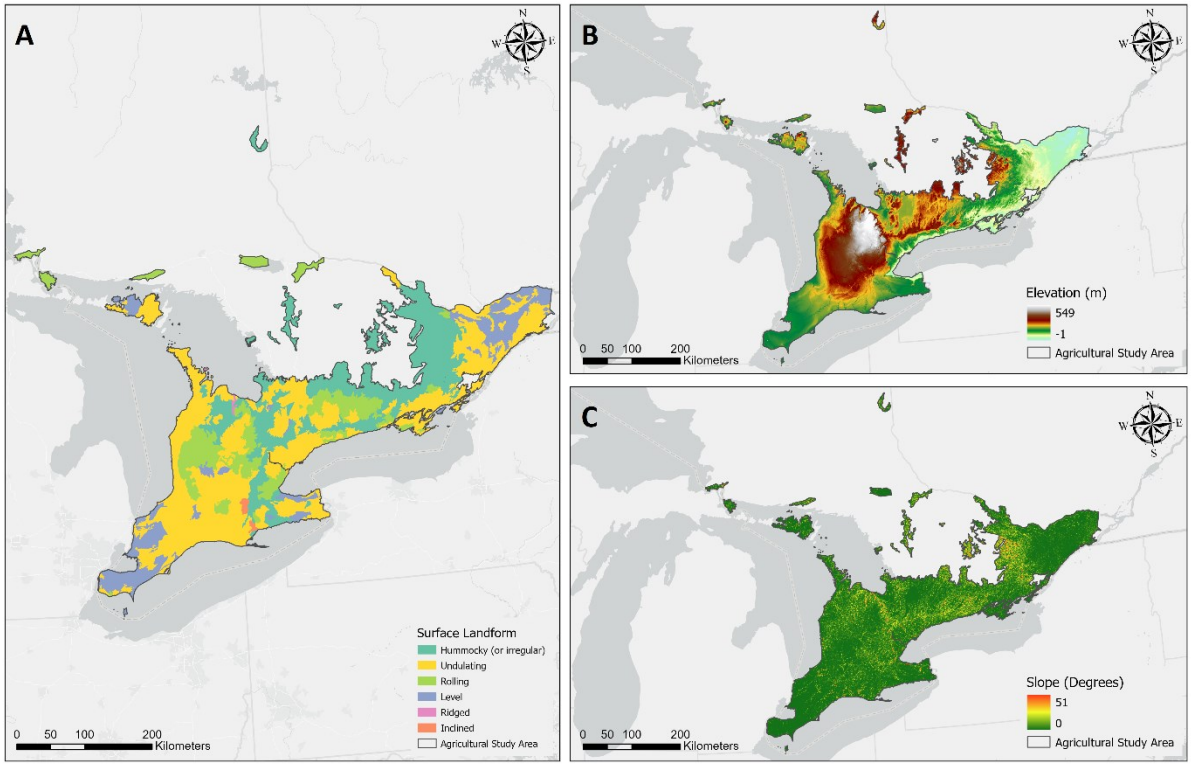

Figure 3.6. Map of geophysical drivers related to land surfaces, including: (A) surface landforms, (B) elevation, and (C) slope (Data sources: AAFC & MNRF).

The second group of data inputs are geophysical factors related to regional drainage patterns and play a key role in determining P loss transport pathways (Figure 3.3). These land drivers include geomorphological variables, surficial geology and parent soil texture material, and hydrological features such as stream density, tile drainage densities, and stream discharge (Figure 3.7). The surficial geology dataset was compiled from the Geological Survey of Canada's (2015) surficial geology map collection disseminated by Natural Resources Canada (NRC). Figure 3.7 depicts the primary material of the unconsolidated deposits within the soil profile, ranging from surface to bedrock, derived from the surficial geology data input (Geological Survey of Canada, 2015). The parent soil texture material dataset was obtained from Soil Landscapes of Canada, the same source as the surface landform (Soil Landscapes of Canada Working Group, 2010). The soil texture dataset in Figure 3.7 classifies the parent material into 18 distinct texture classes and is compatible with the USDA Texture Classes (Soil Landscapes of Canada Working Group, 2010). The soil texture indicator

defines the soil particle size classes based on the A Horizon in the soil profile (Soil Landscapes of Canada Working Group, 2010).

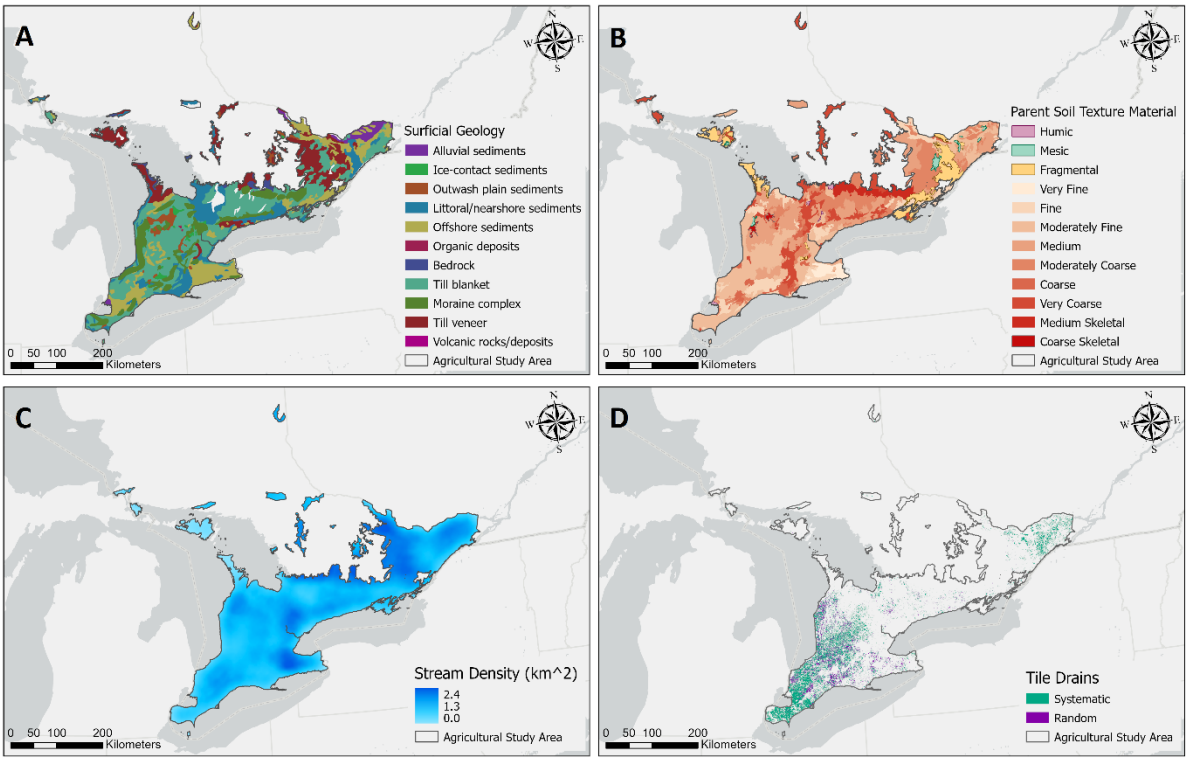

Figure 3.7. Map of geophysical drivers related to drainage patterns, including: (A) surficial geology, (B) parent soil texture material, (C) stream density, and (D) tile drains (Data sources: AAFC, MNFR & OMAFRA).

The datasets linked to hydrological processes and responses in the region were extracted from Land Information Ontario (LIO; https://geohub.lio.gov.on.ca/), a geospatial hub for public and private sectors to access Ontario-specific geographic data (Figure 3.7). More specifically, the data required to calculate stream density was extracted from the Ontario Integrated Hydrology (OIH) dataset since these parameters are linked to hydrological responses (MNFR, 2019b). The OIH package developed by MNRF contains a collection of mapped hydrological features that can be used for watershed delineation and generating other water cycle-related parameters (MNFR, 2019b). The tile drain parameter was collected from the Ontario Ministry of Agriculture, Food, and Rural Affairs (OMAFRA). The dataset illustrates the locations of agricultural field tile drains, the type of installation, and the system that receives the tile drain runoff (MNRF, 2019a). For stream discharge,

the data was obtained from the HYDAT database established by the Water Survey of Canada (WSC), a Canada-wide organization responsible for standardizing water resource data across Canada (WSC, 2021). The HYDAT database includes monthly streamflow data for stations across the study area, as shown in Figure 3.8.

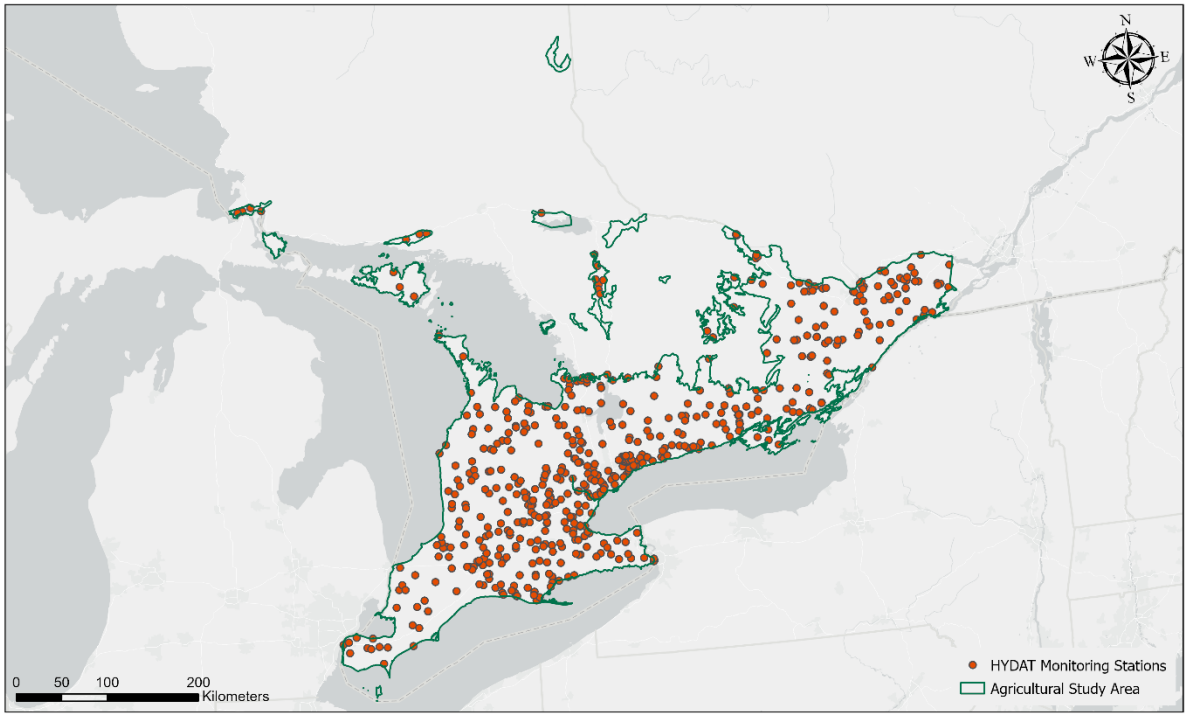

Figure 3.8. Map showing HYDAT monitoring stations collected from 2000 to 2020 within the agricultural study area (Data source: WSC).

The third and final category of parameters consisted of land management factors, including LULC and agricultural farming systems (Figure 3.9). The Annual Crop Inventory (ACI) dataset provided by AAFC was used for the farming systems, which classifies the agricultural landscape into more than 50 categories based on crop type and/or farming system (AAFC, 2018b). To represent agricultural production systems, the crop type classes in the ACI dataset were clustered into broader categories based on analogous P loss effects (Macrae et al., 2021). Lastly, the LULC data input was acquired from the AAFC Land Use Time Series dataset, also provided by AAFC (AAFC, 2018a). The LULC data input represents the surface cover of the earth and includes classes such as settlement, forest, water, grassland, and cropland (AAFC, 2018a). The dataset classified land cover and land use types

into a 30m resolution raster grid based on a meta-analysis of three decades of exceptional spatial datasets from 1990 to 2021 (AAFC, 2018a).

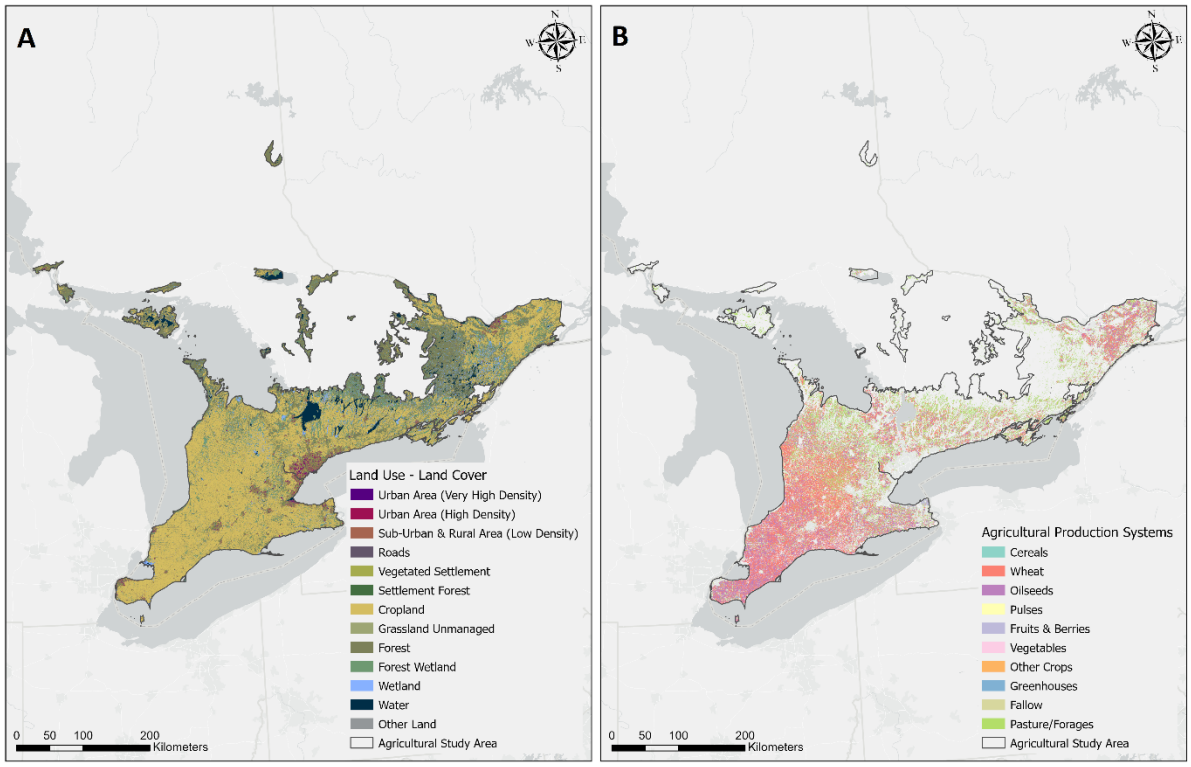

Figure 3.9. Map of geophysical drivers related to land management factors, including: (A) LULC and (B) agricultural production systems (Data source: AAFC).

3.2.3 Water Quality Parameters

The datasets pertaining to water quality parameters include two macronutrients and their respective form, which are associated with the impact of P loss across the region (Figure 3.3). The nutrient factors consist of total and dissolved nutrient parameters, including SRP, TP, and nitrates ($NO3^-$). In addition, turbidity was selected as the fourth parameter to indicate the presence of suspended sediments in the water column. The nutrient data for all four parameters were obtained from the Provincial (Stream) Water Quality Monitoring Network (PWQMN) dataset provided by the Ministry of Environment, Conservation, and Parks (MECP) (Kaltenecker, 2020). The PWQMN dataset consists of stream and river water quality from Ontario spanning two decades (2000 to 2020)

(Kaltenecker, 2020). Within the limits of the agricultural study area, there are over 200 sampling points, as shown in Figure 3.10.

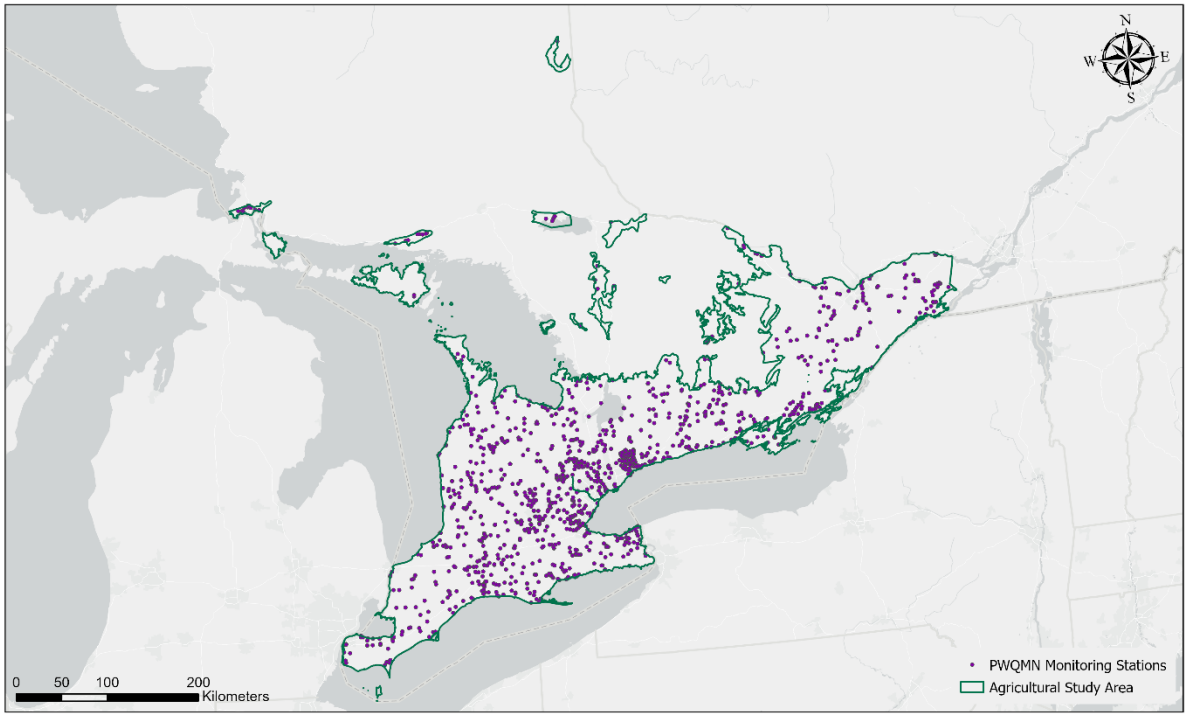

Figure 3.10. Map showing PWQMN monitoring stations collected from 2000 to 2020 within the agricultural study area (Data source: MECP).

3.3 Data Analyses

3.3.1 Clustering Analysis

Before beginning the cluster analysis, preprocessing steps were taken to ensure all the datasets were uniform in resolution and extent. The agricultural study area (Figure 3.1B) was established to ensure that all datasets were restricted to the agriculturally productive regions of the Great Lakes-St Lawrence Basin (Figure 3.1A). The soil texture dataset (Figure 3.7B) was used to clip all other datasets to this new extent in the latest version of ArcMap 10.8. Additionally, all datasets in vector format were converted to raster (Figure 3.12) and, if they were not already at a 30 m spatial resolution, were transformed to the exact grid resolution of 30 m x 30 m in the NAD83 / Ontario MNR Lambert projection. More specifically, for the climate datasets, as shown in Figure 3.11, the

weather station shapefile was interpolated using the Simple Kriging tool in ArcMap. The output pixel size was determined using the inspection density equation documented in Hengl (2006). The inspection density equation takes into account the total area (A) and the number of points (N). The resulting climate raster datasets were resampled from 2370 m spatial resolution to 30 m to match the pixel size of the elevation dataset (included in the climate cluster analysis).

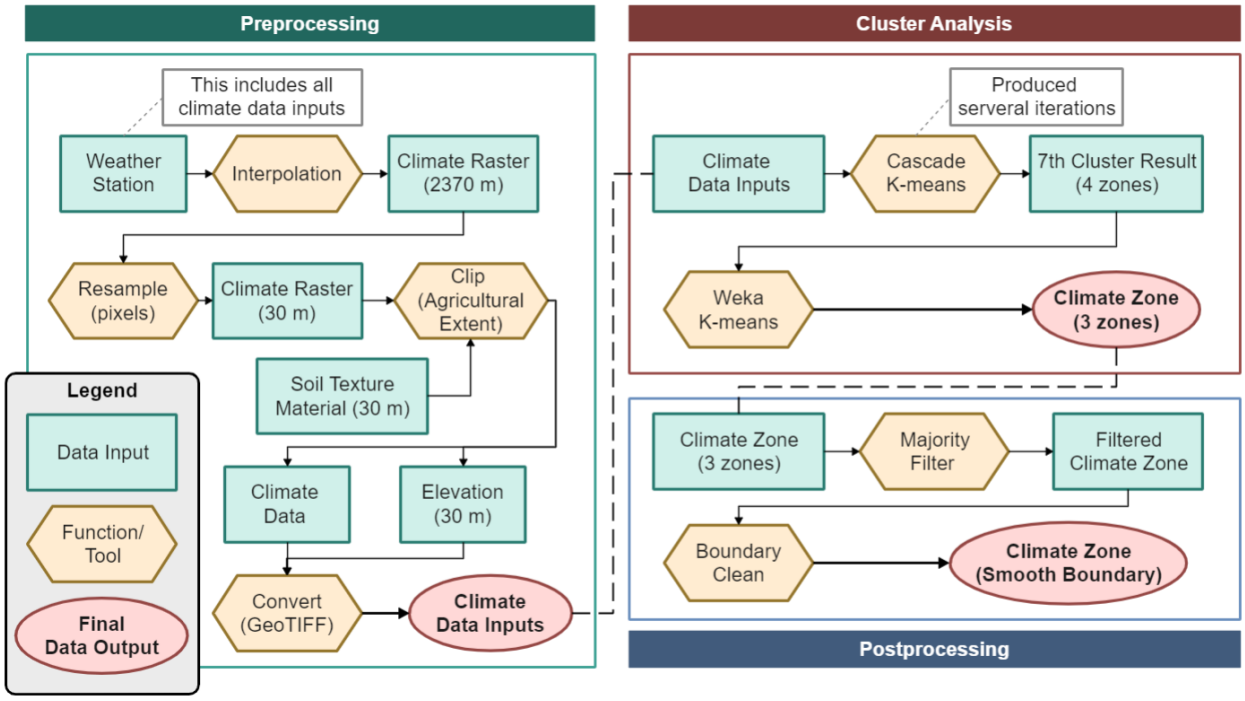

Figure 3.11. The flow diagram depicts the step-by-step data analysis process for generating climate zones, encompassing three methodological stages: preprocessing, cluster analysis, and postprocessing.

Following the preprocessing steps, the clustering analysis was performed using Google Earth Engine (GEE). The clustering analysis was executed separately on climate and land datasets, and the function was run iteratively with varying combinations of inputs to determine the level of influence each factor had on the overall outcome. The cascade K-means function, which selects the best K value (number of clusters) based on the inputs, was run several times for the climate cluster analysis (Figure 3.11). The selected version resulted in four distinct climate zones, and the final inputs included rainfall, snowfall, maximum temperature, minimum temperature, GDD, and elevation. In order to account for seasonal variability, this version was chosen as it eliminated the redundancy

associated with using averages (i.e., total precipitation and average temperatures) and opted to include the components of the whole (i.e., rainfall, snowfall, maximum temperature, and minimum temperature). Further inspection of the different clusters revealed that climate values for clusters 2 and 3, which spanned the middle portion of the study area, were more comparable across all data inputs. The analysis was rerun using the same data inputs, but the K value was limited to three using the Weka K-means function, and the resulting cluster zones merged the former cluster zones 2 and 3 into 1, now considered cluster zone 2 and cluster 4 is now cluster 3 (Figure 4.1).

Similarly, the land cluster analysis was also executed iteratively, albeit with fewer systematic steps. In contrast to the climate datasets, most of the geophysical data were non-continuous (vector format), which increased fragmentation in the results. To circumvent this, some data were excluded from the analysis and used to support the nutrient data analysis (see subsection 3.3.2), while others were used to provide context for the emerging geophysical zones (see chapters 4 and 5). The categories of the vector inputs in the soil texture datasets were reduced from 12 classes to 5 to further reduce fragmentation and noise (Figure 3.13). The final inputs consist of surface landforms, elevation, slope, and soil texture (broadened version) (Figure 3.12). Additionally, to minimize noise in the results, the Weka K-means function was used, and the K-value was restricted to three clusters because higher values resulted in more speckle noise in the raster.

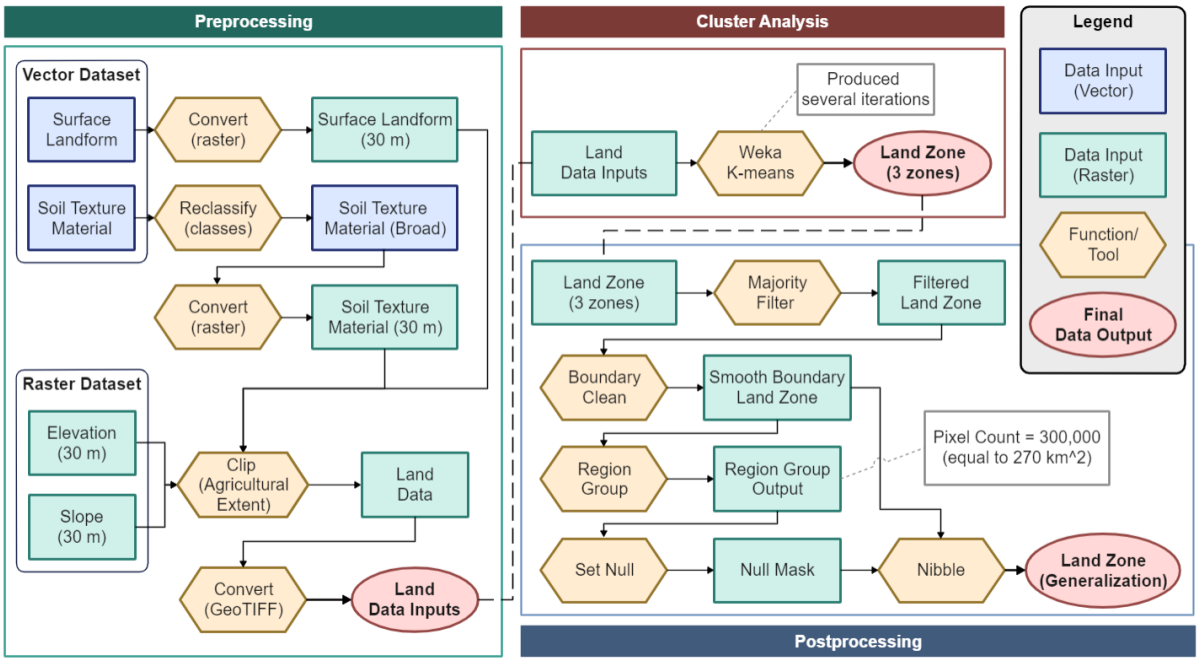

Figure 3.12. The flow diagram depicts the step-by-step data analysis process for generating land zones, encompassing three methodological stages: preprocessing, cluster analysis, and postprocessing.

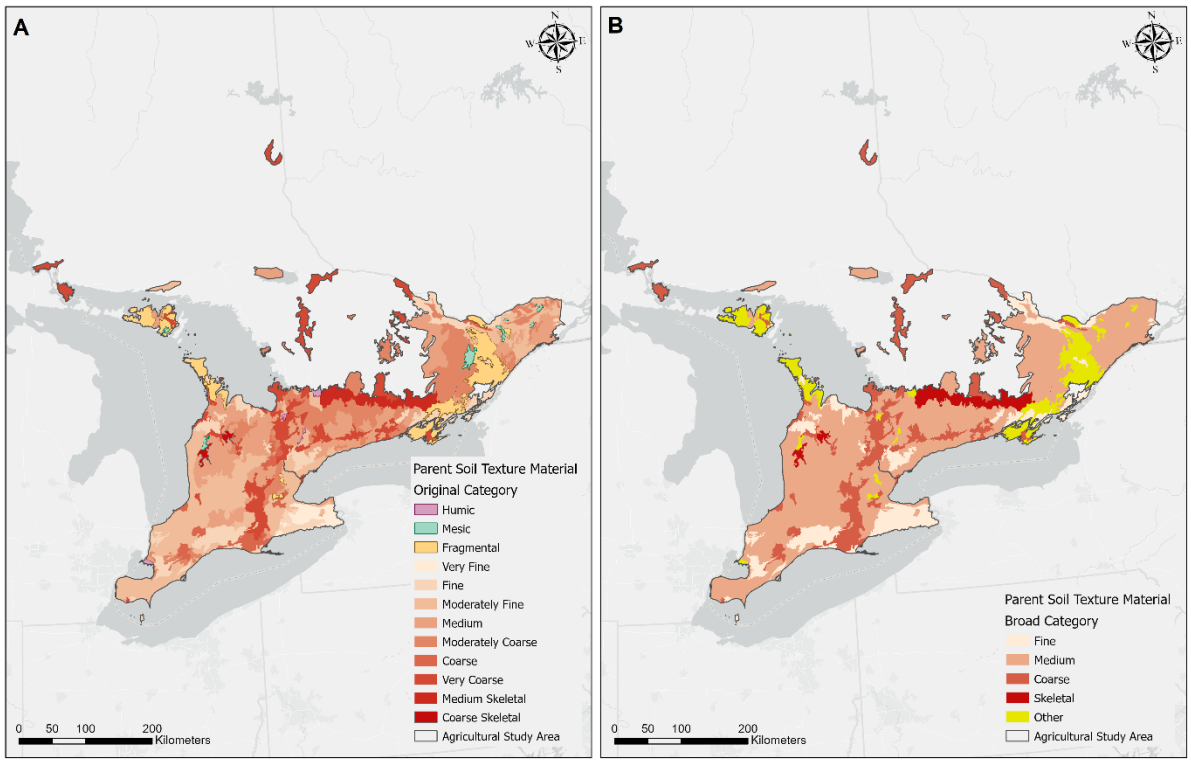

Figure 3.13. Map showing broad categories of parent soil texture material compared to the original classification.

To further reduce both speckle noise and fragmentation, the cluster outputs were post-processed using a combination of three steps in the ArcGIS Spatial Analyst tool from the Generalization toolset. The climate cluster results required fewer postprocessing steps than the land cluster results, as shown in Figures 3.10 and 3.11. The first step filtered the cluster output using the Majority Filter tool to remove outliers and noise in both raster datasets. The second step uses the Boundary Clean tool to remove jagged polygons from both cluster results. The final step was only applied to the land zone results, where the cluster zones were generalized using three tools, Region Group, Set Null and Nibble tools, to eliminate isolated areas less than 270 km2 from the output (Figure 3.11). The 270 km2 is smaller than the fourth level of the watershed subdivision used by the OIH package, as described in the previous section.

Finally, the climate and geophysical cluster analysis results were combined to create the merged zones. The intersect tool in ArcGIS was used to create the merged zones. This resulted in 12 distinct zones, with three geophysical zones for each of the four climate zones. The merged zone is the final product of the cluster analysis steps.

3.3.2 Water Quality Data Analysis

All the preprocessing steps for the water quality data analysis were completed in R (3.6.1). The PWQMN datasets included 20 merged CSV files, and all essential spatial information (i.e., latitude and longitude values) was attached to each PWQMN station. Additionally, further procedures were required to ensure that the data could be displayed in ArcGIS Pro software. The data was originally stored in a one-to-many relationship table to generate plots in R, meaning that one station had multiple parameter values. However, the data was converted to a one-to-one relationship to export the CSV files to ArcGIS Pro so that each unique station number occupied one row.

3.3.3 Future Climate Data Analysis

All the preprocessing steps for the future climate datasets were performed in ArcGIS Pro. The annual and seasonal data were converted from netCDF files to single raster datasets for each climate factor. NetCDF or Network Common Data Form files store multidimensional data, and many climate change datasets are typically available in this format. Each of the netCDF files included four variables: latitude, longitude, standard time (ranging from the year 1950 to 2100), and the climate variable (e.g., annual precipitation). For seasonal datasets, each standard time slice represented the average values across three months (e.g., Winter = December + January + February) for each year.

First, a subset slice was extracted from each netCDF file using the Subset Multidimensional Raster tool in ArcGIS Pro for each time range: (1) contemporary range: 1981 to 2005, (2) future range 1: 2040 to 2069, and (3) future range 2: 2070 to 2099. There is a discrepancy between the contemporary time range in the future climate dataset and the original climate normal data (1981 to 2010). Apart from the evident advantage of ensuring consistency in data analysis, the primary motivation factor in utilizing the same dataset was that the extreme climate indices (such as extreme precipitation and temperature days) were unavailable in the climate normal dataset. Moreover, for each climate factor, three emission scenarios were stored in separate netCDF files, and so they were extracted separately

as well. Second, the Aggregate Multidimensional Raster tool was then used to generate a single raster file for each climate variable and time range under each emission scenario.

3.4 Statistical Analyses

Similar preprocessing steps were taken before performing statistical analytical techniques on each of the results from the data analysis steps discussed in Section 3.3. First, the Tessellation tool was used to create a 100 km^2 hexagon grid and clipped to extend across the agricultural study area. Then, using the Feature to Point tool, a representative distribution of sampling points was generated from the centroid of each hexagon grid. These sampling points were used to identify dominant data inputs within each climate and land zone result. The Select by Location tool was used for each sampling point to assign a climate, land and merged zone value. Then, for each climate and land data input listed in Figure 3.2, the Zonal Statistic tool was used to generate mean values for continuous datasets and majority values for categorical datasets. The same steps were taken for future climate datasets.

In addition to assigning a specific zone code for climate and land and consolidated results to each water quality monitoring station, a new LULC class was developed. The water quality dataset in wide format was imported into ArcGIS, and the Select by Location tool was used to determine and designate climate zone, land zone, merged zone, and LULC values for each nutrient station. For the LULC, the original 13 classes were broadened to 4 categories, and the fifth category, pastures, was assigned using the classes from the agricultural production dataset, pasture/forages and fallows (Figure 3.9). A radius of 20 m was used in the Select by Location tool to avoid assigning small, isolated regions as the primary land type for each water quality station. Subsequently, the agricultural production system shapefile was used to assign the pasture class to the water quality dataset. Moreover, the farming system dataset was also used to assign LULC categories to ensure that the cropland values were accurately represented.

Chapter 4
Results

4.1 Clustering Analysis of Climate and Land Zones

Three climate zones were identified in the analysis. These climate zones, defined by the cluster analysis (Figure 4.1), largely reflect latitude, with climate zone 1 (C1) being the furthest north, climate zone 3 (C3) being the furthest south, and climate zone 2 (C2) extending across the middle part of the agricultural study area. Of the three zones, C1 has the lowest area percentage and mainly overlaps with Lake Huron's watershed, as well as Georgian Bay. Conversely, C2 encompasses the largest proportion of the research site (over 50%) and intersects with each of the principal sub-basins of the Great Lakes. C3 is 8.39% larger than C1 and extends over some portions of Lake Huron, Ontario, and all of Lake Erie watersheds. The extent of the agricultural study area falls within the humid continental temperate Köppen climate classification (Df). In contrast to the other two zones, C3 is within two Köppen climate classifications, the hot-summer (Dfa) and warm-summer (Dfb) sub-types. Most of the zone falls within Dfb like the other two zones but extends marginally into Dfa near Windsor, Ontario. In addition, the study area extends within two Canadian Ecozones. All three zones are within the Mixedwood Plains Ecozones, but the northeastern portions of C1 and C2 extend into the Boreal Plains zone.

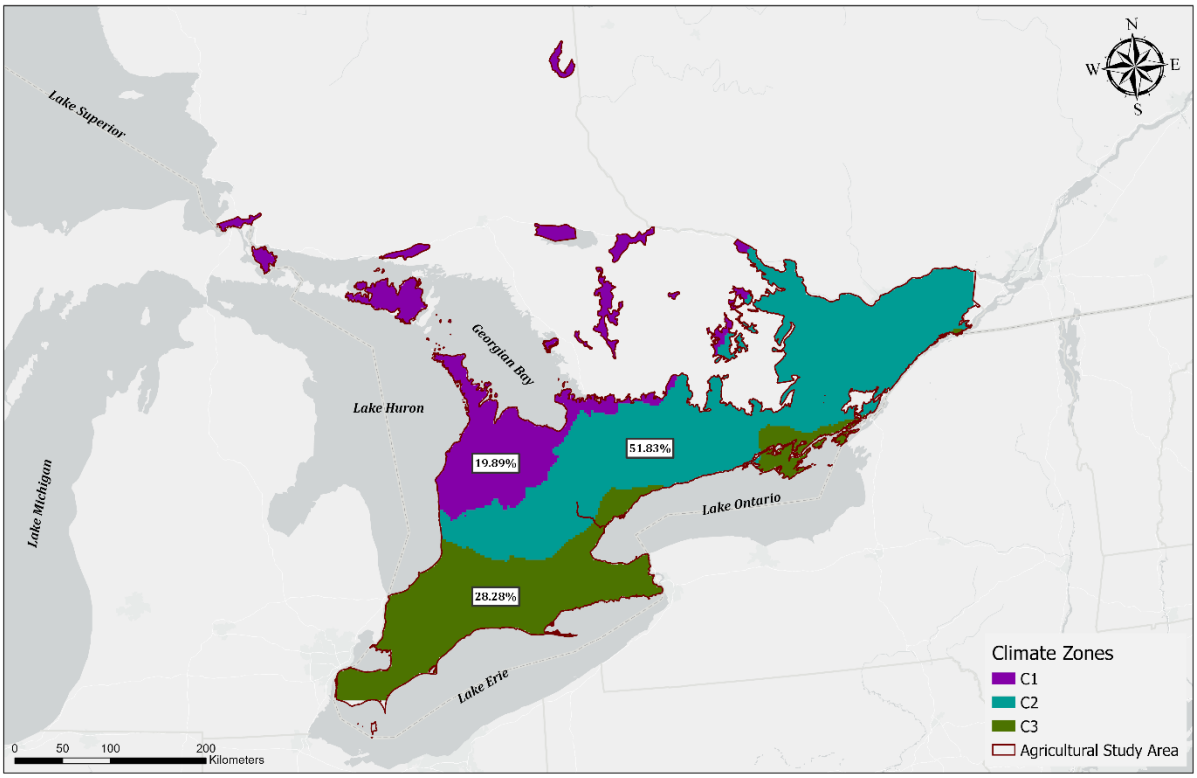

Figure 4.1. Map illustrating the cluster analysis results based on climate inputs produced in three climate zones across the agricultural extent within the study area. The percentage area coverage is overlaid for each zone.

While the climate zones primarily reflected latitudinal differences, precipitation and air temperature patterns were analyzed to determine the climate variables responsible for the cluster patterns. Compared to C2 and C3, total annual precipitation is greatest in C1, with C2 having the lowest average overall (Figure 4.2A). Although rainfall accounts for the majority of precipitation across all three zones, there are distinct differences in precipitation characteristics across the three climate zones. The greater precipitation totals received in C1 are a result of substantially greater snowfall amounts (~ 300 mm, Figure 4.2A) relative to the other two zones (~150 mm, Figure 4.2A). Although C2 and C3 receive similar amounts of snowfall (~750 mm, Figure 4.2B), C3 receives more rainfall (~800 mm, Figure 4.2B) than either C2 or C1. Overall, rainfall proportions increase from C1 to C3 (with the most rainfall at the southern location, closest to the southern Great Lakes), while snowfall contributions are greatest in the northernmost class (C1), which is adjacent to Lake Huron and Georgian Bay, and decrease from C1 to C3.

As shown in Figure 4.2B, all three temperature dataset results increase in the same direction as rainfall, where C1 is the coolest and C3 is the warmest. C1 has the lowest annual average growing degree units (GDU), which is equivalent to the lowest maximum and minimum temperatures. Furthermore, C2 is approximately 2 degrees warmer and 150 GDU higher than C1. Finally, in every dataset, the distance between C3 and C2 is greater than between C2 and C1. As a result, the maximum and minimum temperatures of C3 are substantially higher than those of C1, and the GDU average exhibits a comparable pattern.

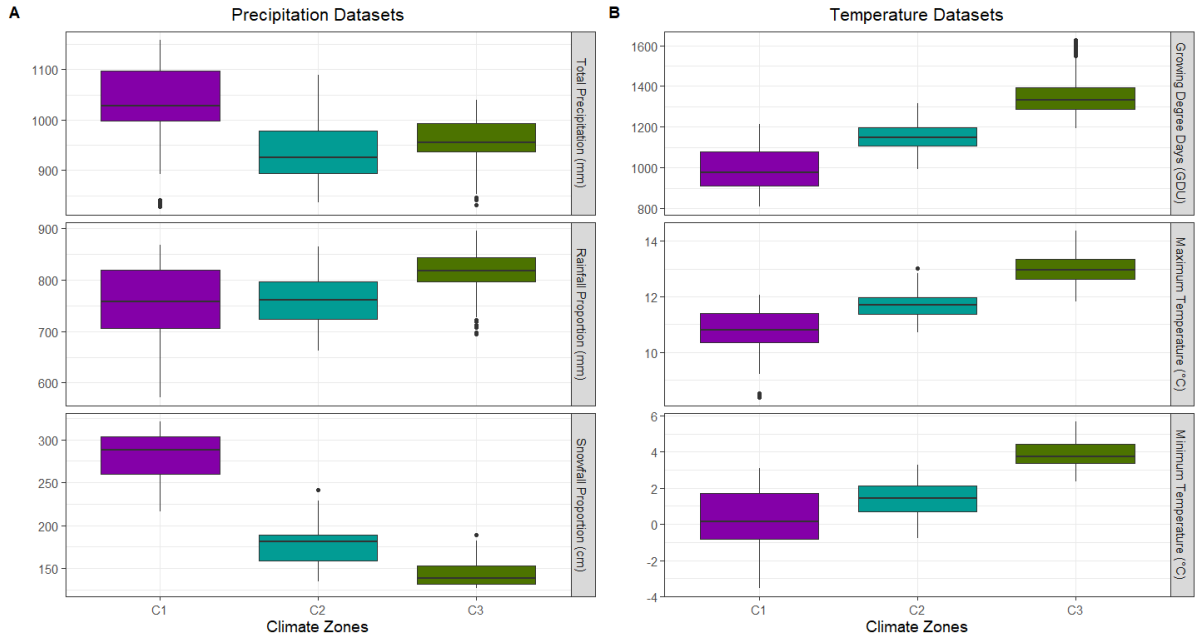

Figure 4.2. Boxplot comparisons between annual averages of 30-year climate normal variables for the three climate zones from 1981-2010: (A) precipitation plot, which includes total precipitation (mm), total rainfall (mm), and total snowfall (cm), and (B) temperature plot, which includes growing degree days (GDU), maximum temperature (°C), and minimum temperature (°C).

Figure 4.3A illustrates that all climate zones maintain a moisture surplus (precipitation – potential evapotranspiration) for the majority of the year except in the summer months of June, July, and August, when there is a moisture deficit. The moisture deficit is especially apparent at C3, the most southern climate class and least apparent at C1 (the northernmost group). Streamflow patterns reflect the moisture surplus and deficit patterns, with the smallest streamflow amounts in the summer months. It is noteworthy that the northernmost region experiences a moisture surplus throughout the

winter months but experiences streamflow peaks in April when stream discharge is significantly higher than at any other time of year across all climate zones. In contrast, C2 and C3 have less seasonality in their atmospheric moisture budgets (Figure 4.3A). Similar to C1, C2 experiences higher peak flow in spring (April), whereas C3 experiences greater flow throughout the winter months and does not exhibit the same peak flow in springtime.

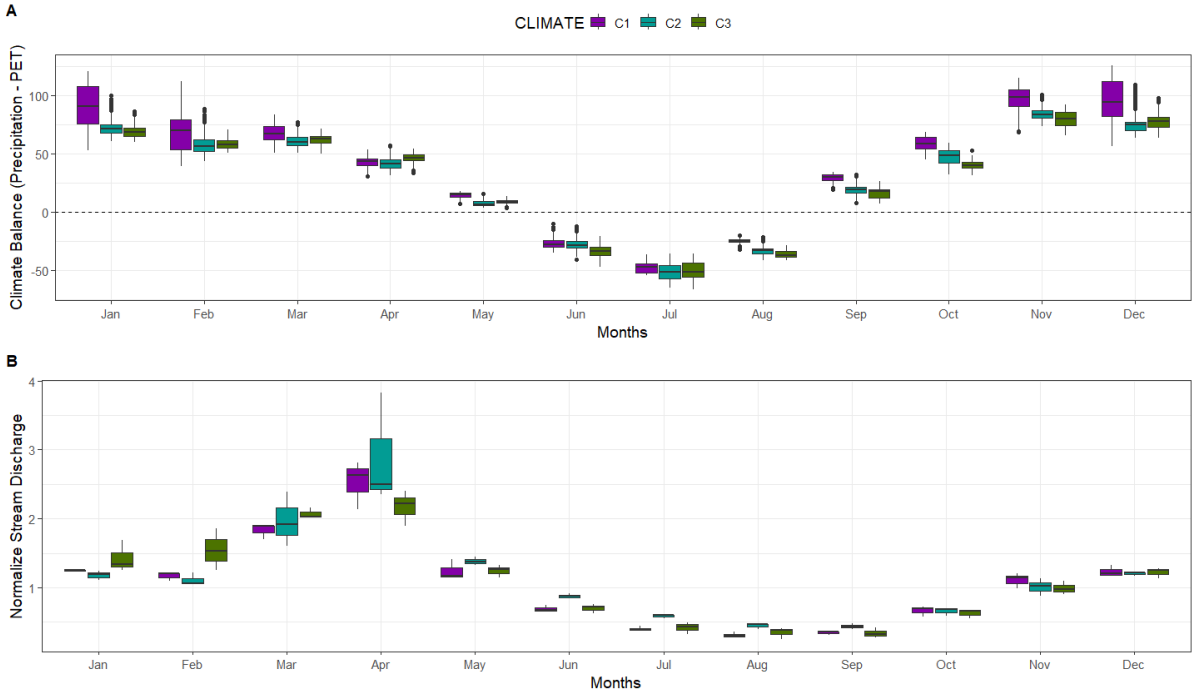

Figure 4.3. Boxplot comparisons between monthly averages of 20-year ranges for the three climate zones: (A) climate balance plot, based on climate normal data from Figure 4.2, and (B) normalized stream discharge plot, based on monthly average flow relative to the median from HYDAT datasets ranging from 2000 to 2022.

In contrast to the cluster analysis results for climate variables, the clustering of land zones (n = three) exhibits a greater degree of fragmentation, with several isolated regions within each zone across the study area (Figure 4.4). Furthermore, the areas of the three land zones are more similar in size compared to climate zones. Land zone A (LA), the most expansive of the three zones (encompassing over 40 percent of the total area), extends latitudinally to the two farthest points within the agricultural study area. The LA area shares boundaries with most of Lake Erie, a portion of the St. Lawrence River, and the coastline of the Lake Huron watershed. On the other hand, land zone

B (LB) has the smallest percentage area. The central portion of the LB zone extends from the Haliburton Highlands to the Ottawa Valley. Other isolated regions that fall within the LB class include the Norfolk sand plain (Western edge of Lake Ontario) and the Bruce Peninsula (between Lake Huron and Georgian Bay). There are also small pockets in areas surrounding the Sault Ste. Marie Island and Lake Nipissing in northern Ontario. Lastly, land zone C (LC) covers a substantial region in the middle of the Southwestern part of Ontario, extending across most of the Lake Huron watershed but outside of the areas immediately adjacent to the lake. In addition to encompassing areas north of LB's central region, the LC zone borders Haldimand County.

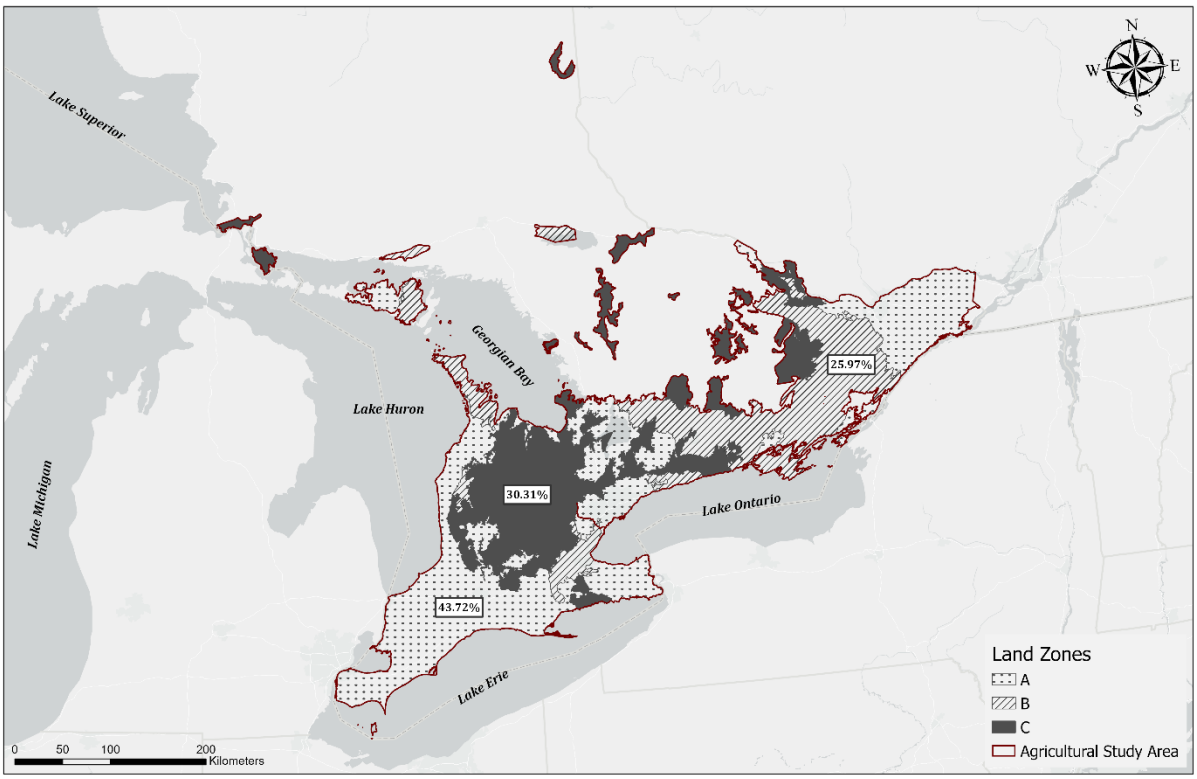

Figure 4.4. Map illustrating cluster analysis results based on geophysical inputs produced in three land zones across the agricultural extent within the study area. The percentage area coverage is overlaid for each zone.

Land surfaces in the three land zones are distinctly differentiated by means of surface landforms, slope, and elevation. Figure 4.5 illustrates that increases in surface variability coincide with increases in surface steepness and higher elevations. As depicted in Figure 4.5A, there is a concurrent increase in both elevation and slope from LA to LC. Specifically, the vertical distance separating LC from the

remaining zones surpasses that of the slope. Similarly, Figure 4.5B follows the pattern where surface variability increases from LA to LC as the dominant landform shifts from undulating and level surfaces to hummocky and rolling surfaces. These findings indicate that LA is flat and low-lying with non-variable surfaces, while LC is a steep upland with variable surfaces. Compared to LA, LB is a steeper transition zone at higher elevations, with a mix of non-variable and variable surfaces (i.e. intermediate between LA and LC).

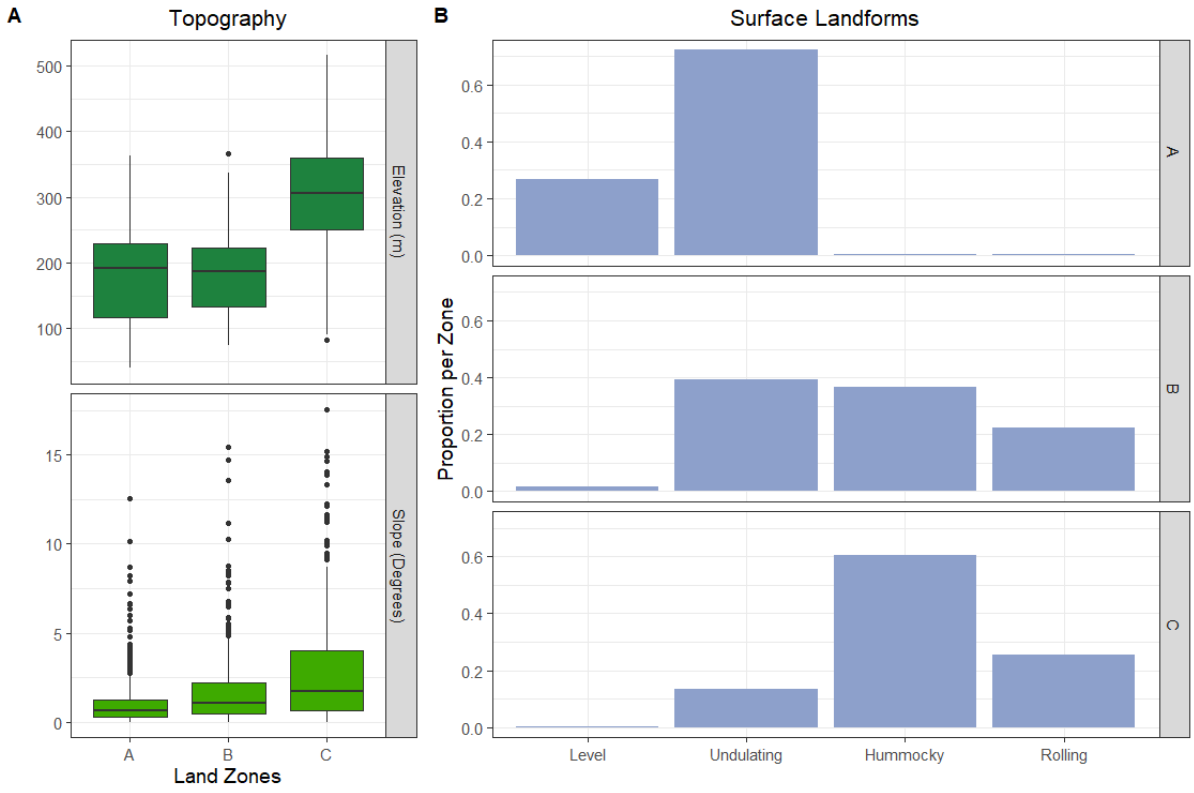

Figure 4.5. Comparison of land surfaces across three land zones: (A) topography plot, boxplot comparison of mean elevation (m) and mean slope (degrees), and (B) surface landform plot, bar chart including four landform classes.

A combination of findings linked to geological processes and hydrological variables aid in understanding dominant drainage patterns across land zones. For geological processes, Figure 4.6A shows the surficial geology related to the soil texture in each land zone depicted in Figure 4.6B. LA is dominated by fine soils, mainly sourced from similar portions of till and littoral sediments and some alluvial deposits. On the other hand, both LB and LC have high proportions of coarse-textured soils

derived from till material, some littoral deposits, and exposed bedrock. However, LB exhibits a higher percentage of rock fragments within the coarse soils, while LC primarily comprises soils with medium and fine textures. Stream density remains relatively constant within the land zones with minor variations (Figure 4.6C). LC has a slightly higher stream density than LB, while LA has the lowest density. Tile drainage densities throughout the study area are consistent with findings shown in Figures 4.5 and 4.6 A and B (Figure 4.5C). Higher tile drainage usage is found in LA because the land surface and geological processes suggest poor drainage patterns and a higher water table. In contrast, LB is characterized by well-drained soils and steep, sloping, variable surfaces, which are different from LA; this corresponds to the zone's lower tile drainage installations. Finally, LC has the highest slopes and elevations compared to LB but has a greater portion of medium and fine-textured soils, which indicates poorer drainage patterns and results in a higher tile drainage density than LB but a lower one than LA.

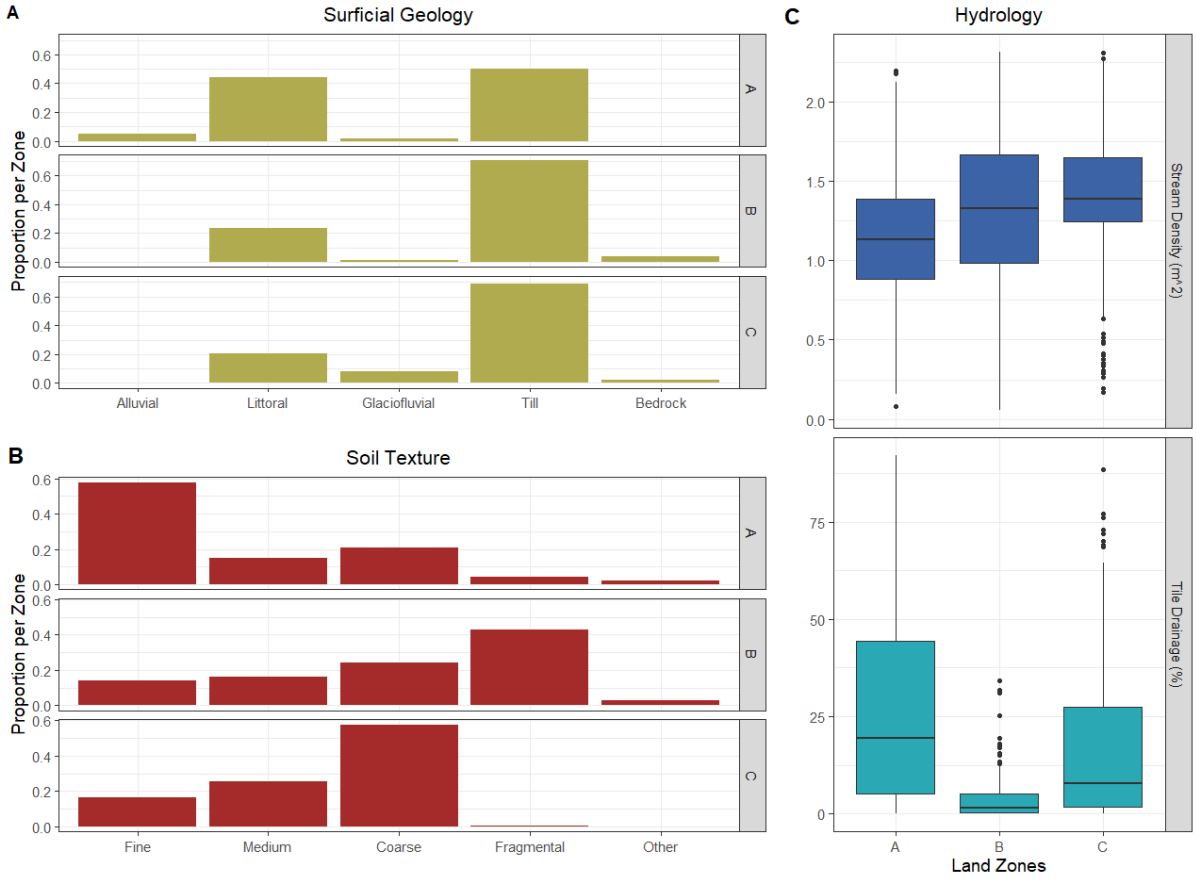

Figure 4.6. Comparison of drainage patterns across three land zones: (A) surficial geology plot, bar

chart including five broad geology classes, (B) soil texture plot, bar chart including five broad soil classes, and (C) hydrology plot, boxplot comparison of stream density (m2) and tile drainage density (%).

The dominant LULC types, shown in Table 4.1, highlight the broad categories across the land zones. However, the farming production systems, illustrated in Table 4.2, are a subset of two LULC types—pastures and croplands— precisely the broad farming system types practiced within croplands. Croplands predominate in LA, with grains and oilseeds constituting the principal production systems, respectively. This provides additional justification for this zone's high tile drainage installation (Figure 4.6C) to prevent field waterlogging risks. Conversely, LB has a higher proportion of natural areas and slightly more pastures than croplands. Once more, this aligns with the results presented in Figure 4.6C, which indicate that the average tile drainage usage is close to 0%. Grains and oilseeds equally dominate the farming systems in LB, but since there are more pastures than croplands in this zone, pastures are shown to occupy a greater area of the land. Lastly, LC has a mixture of croplands, pastures, and natural regions, with the latter comprising a greater extent than the rest. LC exhibits a comparable pattern to LA, wherein oilseeds and grains are the prevailing crop types. However, unlike LA, LC comprises a greater proportion of pastures, surpassing the area occupied by grain systems. These findings also match tile drain densities where LC has a higher density and more cropland than LB but smaller proportions than LA.

Table 4.1. Comparison of proportions of LULC types (%) across three land zones, including four broad LULC classes.

Land Zones	**Cropland** (%)	**Pasture** (%)	**Urban** (%)	**Natural** (%)
A	45.44	11.84	21.75	20.97
B	10.20	20.39	12.17	57.24
C	21.93	18.80	9.14	50.13

Table 4.2. Comparison of proportions of farming production system types (%) across three land zones. Four of the farming production systems are sub-classes of the cropland LULC type shown in Table 4.1, where the sub-classes add up to 100 percent of the croplands within Table 4.1. The pasture class is equivalent to the proportions of pastures shown in Table 4.1 but is demonstrated in comparison with other farming production system types in this Table.

Land Zones	**Cropland** (Sub-Types)			
	Grain (%)	**Oilseed** (%)	**Pulse** (%)	**Pasture** (%)
A	42.14	35.36	0.71	21.79
B	16.31	16.30	0.00	67.39
C	29.41	21.57	1.96	47.06

4.1.1 Analysis of Merged Zones

The combination of climate and land zones yields merged zones that illustrate the extent of overlap between the two across the agricultural study area, with a specific focus on the three land zones contained within each climate zone. Hence, Figure 4.7 depicts that land zones occupy varying percentages within the three climate zones. The combined coverage of LA and LB (9.48%) in C1 is nearly equivalent to that of LC (10.41%). In contrast, the percentage areas of all three land zones within C2 are comparable. Among the climate zones, C3 has the highest variation between the land zones, where LA (21.92%) is five times the size of LB (4.08%) and nine times the size of LC (2.28%).

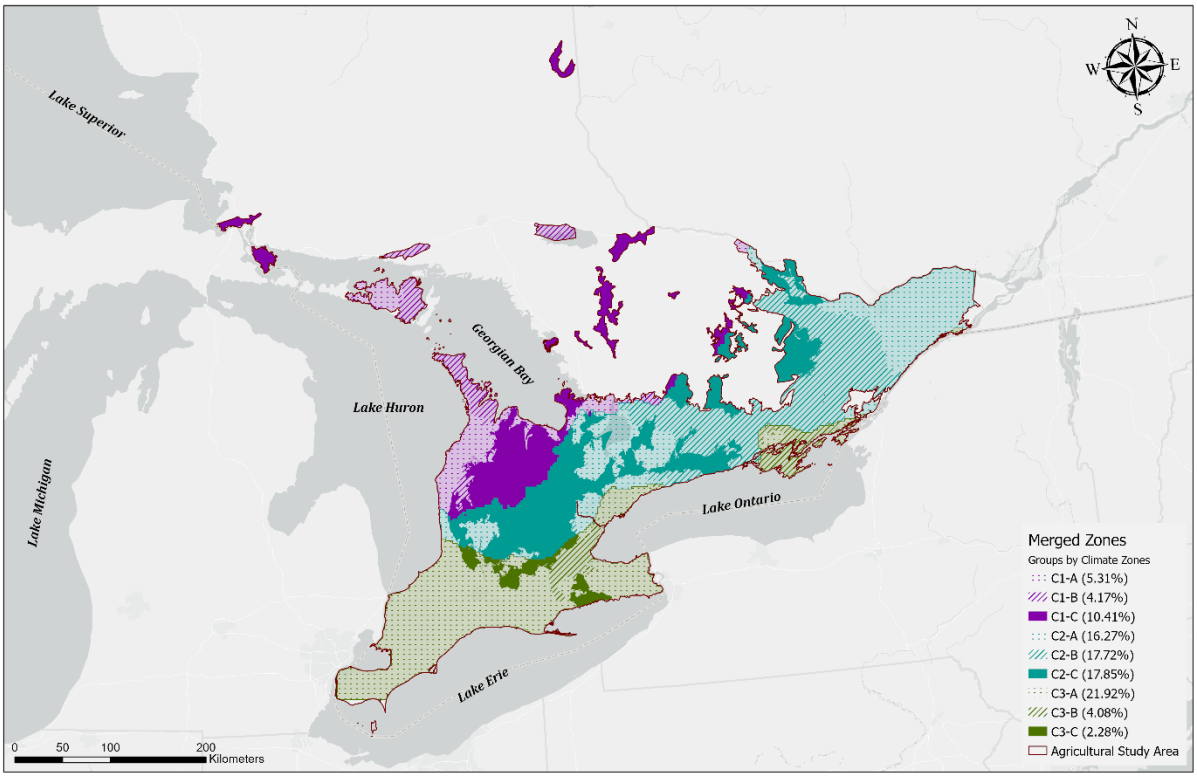

Figure 4.7. Map illustrating the intersection between the climate and land zones resulted in 9 distinct zones grouped by climate zones across the agricultural extent within the study area.

The findings in Figure 4.8 are identical to the stream discharge data presented in Figure 4.3B, except this plot separates the climate zones by land zones for each month. With minimal variations, the land zones in climate zones C2 and C3 adhere to an equivalent overall annual discharge pattern. For instance, while LA and LC consistently exceed LB most of the year, C3 peaks earlier than C2. Conversely, in C1, the land zones deviate from the pattern. In particular, C1-B deviates from the general seasonal pattern by reaching its maximum in July, as opposed to April, during the spring. Furthermore, LA and LB mainly drive the peaks observed in C1. Both land zones are consistently higher than LC most of the year. In addition, LB experiences a substantially greater discharge during the winter months than the other two zones.

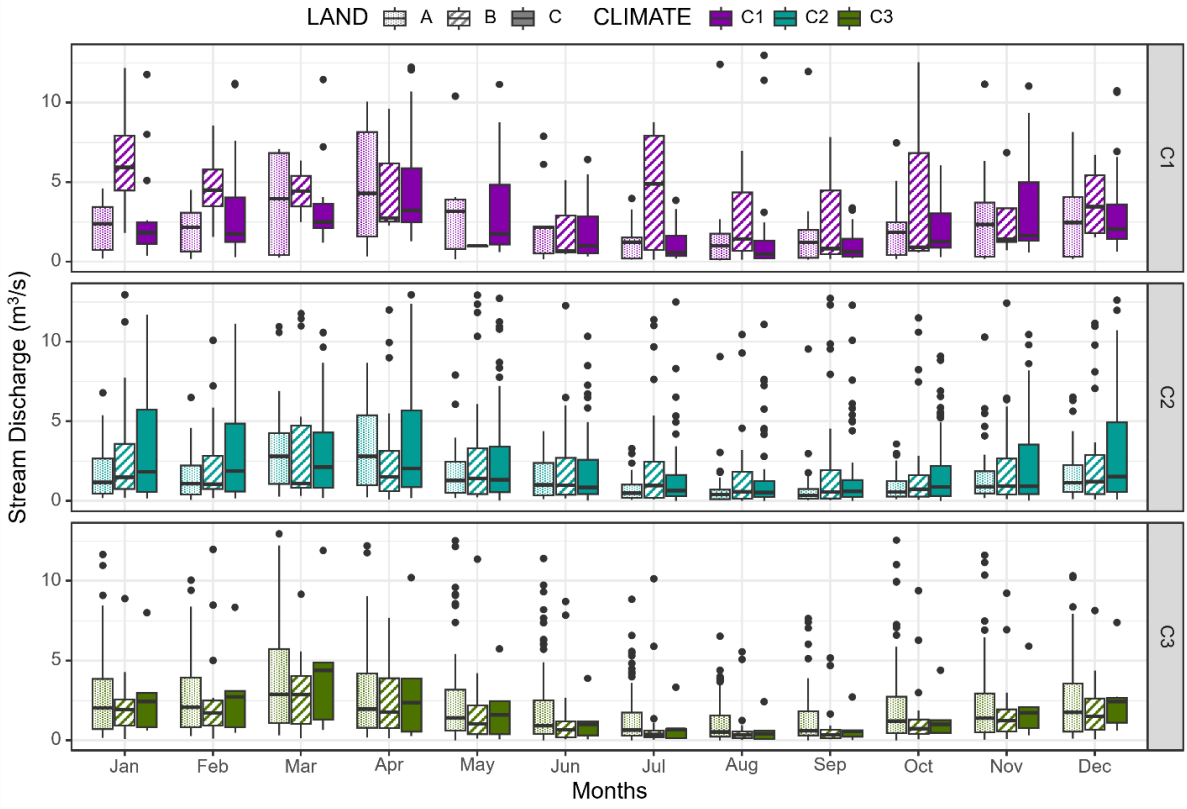

Figure 4.8. Stream discharge boxplot comparisons between monthly averages of 20-year ranges for the nine merged zones grouped by climate zones based on monthly averages from HYDAT datasets ranging from 2000 to 2022.

Figure 4.9A provides insight into the timing of annual flow. The greatest flow occurs in April across all zones, which coincides with snowmelt and the onset of the growing season. The degree of variability between land zones is greater in climate zones C1 and C2 than in C3. Overall, Figure 4.9B shows that both the growing and non-growing seasons contribute relatively equally to the average streamflow across all nine zones. However, the non-growing season provides more flow in the northern zones and zones LB and LC than in LA.

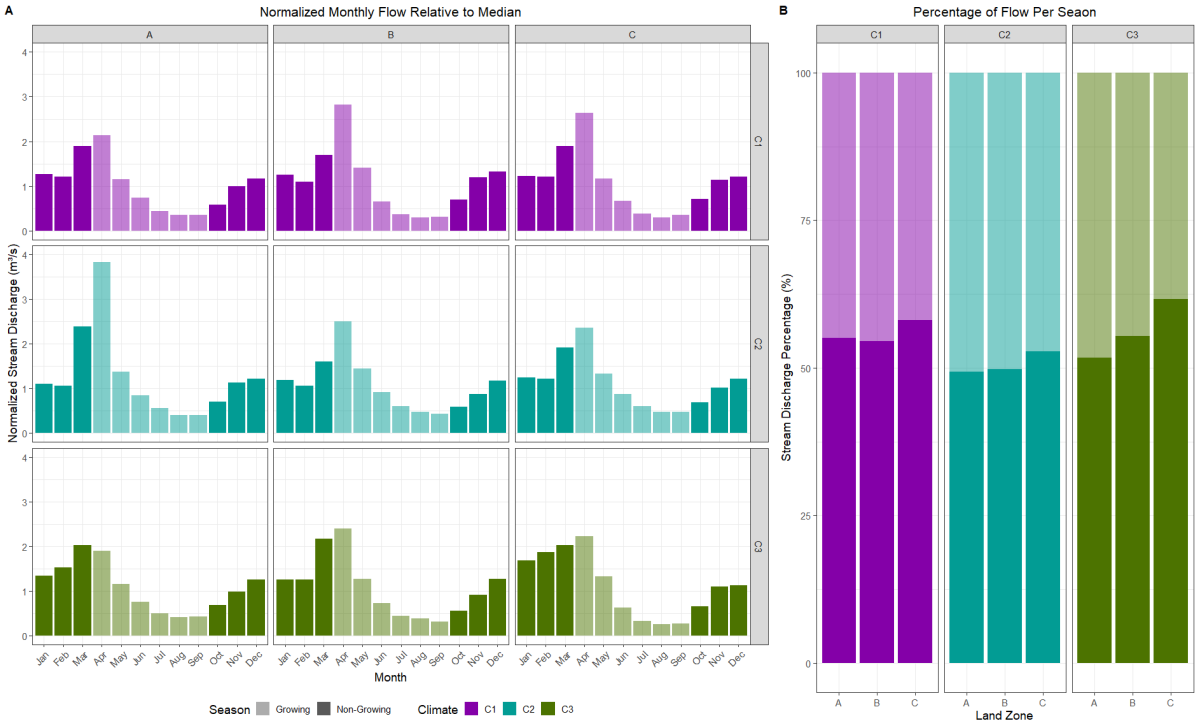

Figure 4.9. Stream discharge comparisons between growing and non-growing seasons for the nine merged zones based on HYDAT datasets, which range from 2000 to 2022: (A) Normalized Monthly Flow plot, bar chart of annual, monthly average flow relative to the median, and (B) Percentage of Flow Per Season, bar chart of the percentage of stream discharge per growing/non-growing season.

Figure 4.10 displays the same dataset found in Table 4.1; however, the proportions of LULC types were split between climate zones within each land zone. Similar to the findings shown in Table 4.1,

LA has the highest proportion of croplands and the lowest number of natural landscapes, while LB has the opposite proportions of LULC types. On the other hand, LC has similar proportions of croplands and natural landscapes. Figure 4.10 illustrates that croplands, pastures, and urban regions across all land zones increase while natural landscapes decrease from C1 to C3. These patterns are especially apparent in the differences between natural land and croplands. For instance, C3-C accounts for 60 percent of croplands while C1-C is less than 20 percent, but, on the other hand, C3-C only accounts for 10 percent of natural landscapes while C1-C is more than 50 percent. In addition, C1-A has similar proportions of croplands and natural landscapes, but C3-A accounts for more than 60 percent of croplands and less than 10 percent of natural land.

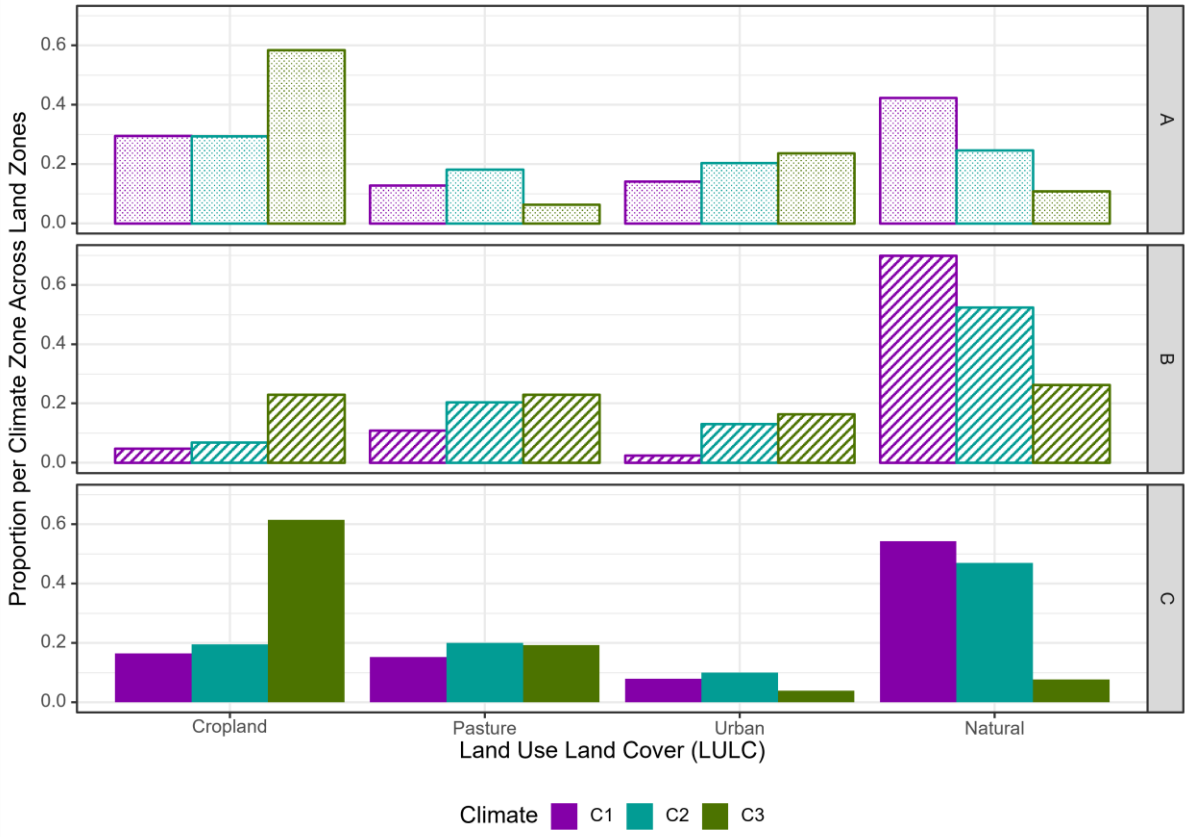

Figure 4.10. Comparison of proportion of land cover – land use (LULC) types across climate zones within each land zone.

4.2 Differences in Water Quality Parameters Across Clustered Zones

Figure 4.11 highlights the sources of both SRP and TP within broad LULC types across climate and land zones. Across both plots, sources of P within climate zones are increasing from C1 to C3, which matches the direction of temperature rise, growing degree day increase and transition to rainfall-dominance. Furthermore, C3, the warmest, rainfall-dominant zone, has consistently elevated P concentrations irrespective of LULC type and across land zones. More specifically, croplands in C3 exhibit the highest P levels across all land zones. The highest P source among all LULC varieties is located in LA, a flat, low-lying region with non-variable surfaces, which overlaps with high tile drainage installations within C3. With the exception of croplands for both plots, LB has the lowest P levels among the three land zones across all LULC types.

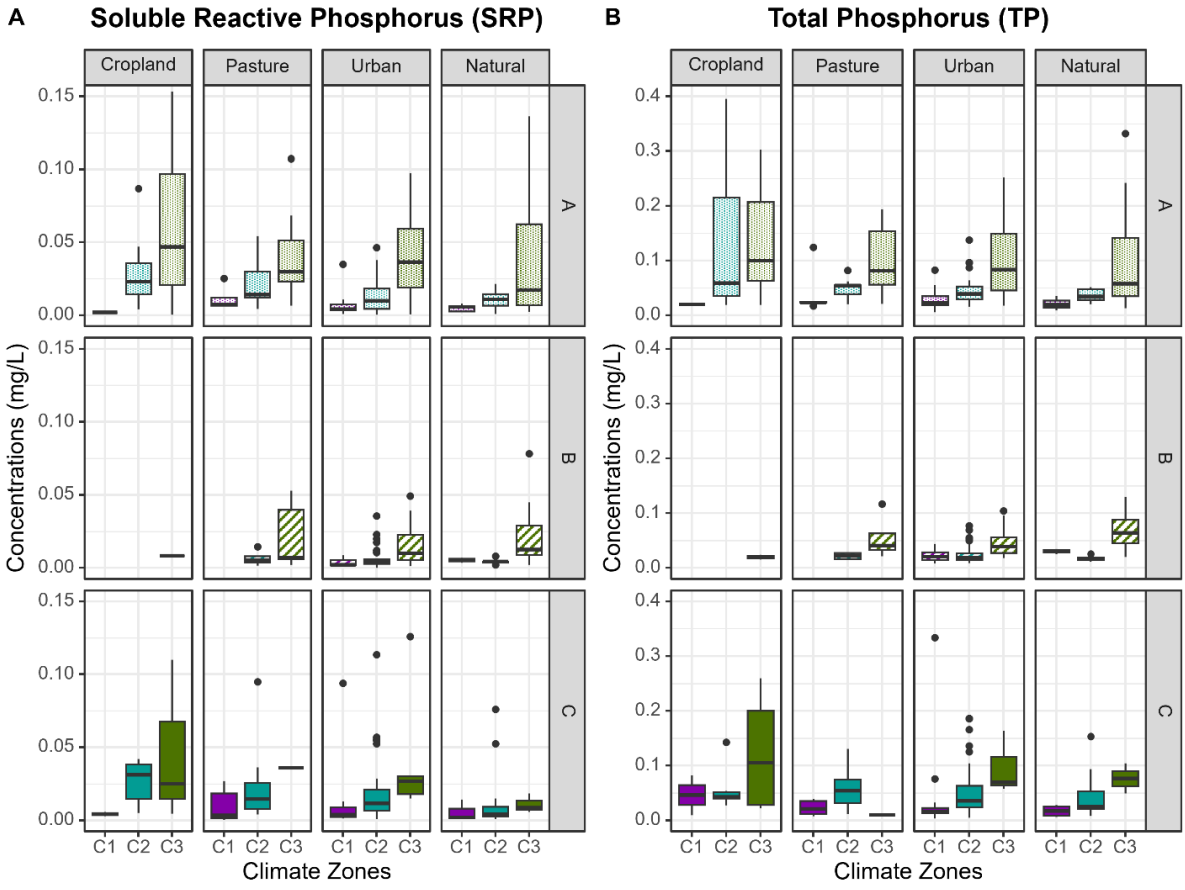

Figure 4.11. Boxplot comparisons between fractions of P nutrients within all nine zones grouped by land zones across landscape types: (A) SRP plot and (B) TP plot.

Figures 4.12 and 4.13 illustrate the spatial distribution of the data presented in Figure 4.11, explicitly highlighting the locations of all PWQMN monitoring stations within the agricultural study area and the stations with elevated nutrient concentrations. Figures 4.12A and 4.13B demonstrate that the stations above the acceptable limits for streams with Ontario are concentrated across the southwestern portion of the study area. The presence of SRP and TP elevated stations (i.e., above 0.03 mg/L for SRP and 0.1 mg/L for TP) is greatest in the LA and LC zones, especially when they overlap with climate zones C2 and C3. Even though LB has the smallest occurrence of elevated SRP and TP stations, the few stations in this zone overlap with C3 and border zones C3-A and C3-C.

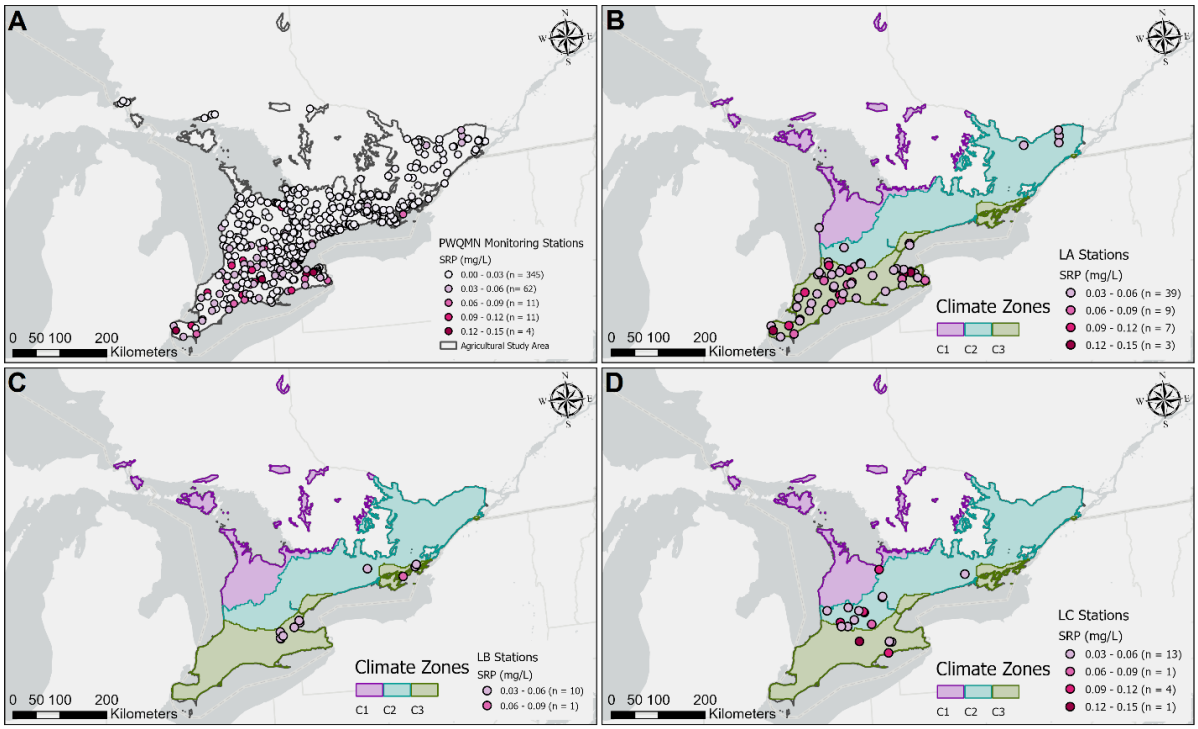

Figure 4.12. Spatial distribution of PWQMN monitoring stations showing SRP concentrations across the agricultural study area. Map A includes all PWQMN stations with SRP values within the study

area, while maps B, C and D include PWQMN stations within each land zone with SRP values above 0.03 mg/L across the three climate zones.

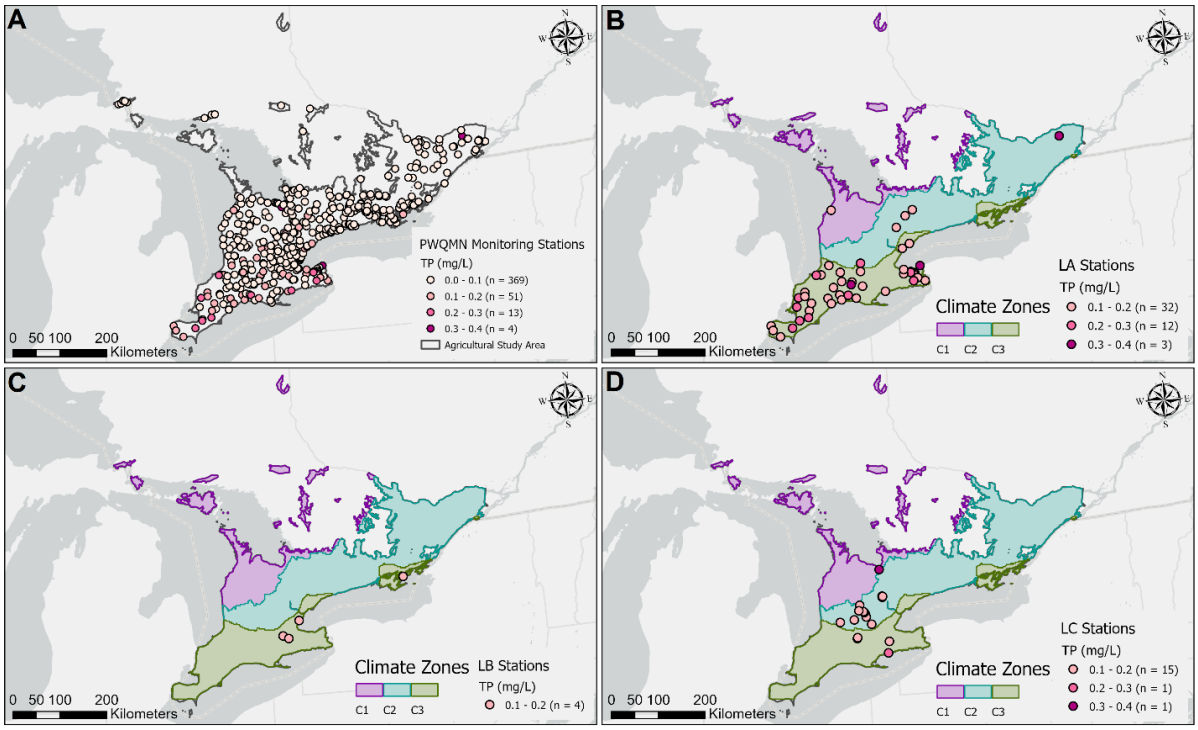

Figure 4.13. Spatial distribution of PWQMN monitoring stations showing TP concentrations across the agricultural study area. Map A includes all PWQMN stations with TP values within the study area, while maps B, C and D include PWQMN stations within each land zone with TP values above 0.1 mg/L across the three climate zones.

With the exception of climate zones C3-C, all plots in Figure 4.14 illustrate a positive linear relationship between stream discharge and P loads across all land and climate zones, which is to be expected. Figure 4.14B demonstrates a robust positive correlation between TP and discharge, where R2adj exceeds 0.7 for almost all climate and land zones. In contrast, relationships between SRP and flow were weaker (Figure 4.14A).

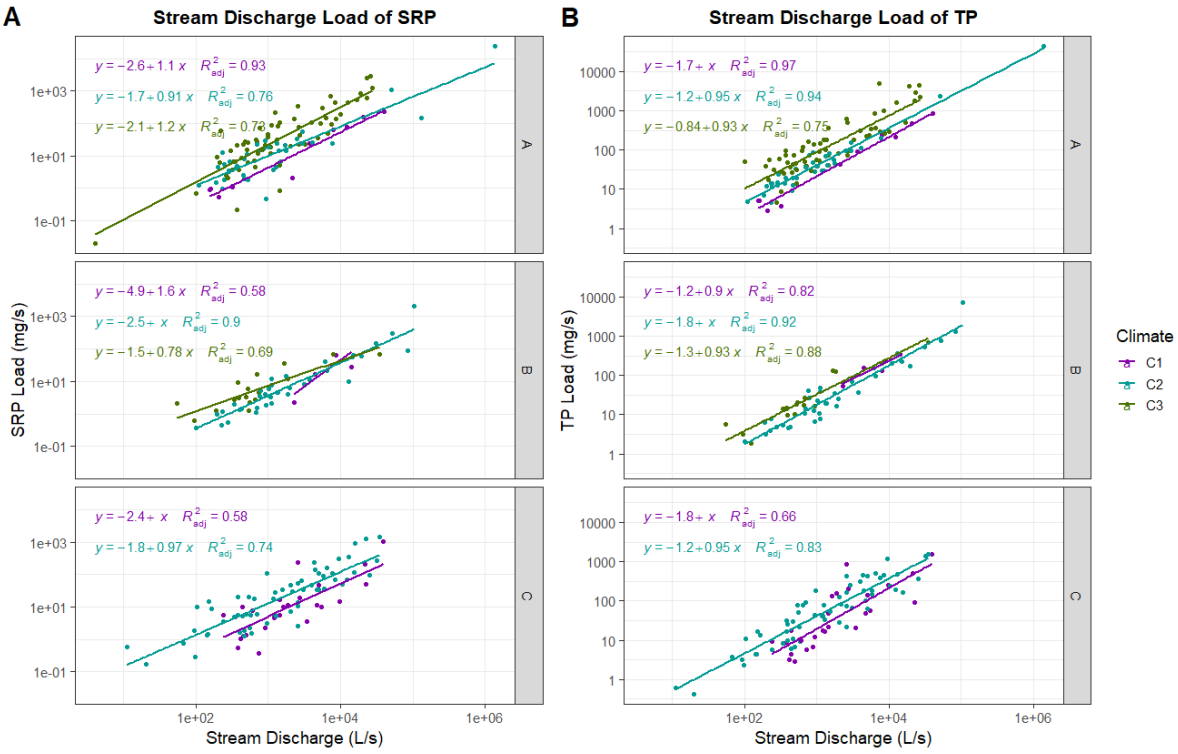

Figure 4.14. Logarithmic transformed (log10) scatterplot comparisons between stream discharge of P loads within all nine zones grouped by land zones: (A) Stream Discharge Load of SRP plot and (B) Stream Discharge Load of TP plot.

Figure 4.15 captures the seasonal variability in SRP and TP concentrations across all land zones within each climate zone. Across all climate zones, LA and LC have higher SRP and TP concentrations than LB and P concentrations, which generally increase from C1 to C3. There are notable seasonal differences. For example, P concentrations are smallest in winter in C1 but greatest in winter in C3. Differences across the other seasons are less apparent.

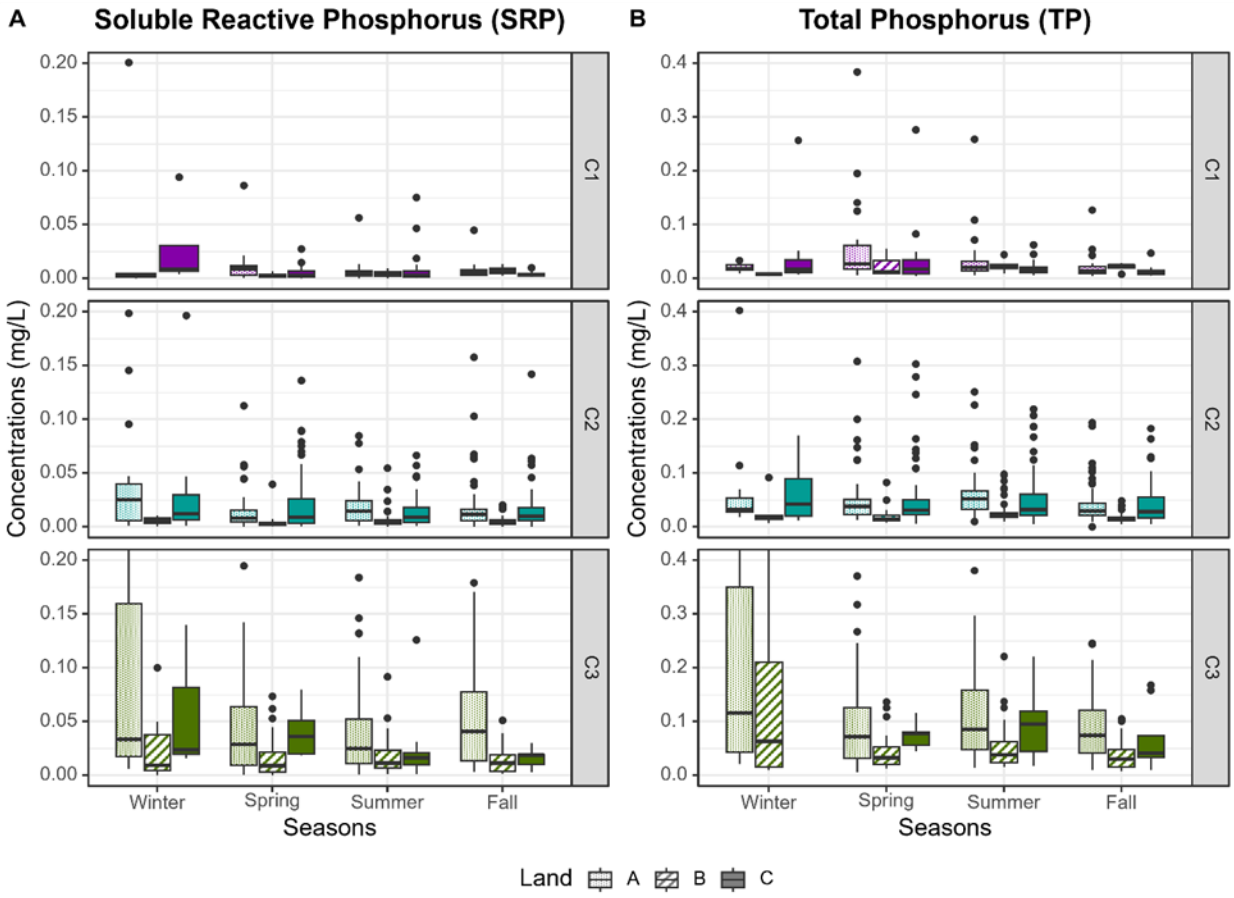

Figure 4.15. Boxplot comparisons between fractions of P nutrients within all nine zones grouped by climate zones across seasons (i.e., Winter (Dec-Jan-Feb), Spring (Mar-Apr-May), Summer (Jun-Jul-Aug), and Fall (Sep-Oct-Nov)): (A) SRP plot and (B) TP plot.

Figure 4.16 follows a similar pattern to Figure 4.11, where C3 is a consistent source of a substantial amount of nitrate and suspended sediment (i.e., turbidity), and this is apparent in both LA and LC but is less evident in LB. Although fewer stations collect turbidity observations, Figure 4.16B shows that suspended sediment is elevated in LA in C3, irrespective of land use, but this is not observed in C1 or C2. There is less data for zones B and C, but no clear patterns are observed.

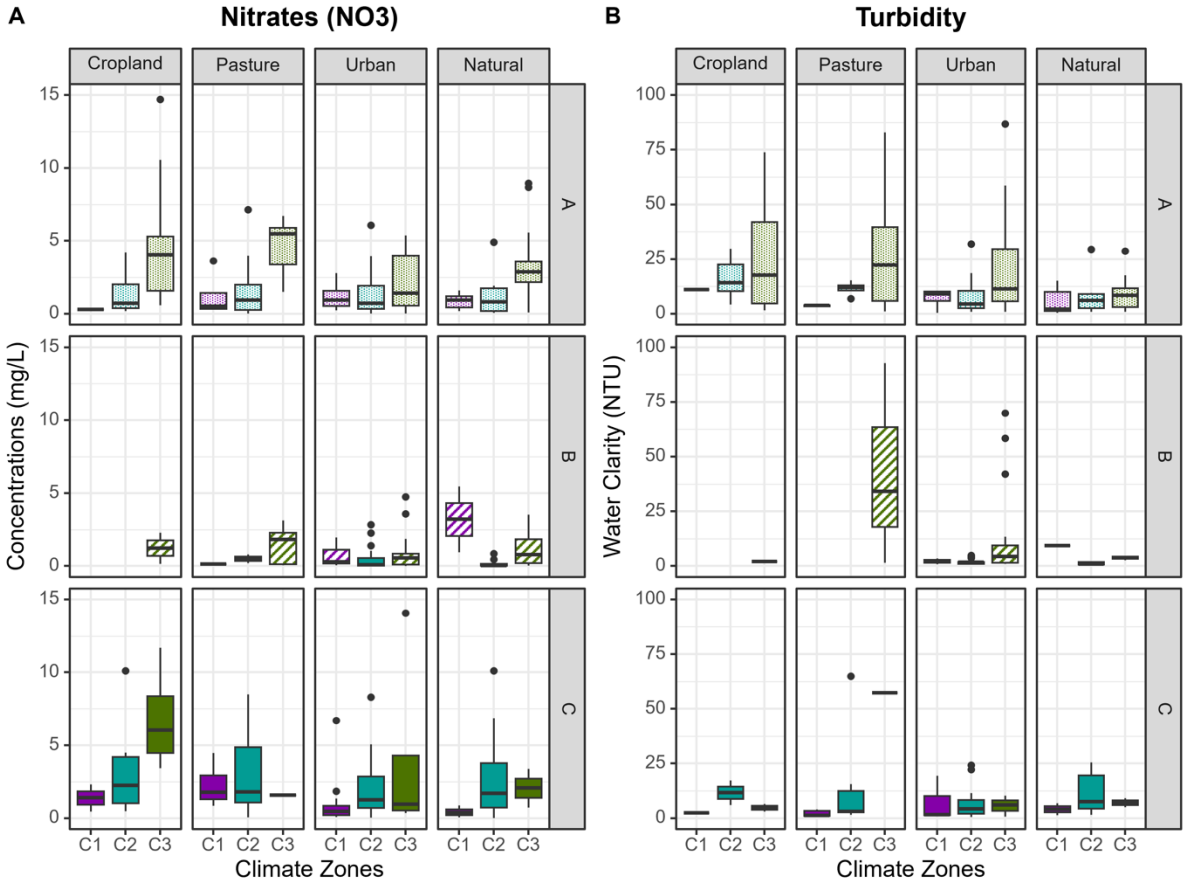

Figure 4.16. Boxplot comparisons between supporting nutrient factors within all nine zones grouped by land zones across landscape types: (A) Nitrate (NO3) plot and (B) Turbidity plot.

Similar to Figures 4.12 and 4.13, Figures 4.17 and 4.18 illustrate the spatial distribution of the data presented in Figure 4.16, explicitly highlighting the locations of all PWQMN monitoring stations within the agricultural study area and highlighting elevated stations. Analogously, Figures 4.17A and 4.18B demonstrate that the stations above the acceptable limits for streams with Ontario are concentrated across the southwestern portion of the study area. Compared to the abundance of SRP and TP elevated stations, elevated nitrate locations (i.e., above 10 mg/L) only exist in limited numbers within LA and LC. On the other hand, in Figure 4.18, turbidity hotspots (i.e., 10% above natural levels, which is 10 NTU) are found in high quantities across all land zones. Both nitrate and turbidity hotspots within LA and LC overlap with C3 and C2.

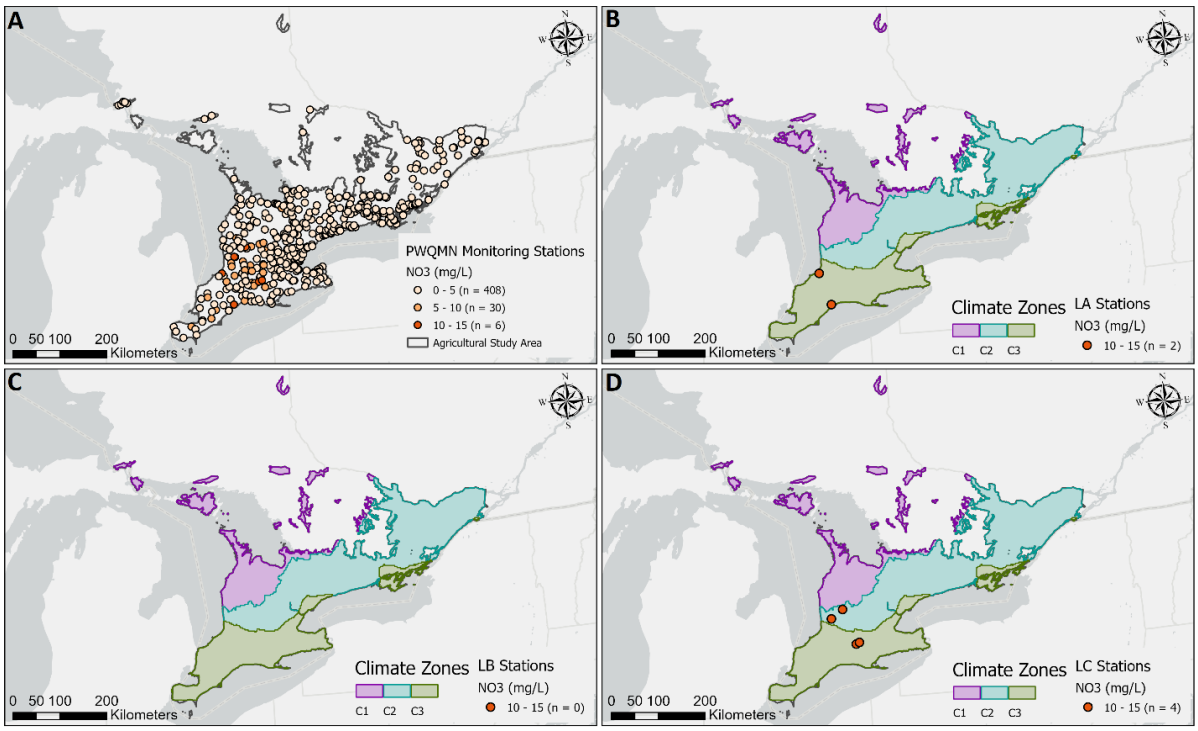

Figure 4.17. Spatial distribution of PWQMN monitoring stations showing NO3 concentrations across the agricultural study area. Map A includes all PWQMN stations with NO3 values within the study area, while maps B, C and D include PWQMN stations within each land zone with NO3 values above 10 mg/L across the three climate zones.

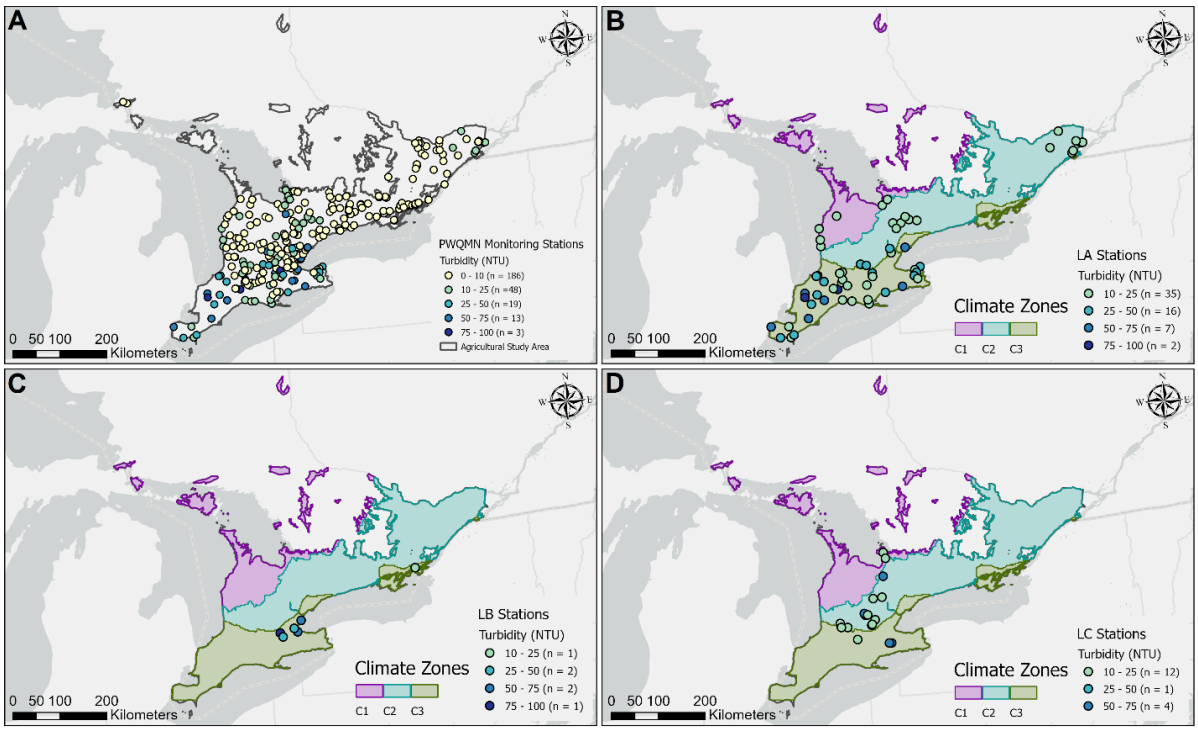

Figure 4.18. Spatial distribution of PWQMN monitoring stations showing turbidity levels across the agricultural study area. Map A includes all PWQMN stations with turbidity values within the study area, while maps B, C and D include PWQMN stations within each land zone with turbidity values above 10 NTU across the three climate zones.

Similar to Figure 4.14, all plots in Figure 4.19 illustrate a positive linear relationship between stream discharge and nitrate loads, except for C3-C. As shown in Figure 4.19, the climate zones have different slopes and R2adj across land zones. For instance, in LA, all the climate zones are strongly correlated, but in LB, the correlation is weak across climate zones. Moreover, climate zones in LA share similar slope values, but these values vary in LB.

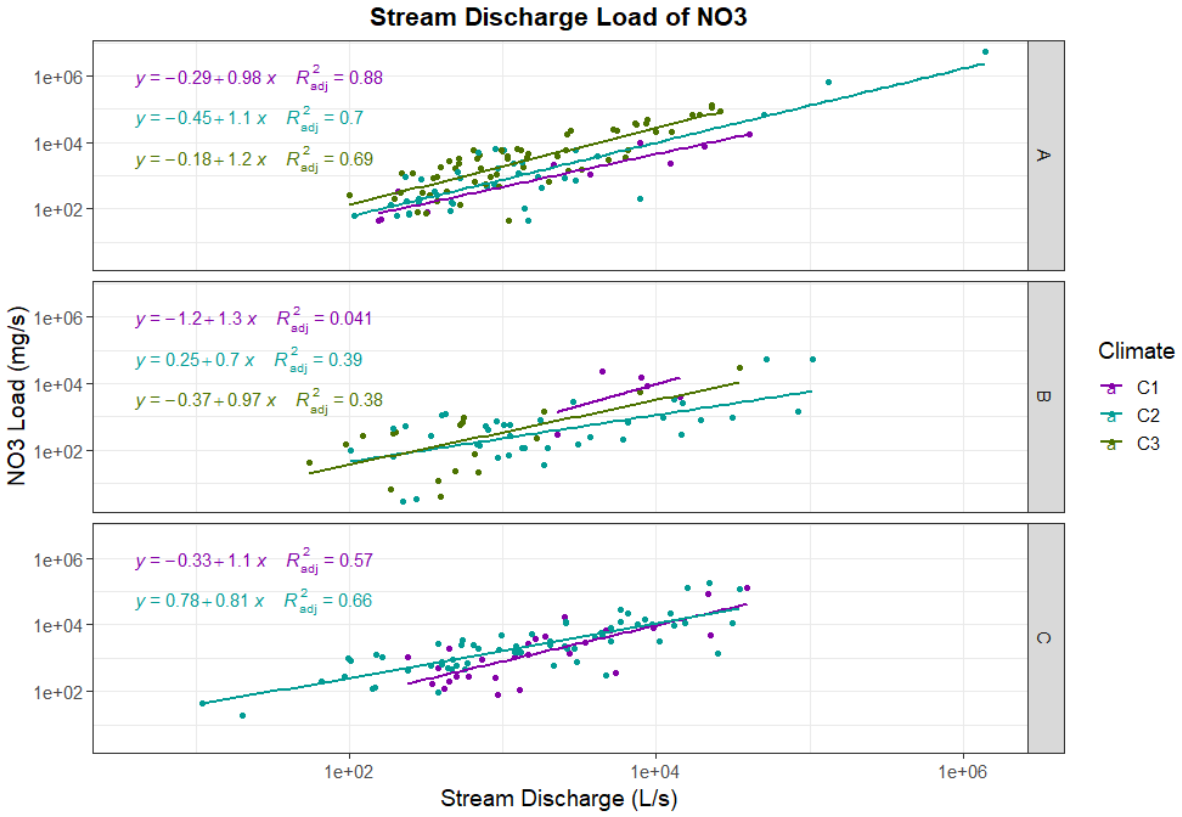

Figure 4.19. Logarithmic transformed (log10) scatterplot comparisons between stream discharge of NO3 loads within all nine zones grouped by land zones.

Similar to the findings shown in Figure 4.17, Figure 4.20 captures the seasonal variability in nitrate concentrations and suspended sediment prevalence across all land zones within each climate zone. Across all climate zones, LA and LC have higher levels of nitrates and turbidity than LB, and concentrations increase from C1 to C3. Similar to Figure 4.15, nitrates and turbidity concentrations are elevated within C3-A and C3-C but follow different seasonal patterns. Analogously, C3-A remains elevated year-round, while in C3-C, nitrates peak in winter, and turbidity is highest in fall.

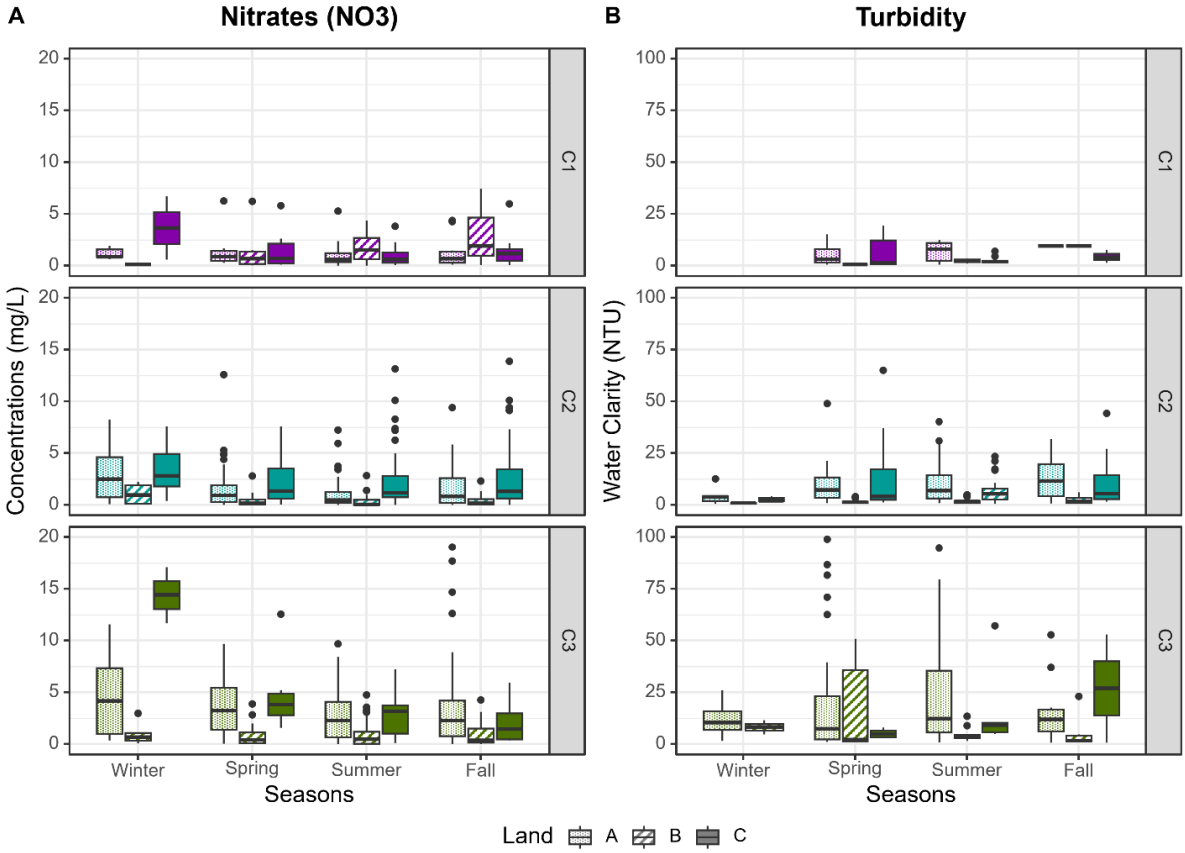

Figure 4.20. Boxplot comparisons between supporting nutrient factors within all nine zones grouped by climate zones across seasons (i.e., Winter (Dec-Jan-Feb), Spring (Mar-Apr-May), Summer (Jun-Jul-Aug), and Fall (Sep-Oct-Nov)): (A) Nitrate (NO3) plot and (B) Turbidity plot.

4.3 Shifts in Climatic Variables Within the Clustered Climate and Land Zones Under a Changing Climate

In Figure 4.21, precipitation levels in both future time ranges are higher than in the contemporary range. However, the disparity between the two future ranges widens as one progresses from low to high emission scenarios. Furthermore, in the high emission scenario (RCP 8.5), the zone with the lowest contemporary precipitation rates (C2) will have higher future rates than the average rates of C1's contemporary rates. Additionally, while every zone experiences an equal impact, future precipitation levels are anticipated to increase drastically in C1 (by at least 50 mm/year), which already receives the most precipitation under contemporary conditions, and precipitation in C2 and

C3 has the potential to increase to what C1 currently received under RCP 8.5. The increases in precipitation appear to be predominantly in winter and, to a lesser extent, in spring and fall, but no changes will be observed in summer rainfall totals (Figure 4.22). The spatial patterns across the different climate zones are not projected to change. These patterns are also highlighted in Figure 4.23.

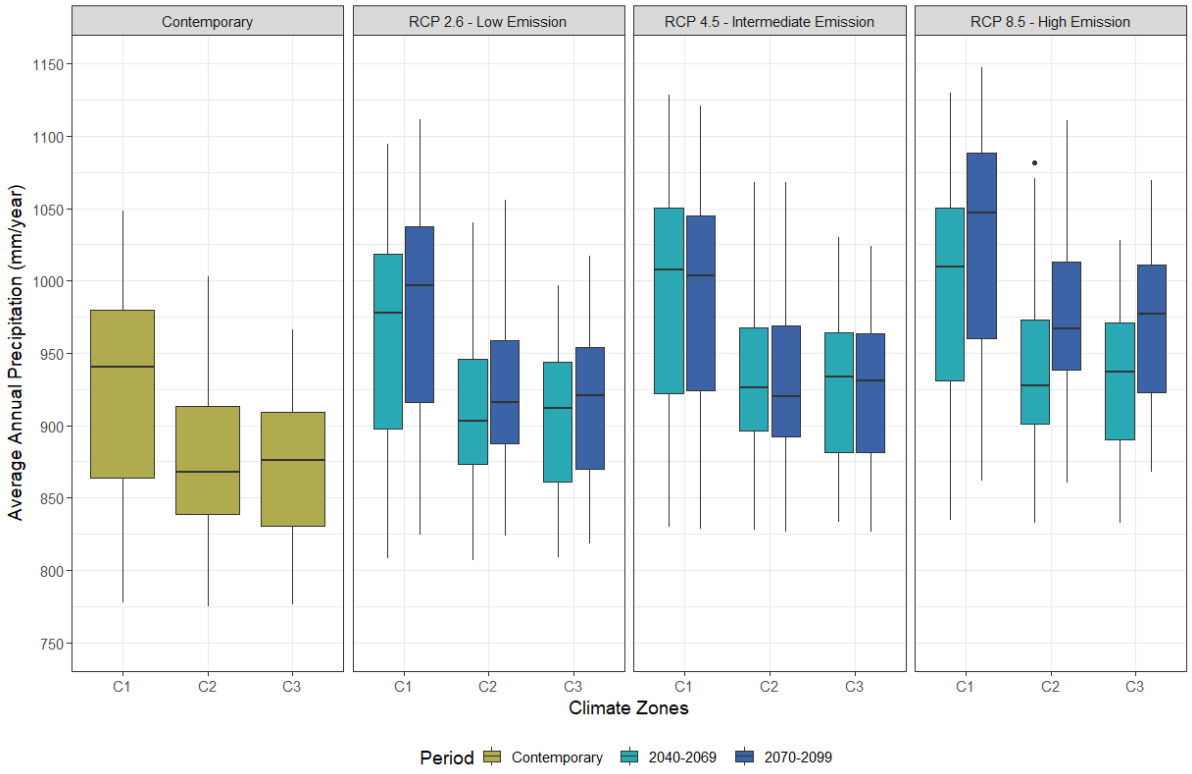

Figure 4.21. Boxplot comparisons of average annual precipitation within climate zones across three time periods, including the contemporary period ranging from 1981 to 2006 and two future time ranges, and three emission scenarios.

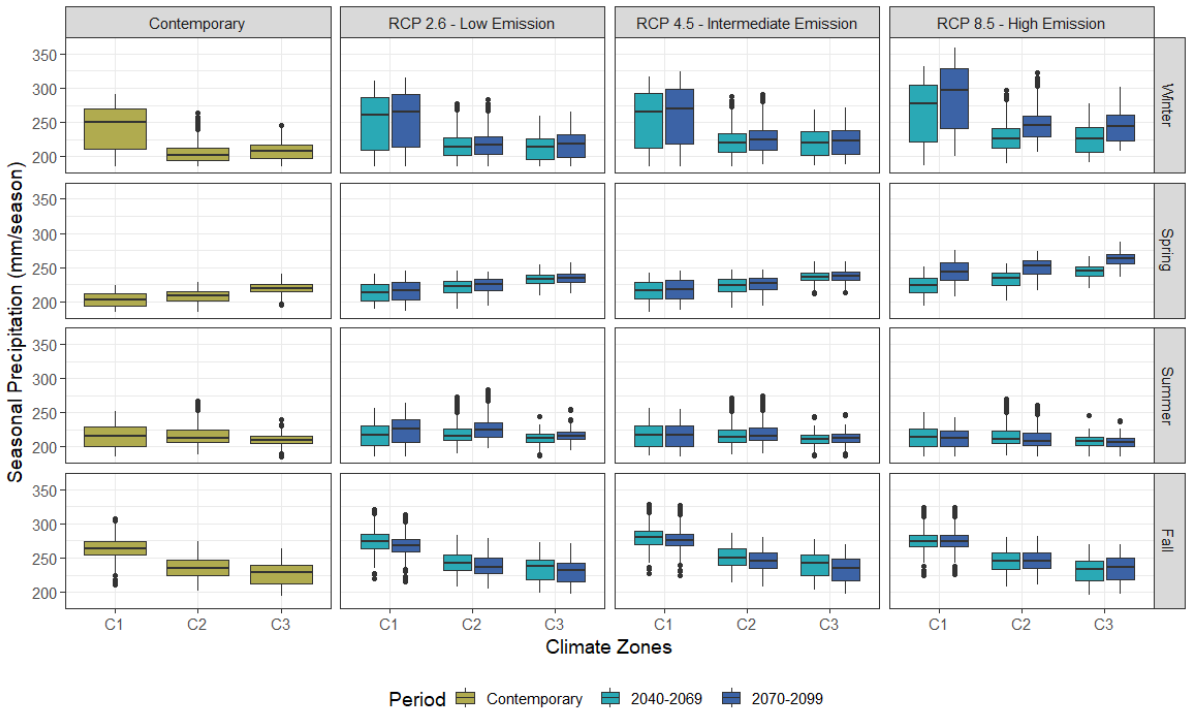

Figure 4.22. Boxplot comparisons of seasonal precipitation within climate zones across three time periods, including the contemporary period ranging from 1981 to 2006 and two future time ranges, and three emission scenarios.

The spatial precipitation pattern shown in Figure 4.23A is consistent with Figure 4.21, where the highest precipitation rates occur in C1 near Owen Sound, Ontario. Future emission scenarios predict that the average precipitation rates in this area will spread southwards along the Lake Huron coastline towards Lake Erie. More specifically, the 1100 mm contour polygon will spread from C1 to C3 even under the low-emission scenario. This finding once more aligns with Figure 4.21, which indicates that C3 will be most substantially affected by higher emission scenarios during the later time period. An additional area that will experience a heightened precipitation rate is along the Ontario-Quebec border in the east (C2). The impact rate mirrors the western portion of the agricultural extent, where C2-A and C3-C will account for similar precipitation rates in the future.

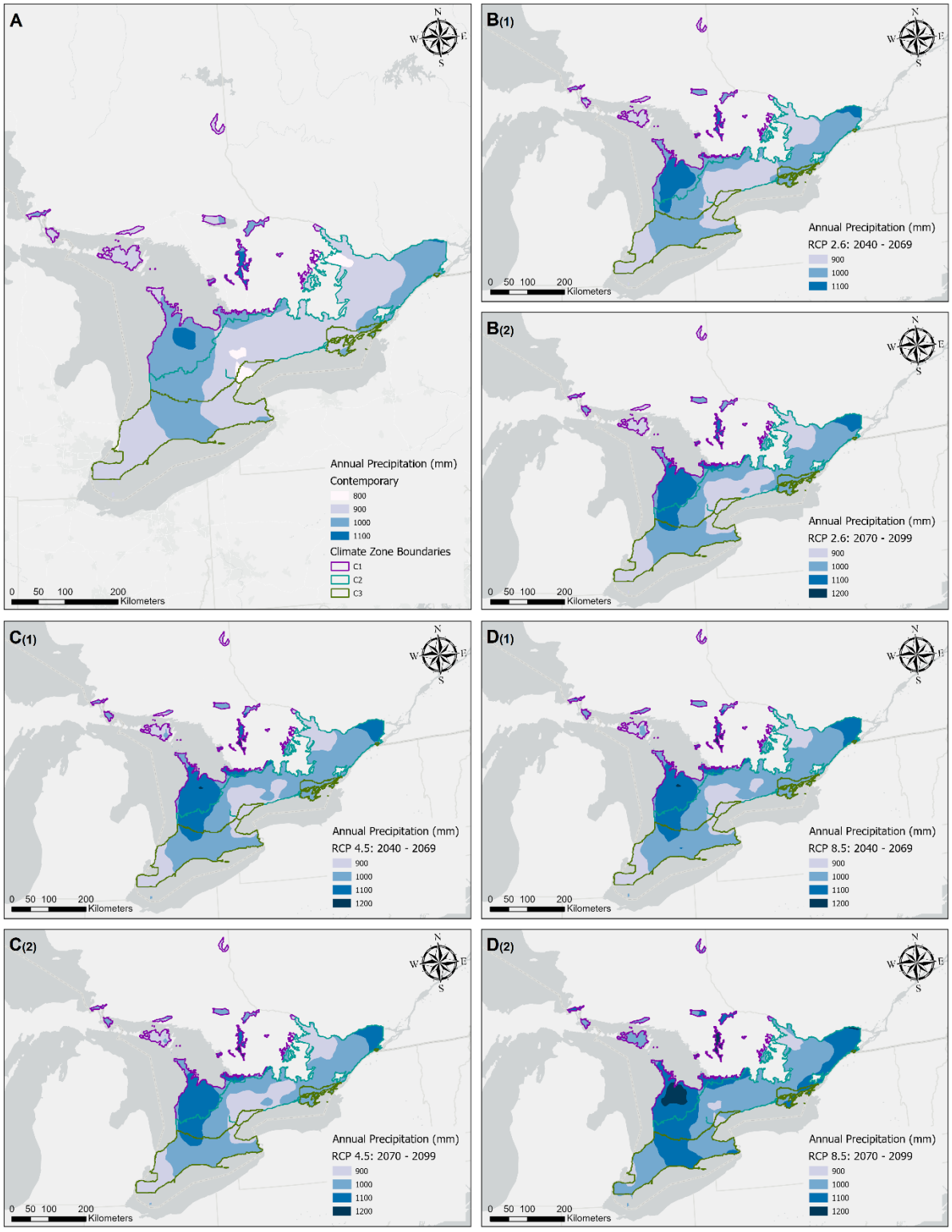
A
Annual Precipitation (mm)
Contemporary
800
900
1000
1100
Climate Zone Boundaries
C1
C2
C3
0 50 100 200
Kilometers
B(1)
Annual Precipitation (mm)
RCP 2.6: 2040 - 2069
900
1000
1100
0 50 100 200
Kilometers
B(2)
Annual Precipitation (mm)
RCP 2.6: 2070 - 2099
900
1000
1100
1200
0 50 100 200
Kilometers
C(1)
Annual Precipitation (mm)
RCP 4.5: 2040 - 2069
900
1000
1100
1200
0 50 100 200
Kilometers
D(1)
Annual Precipitation (mm)
RCP 8.5: 2040 - 2069
900
1000
1100
1200
0 50 100 200
Kilometers
C(2)
Annual Precipitation (mm)
RCP 4.5: 2070 - 2099
900
1000
1100
1200
0 50 100 200
Kilometers
D(2)
Annual Precipitation (mm)
RCP 8.5: 2070 - 2099
900
1000
1100
1200
0 50 100 200
Kilometers

Figure 4.23. Map illustrating the spatial extent of average annual precipitation levels within three different climate emission scenarios and three-time period ranges across the agricultural extent within climate zones: (A) Contemporary conditions, (B) Low emission scenario (RCP 2.6), (C) Intermediate emission scenario (RCP 4.5), and (D) High emission scenario (RCP 8.5).

As observed for precipitation, annual maximum temperatures are also projected to increase across all climate zones (Figure 4.24). Maximum temperatures, which are currently lowest in C1, will be as warm as C3 under all emission scenarios, whereas C2 and C3 will observe considerably warmer maximum temperatures than are currently experienced in Ontario. The maximum emission scenario yields the most dramatic results, with substantially warmer maximum temperatures by the end of the century (Figure 4.24). In contrast, seasonal patterns in maximum air temperature (Figure 4.25) are not anticipated to change in the same way that precipitation will (Figure 4.23). Where precipitation increases primarily occur during the winter and shoulder seasons, air temperatures will increase across all seasons. Notably, where mean maximum temperatures in winter are below the freezing mark in zones C1 and C2, mean maximum temperatures in winter will be at the freezing mark in these zones under the low and intermediate scenarios and above the freezing mark in the high emission scenario.

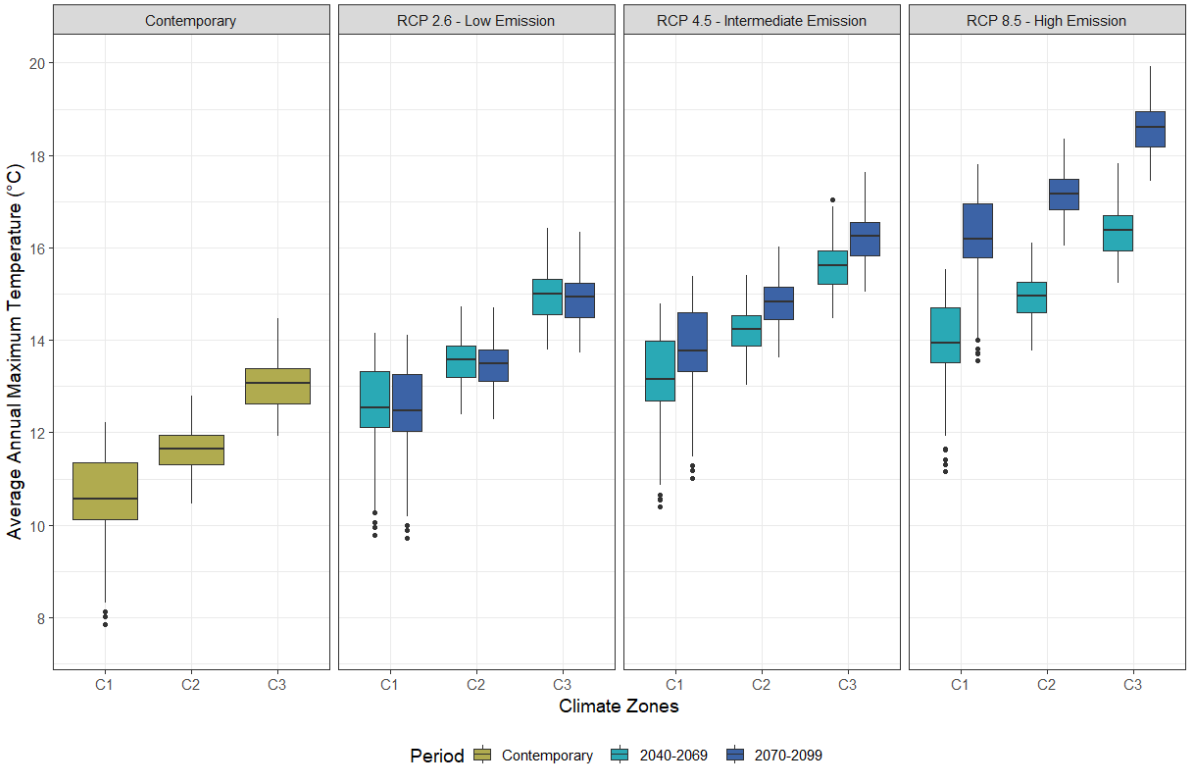

Figure 4.24. Boxplot comparisons of average annual maximum temperature within climate zones across three time periods, including the contemporary period ranging from 1981 to 2006 and two future time ranges, and three emission scenarios.

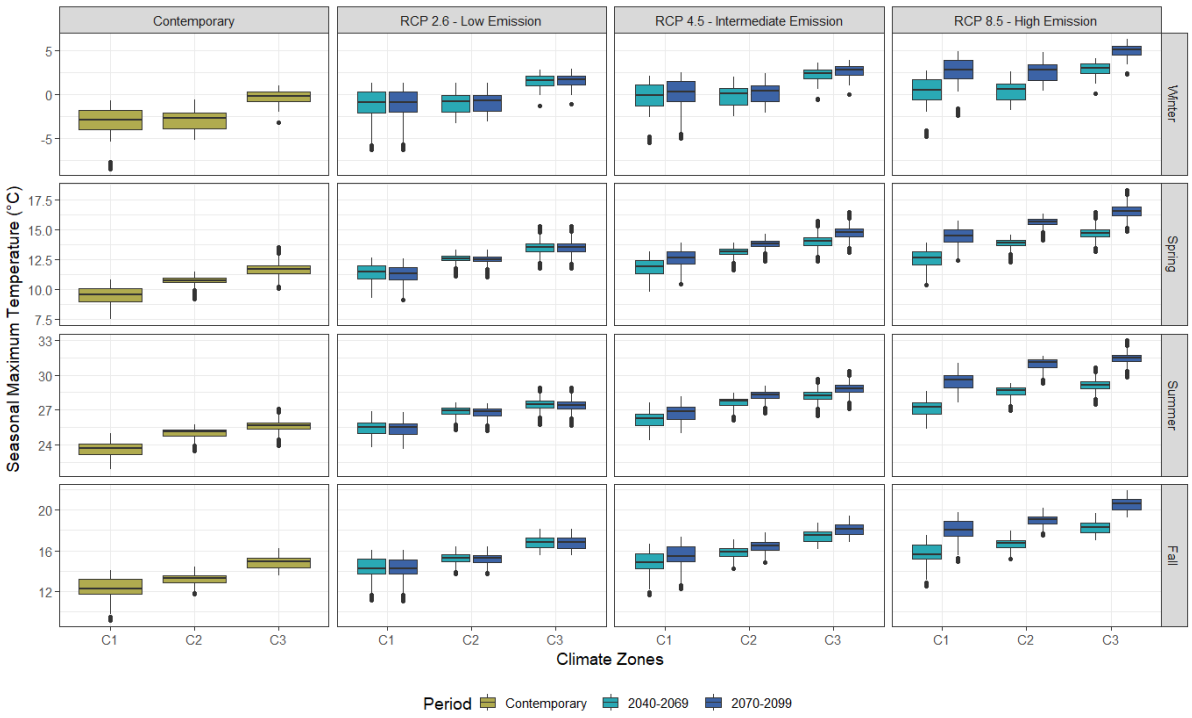

Figure 4.25. Boxplot comparisons of seasonal maximum temperature within climate zones across three time periods, including the contemporary period ranging from 1981 to 2006 and two future time ranges, and three emission scenarios.

Figure 4.26 demonstrates the latitude-driven nature of temperature rates within the region. C3, which covers most of the Lake Erie watershed and has the lowest latitude, accounts for the highest maximum temperature. Across all future scenarios, all climate zones are expected to have an average annual maximum temperature increase of approximately 2 degrees (shift from 12-14 to 14-16 class). Moreover, when considering different emission scenarios and time periods, it is observed that the maximum temperature rises from the south-westernmost point in Windsor, Ontario, to the north-easternmost point in Temiskaming Shores, Ontario. C3 is expected to be impacted the most when maximum temperatures shift from around 12-14 degrees to 18- 20 degrees under the high emission scenario during the latter time period. Although this increase is consistent latitudinally, the region with the highest precipitation rates in C1 (Figure 4.21) has a lower maximum temperature than other regions at comparable latitudes. In addition, this region overlaps with findings shown in Figure 4.5, where LC is a steep upland with variable surfaces.

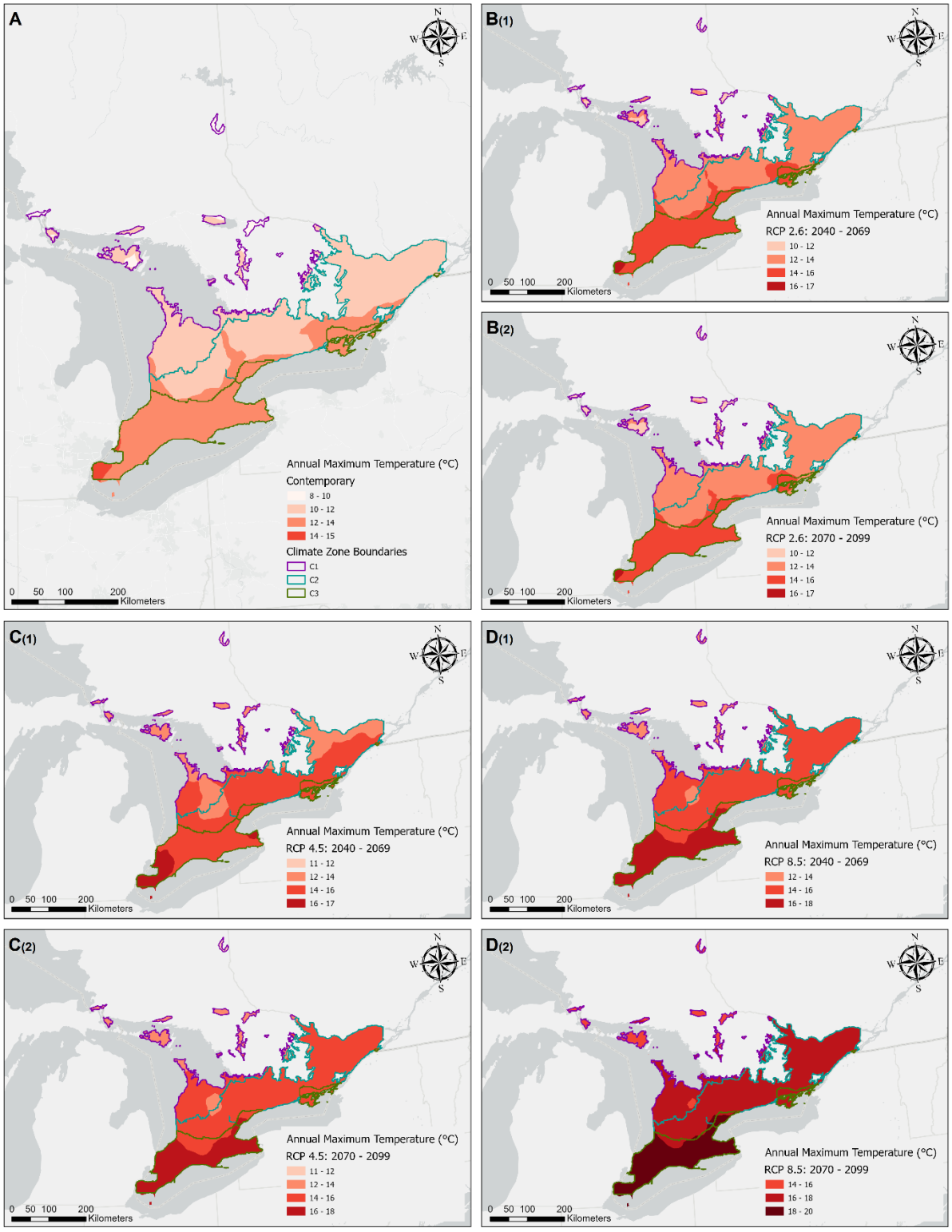
A
Annual Maximum Temperature (°C)
Contemporary
8 - 10
10 - 12
12 - 14
14 - 15
Climate Zone Boundaries
C1
C2
C3
0 50 100 200 Kilometers
B(1)
Annual Maximum Temperature (°C)
RCP 2.6: 2040 - 2069
10 - 12
12 - 14
14 - 16
16 - 17
0 50 100 200 Kilometers
B(2)
Annual Maximum Temperature (°C)
RCP 2.6: 2070 - 2099
10 - 12
12 - 14
14 - 16
16 - 17
0 50 100 200 Kilometers
C(1)
Annual Maximum Temperature (°C)
RCP 4.5: 2040 - 2069
11 - 12
12 - 14
14 - 16
16 - 17
0 50 100 200 Kilometers
D(1)
Annual Maximum Temperature (°C)
RCP 8.5: 2040 - 2069
12 - 14
14 - 16
16 - 18
0 50 100 200 Kilometers
C(2)
Annual Maximum Temperature (°C)
RCP 4.5: 2070 - 2099
11 - 12
12 - 14
14 - 16
16 - 18
0 50 100 200 Kilometers
D(2)
Annual Maximum Temperature (°C)
RCP 8.5: 2070 - 2099
14 - 16
16 - 18
18 - 20
0 50 100 200 Kilometers

Figure 4.26. Map illustrating the spatial extent of average annual maximum temperature levels within three different climate emission scenarios and three-time period ranges across the agricultural extent within climate zones: (A) Contemporary conditions, (B) Low emission scenario (RCP 2.6), (C) Intermediate emission scenario (RCP 4.5), and (D) High emission scenario (RCP 8.5).

Annual minimum air temperatures are also anticipated to increase under all climate change scenarios (Figure 4.27). Additionally, the gap in future minimum temperatures between contemporary averages and time periods widens with the increase in emission scenarios. This is especially apparent under the high emission scenario where no region within the study area will be at or below 0 degrees. As was observed for annual maximum temperatures, annual minimum temperatures will increase across all seasons (Figure 4.28). Notably, minimum winter temperatures will approach the freezing mark and be considerably warmer in summer.

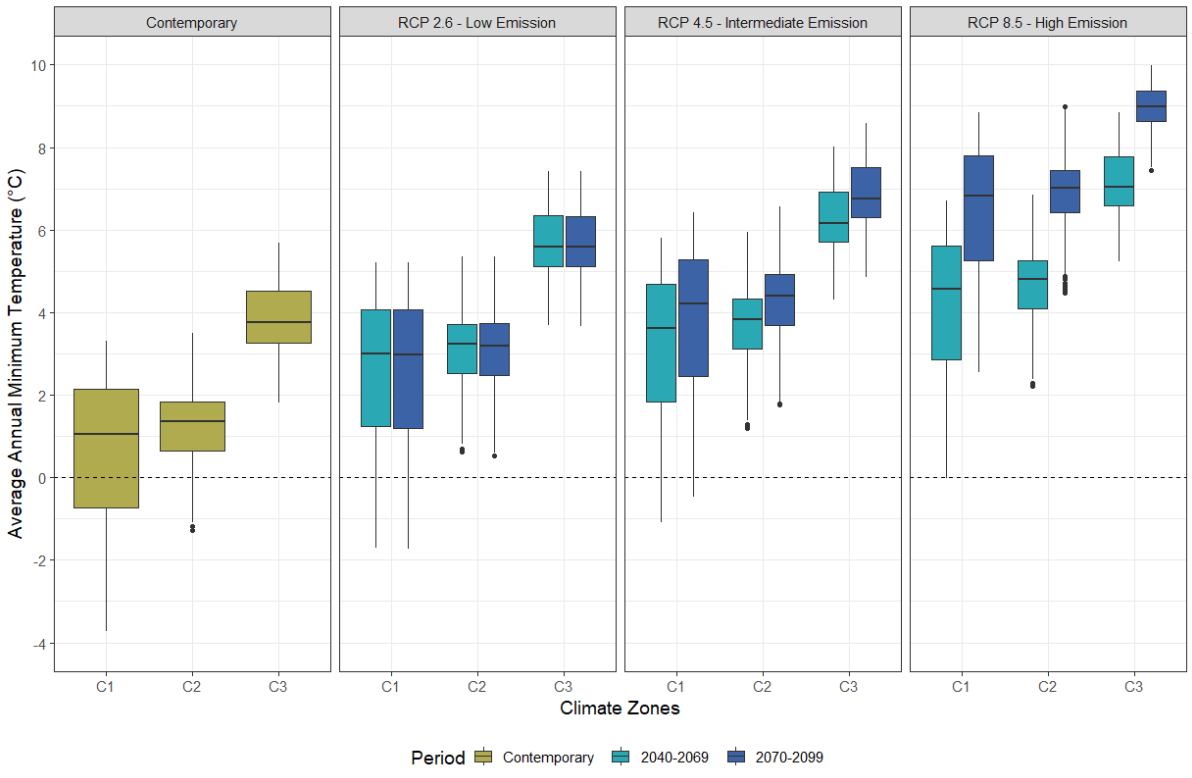

Figure 4.27. Boxplot comparisons of average annual minimum temperature within climate zones across three time periods, including the contemporary period ranging from 1981 to 2006 and two future time ranges, and three emission scenarios.

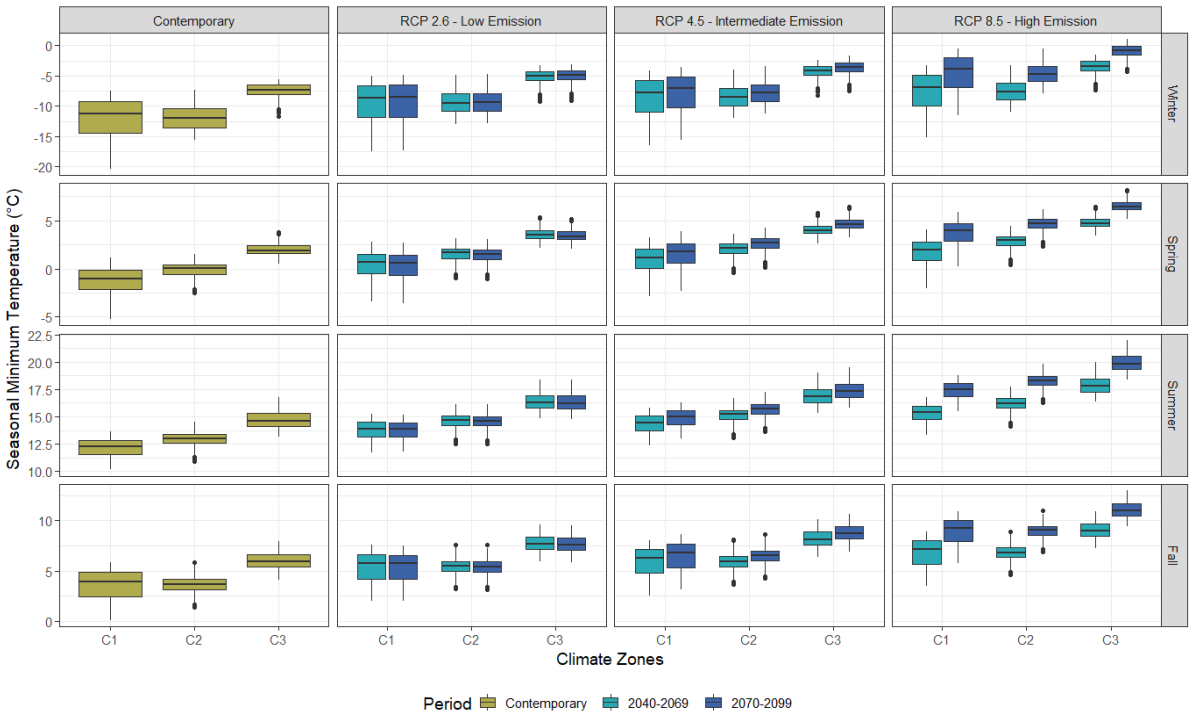

Figure 4.28. Boxplot comparisons of seasonal minimum temperature within climate zones across three time periods, including the contemporary period ranging from 1981 to 2006 and two future time ranges, and three emission scenarios.

Figure 4.29 and Figure 4.26 illustrate similar spatial patterns across the agricultural extent of the study area. Both plots demonstrate a latitude-driven increase from southwest to northeast. In particular, the freeze line is only present under contemporary, low-emission, and intermediate-emission conditions in C1. However, for the latter, the freeze line disappears from 2070-to-2099 under the high-emission scenario, which spans both periods. Once more, the LC bull's eye remains unaffected by latitudinal changes and has a lower average annual minimum temperature than the surrounding region. In Figures 4.29C and D, regions with the lowest maximum temperature have a similar minimum temperature rate under these higher future emission conditions. This spatial pattern is especially evident in Figure 4.29D(2), where the 6-to-8-degree range covers the same area under contemporary regions that experience a maximum temperature range of 8-to-12 degrees.

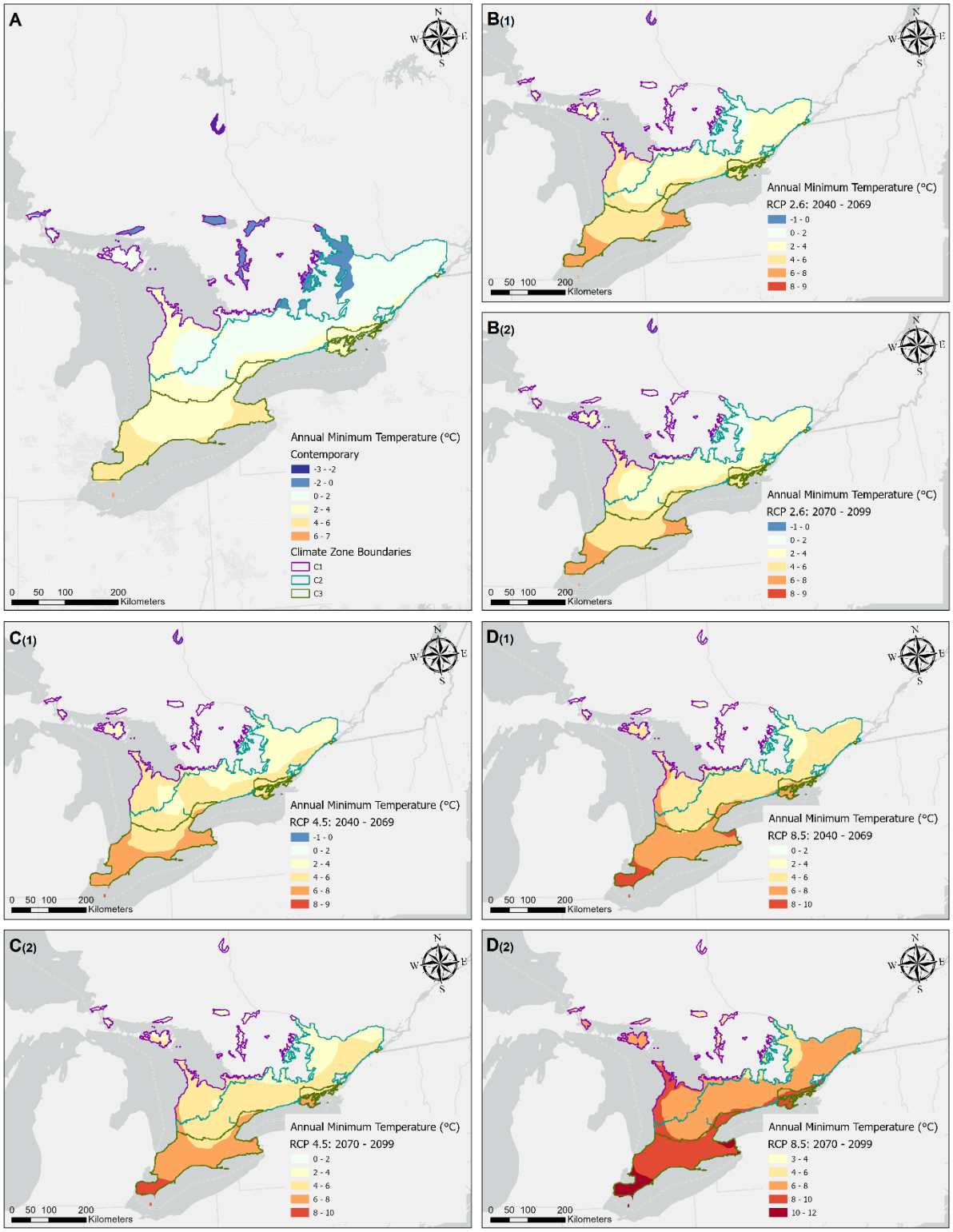
A
Annual Minimum Temperature (°C)
Contemporary
-3 - -2
-2 - 0
0 - 2
2 - 4
4 - 6
6 - 7
Climate Zone Boundaries
C1
C2
C3
0 50 100 200
Kilometers
B(1)
Annual Minimum Temperature (°C)
RCP 2.6: 2040 - 2069
-1 - 0
0 - 2
2 - 4
4 - 6
6 - 8
8 - 9
0 50 100 200
Kilometers
B(2)
Annual Minimum Temperature (°C)
RCP 2.6: 2070 - 2099
-1 - 0
0 - 2
2 - 4
4 - 6
6 - 8
8 - 9
0 50 100 200
Kilometers
C(1)
Annual Minimum Temperature (°C)
RCP 4.5: 2040 - 2069
-1 - 0
0 - 2
2 - 4
4 - 6
6 - 8
8 - 9
0 50 100 200
Kilometers
D(1)
Annual Minimum Temperature (°C)
RCP 8.5: 2040 - 2069
0 - 2
2 - 4
4 - 6
6 - 8
8 - 10
0 50 100 200
Kilometers
C(2)
Annual Minimum Temperature (°C)
RCP 4.5: 2070 - 2099
0 - 2
2 - 4
4 - 6
6 - 8
8 - 10
0 50 100 200
Kilometers
D(2)
Annual Minimum Temperature (°C)
RCP 8.5: 2070 - 2099
3 - 4
4 - 6
6 - 8
8 - 10
10 - 12
0 50 100 200
Kilometers

Figure 4.29. Map illustrating the spatial extent of average annual minimum temperature levels within three different climate emission scenarios and three-time period ranges across the agricultural extent within climate zones: (A) Contemporary conditions, (B) Low emission scenario (RCP 2.6), (C) Intermediate emission scenario (RCP 4.5), and (D) High emission scenario (RCP 8.5).

Figures 4.30, 4.31, and 4.32 include findings from three extreme climate indices; one is related to precipitation rates, while the other two are linked to temperature levels. In contrast to Figures 4.31 and 4.32, Figure 4.30 does not indicate an increased frequency of days with precipitation exceeding 1 mm will occur in climate zones across all emission scenarios. Nevertheless, the number of days will rise with time periods, and this remains consistent with findings in Figures 4.21 and 4.2, where C1 represents the highest precipitation levels. On the other hand, Figures 4.31 and 4.32 demonstrate similar temporal patterns to those depicted in Figures 4.24 and 4.27. As the emission scenarios intensify, there is a concurrent increase in the growing days and the number of days with temperatures surpassing 30ºC. In addition, Figure 4.30 also illustrates a substantial surge in the number of days spanning from climate zone C1 to C3, despite contemporary conditions remaining consistent between climate zones. Even though all climate zones experience change, C3 is particularly affected, with the number of days increasing from a contemporary average below 20 days annually to more than 80 days during the period 2070-to-2099.

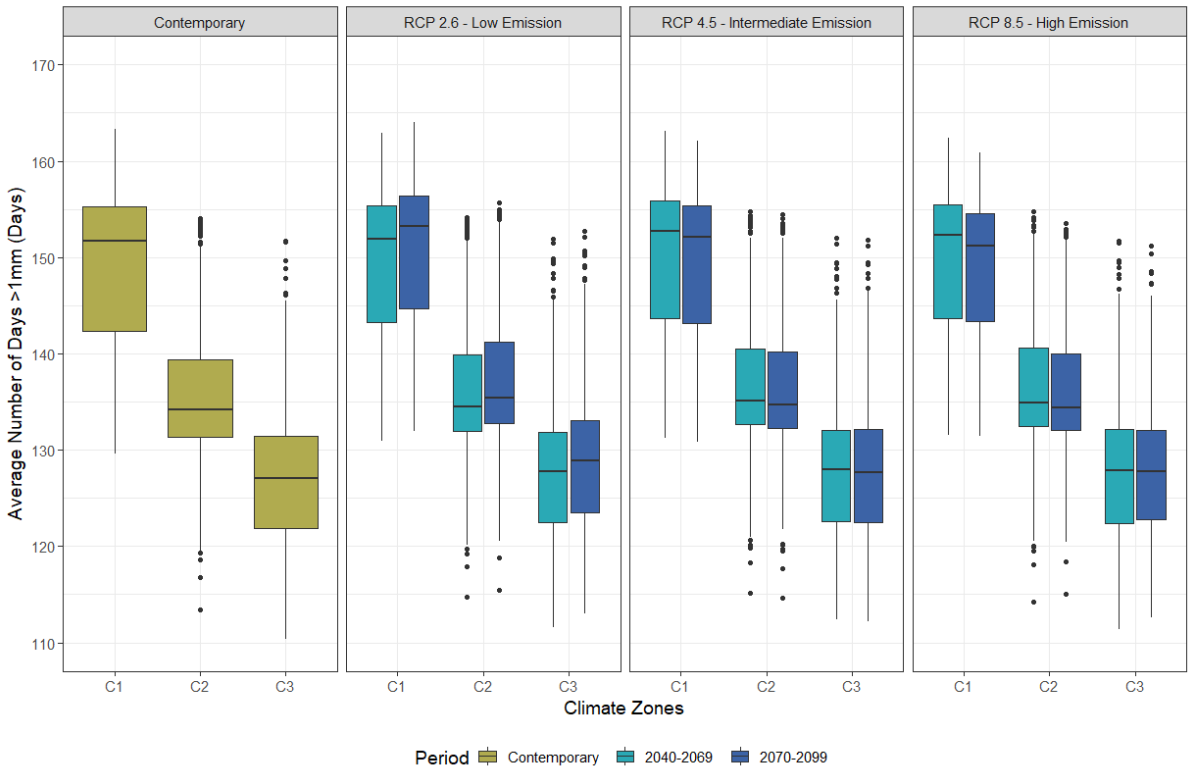

Figure 4.30. Boxplot comparisons of extreme climate index, average number of days with more than 1mm of precipitation within climate zones across three time periods, including the contemporary period ranging from 1981 to 2006 and two future time ranges, and three emission scenarios.

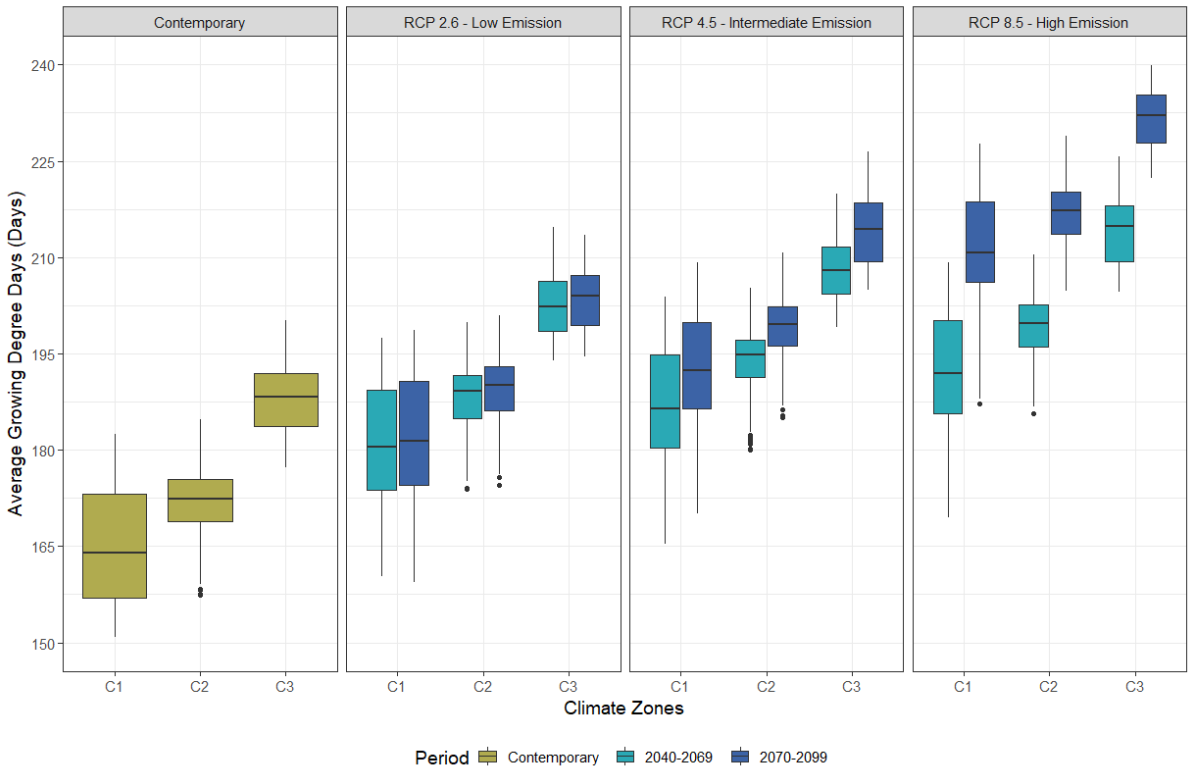

Figure 4.31. Boxplot comparisons of extreme climate index, average growing degree days above 10ºC within climate zones across three time periods, including the contemporary period ranging from 1981 to 2006 and two future time ranges, and three emission scenarios.

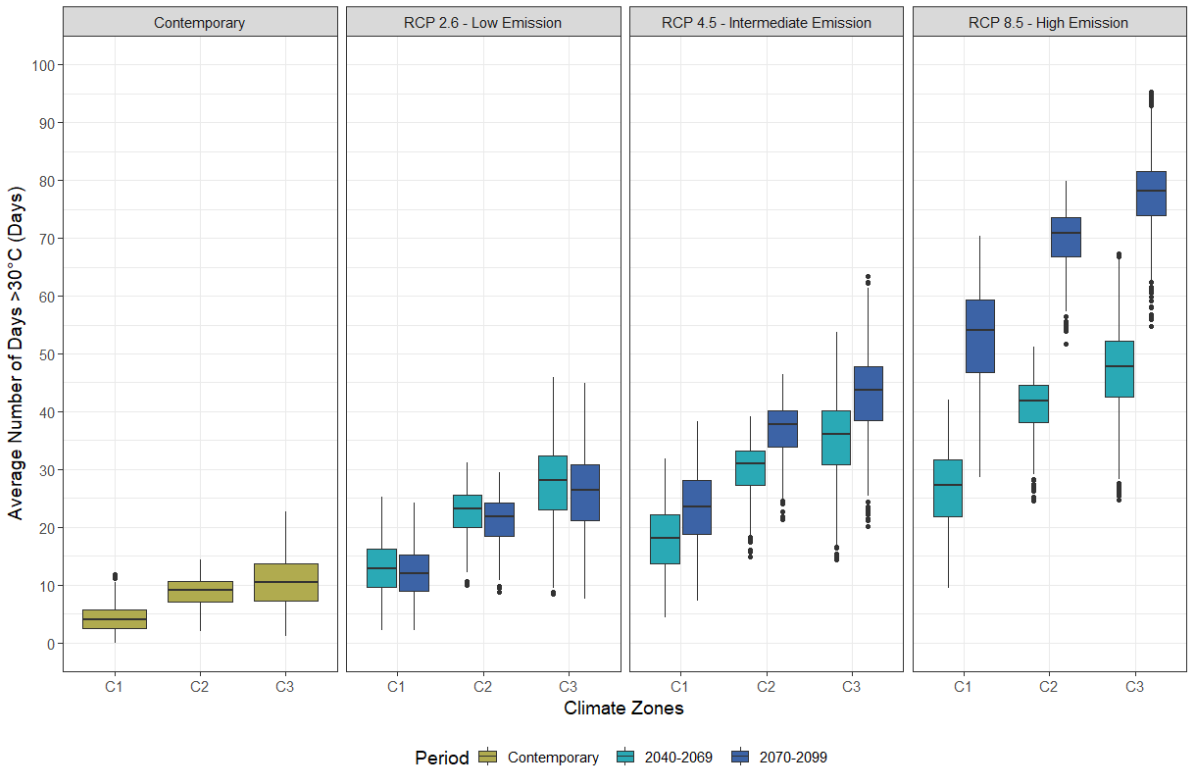

Figure 4.32. Boxplot comparisons of extreme climate index, average number of days above 30ºC within climate zones across three time periods, including the contemporary period ranging from 1981 to 2006 and two future time ranges, and three emission scenarios.

Chapter 5
Discussion

The Lower Great Lakes region features distinct ecoregions with diverse spatiotemporal variables, encompassing variations in climatic conditions, such as precipitation patterns and temperature fluctuations, as well as geophysical characteristics like soil texture and landforms. This dynamic interplay can potentially influence water quality across the region differently. Additional factors, including land use practices and streamflow patterns, contribute to the intricate dynamics shaping the aquatic ecosystems. Recognizing and understanding these complexities is essential for preserving water quality and devising effective water management strategies in the Lower Great Lakes region.

5.1 Characterizing Diverse Ecoregions Through Spatiotemporal Differences

The Lower Great Lakes region comprises three distinct climate ecoregions labelled C1, C2, and C3, moving from north to south, each characterized by unique climatic conditions. These climate differences lead to differences in seasonal streamflow patterns. Moving from north to south, from C1 to C3, there is a notable transition in precipitation dominance, shifting from snowfall to rainfall. This shift correlates with increasing temperatures and longer GDDs. For instance, ecoregion C1, situated in the northernmost region, encompasses areas such as the Lake Huron snowbelt and the Bruce Peninsula, experiencing substantial snowfall accumulation during winter months (Burnett et al., 2003). Consequently, peak streamflow, driven by snowmelt, occurs in spring (April), with discharge rates reaching four times above the median. In contrast, in the more southern region, C3, stream discharge remains elevated throughout multiple cool months (December to March), indicative of rainfall-induced streamflow and intermittent snowmelt. The intermittent snow cover and higher temperatures foster prevalent freeze-thaw patterns within this ecoregion (Reid et al., 2018; Plach et al., 2019). Furthermore, an intersection exists between the identified climate ecoregions and Canada's NRC plant hardiness zones. For instance, zones 7a, 6b, and 6a align with ecoregion C3, while zones 5b and 5a encompass both ecoregions C2 and C1 (NRC, 2014). However, unlike the plant hardiness zones, the climate ecoregions outlined in this study provide a more direct reflection of the lake-effect impact and effectively distinguish between C1's predominant snowfall and the climatic conditions prevalent in the other two zones.

The Lower Great Lakes region encompasses three distinct landscape-based ecoregions labelled LA, LB, and LC, each characterized by varying geophysical features influencing agricultural suitability. Land suitability analysis relies on factors such as soil type and depth, slope, and elevation to assess suitability and potential environmental impacts, such as hydrological connectivity (Akpoti et al., 2019). Moving from LA to LC, there is an increase in slope, elevation, and surface variability. Soil texture dominance transitions from fine to coarse-textured soils, with LB exhibiting a higher proportion of skeletal soils, including rock fragments. As LA features flat, low-lying surfaces, it boasts the highest percentage of croplands among the ecoregions. However, fine-textured soils, particularly those derived from littoral deposits, render fields susceptible to waterlogging, prompting a higher proportion of tile drainage installations in this region. In contrast, LC exhibits steep, upland terrain dominated by natural landscapes, typically less conducive to agricultural activity. Despite this, croplands cover over 20 percent of the region, correlating with higher tile drainage densities in those particular areas. Indeed, although LC features well-drained soils, areas with tile drainage installations often coincide with undulating surfaces and moderately fine-textured soils. The proximity to LA may contribute to the elevated tile drainage density in LC, highlighting the influence of neighbouring ecoregions on agricultural practices (Akpoti et al., 2019). Conversely, LB has the lowest proportion of croplands, reflected in its lower tile drainage density. The presence of rocks, stones, and pebbles in LB's soil matrix renders it less suitable for commercial agriculture, posing challenges for tilling, planting, and harvesting (Hofmann et al., 2005).

Both climate and geophysical variables exert distinct influences on the Lower Great Lakes region, contributing to the dynamic interplay that differentially shapes the mode and timing of stream discharge (Plach et al., 2019; Macrae et al., 2019), as well as land uses within the area which also impact streamflow, mainly as a result of tile drainage. Climate ecoregions are pivotal in determining streamflow timing, with variations observed within each region. LC stands out for the prevalence of peak flow conditions during this period, driven primarily by surface runoff due to its steep slopes and variable surfaces (e.g. Van Esbroeck et al., 2017). In warmer regions (C3), streamflow remains more consistent across the winter months as rainfall-induced runoff swiftly reaches waterways, and there is more tile drainage to facilitate water transfer. Responses are rapid to rainfall events or episodic snowmelt events in winter, and single snowmelt peaks within a season are uncommon (Plach et al., 2019). Although streamflow is lower throughout the growing seasons across all regions, this is the least apparent in the LA zone, especially in region C3-A, possibly due to the large density of tile

drainage in these zones. This intricate interaction between climatic conditions and geophysical features underscores the region's complexity of stream discharge dynamics.

The collective impact of climate and geophysical variables significantly influences the distribution of land uses throughout the region and their suitability for agriculture (Figure 5.1). Croplands, pastures and urban areas all increase, and the natural regions decrease from C1 to C3 (north to south). However, some notable observations can be made. Aside from urban centres in C3-A, agricultural cropland predominates and expansive natural areas are absent. There is also very little pasture or forages, and cropped systems predominate. This reflects the longer GDDs and favourable geophysical conditions conducive to agriculture (Akpoti et al., 2019). Although examples of LA can be found in C2 and C1, these have a higher proportion of pasture in addition to cropped land within these climate zones, possibly owing to their reduced GDDs, particularly in C1. In contrast, LB, primarily situated within climate ecoregion C2, faces challenges for agricultural activity despite its warm conditions due to specific geophysical characteristics that act as barriers (Hofmann et al., 2005). This landscape zone tends to be dominated by natural or urban landscapes. Agricultural activity within LB is mainly concentrated in C3-B, the warmest region, but this is very small. Finally, LC spans all three climate ecoregions, but C3-C exhibits the highest agricultural activity, which overlaps with the warmest region. In contrast, LC in zones C1 and C2 is largely natural land cover. The agriculture in this zone has increasingly more pasture relative to crops in C1 than C2.

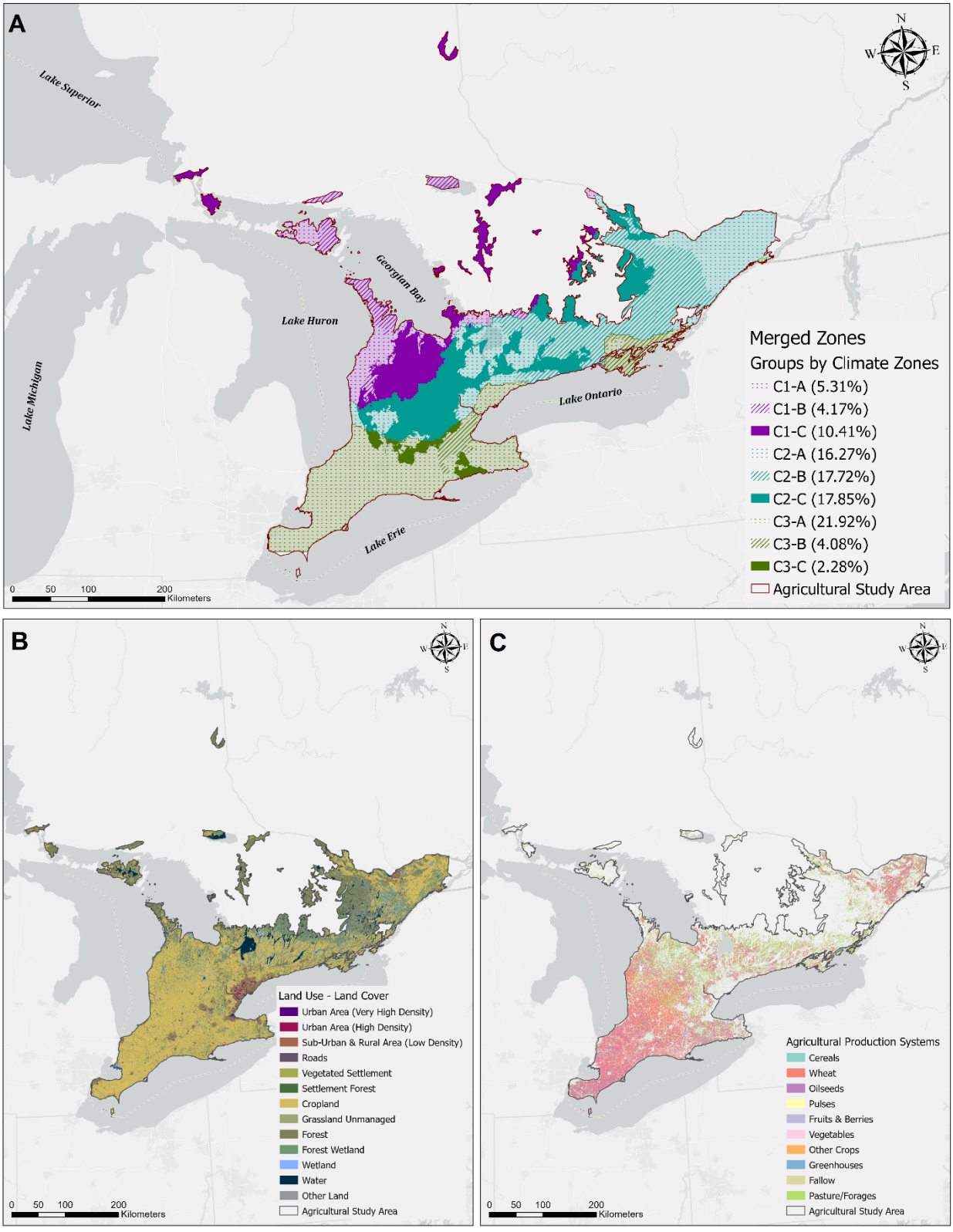
A
Lake Superior
Lake Michigan
Georgian Bay
Lake Huron
Lake Ontario
Lake Erie
N
W
E
S
Merged Zones
Groups by Climate Zones
C1-A (5.31%)
C1-B (4.17%)
C1-C (10.41%)
C2-A (16.27%)
C2-B (17.72%)
C2-C (17.85%)
C3-A (21.92%)
C3-B (4.08%)
C3-C (2.28%)
Agricultural Study Area
0 50 100 200
Kilometers
B
Land Use - Land Cover
Urban Area (Very High Density)
Urban Area (High Density)
Sub-Urban & Rural Area (Low Density)
Roads
Vegetated Settlement
Settlement Forest
Cropland
Grassland Unmanaged
Forest
Forest Wetland
Wetland
Water
Other Land
Agricultural Study Area
0 50 100 200
Kilometers
C
Agricultural Production Systems
Cereals
Wheat
Oilseeds
Pulses
Fruits & Berries
Vegetables
Other Crops
Greenhouses
Fallow
Pasture/Forages
Agricultural Study Area
0 50 100 200
Kilometers

Figure 5.1. The synthesis figure combines both maps from Figures 4.7 and 3.9 to illustrate the overlap of (A) merged ecoregion results and land management factors, (B) LULC types, and (C) agricultural production systems.

5.2 Impact of Ecoregional Disparities on Water Quality Variations

The preceding section has highlighted the diversity among ecoregions, emphasizing their distinct impacts on water quality. These variations contribute to differing risks of nutrient loss, influenced not only by factors affecting nutrient supply and mode of transport but also by the timing of nutrient delivery to adjacent streams. Furthermore, these insights provide an opportunity to categorize ecoregions into source-limited or transport-limited regions, enabling a more nuanced understanding of nutrient dynamics. Peaks in nutrient concentration are expected to coincide with areas supporting agricultural activities, particularly those with longer growing seasons and flatter landscapes.

Ecoregions exhibit notable variability in nutrient supply, with concentrations of SRP, TP, and NO3 increasing from cooler (C1) to warmer (C3) regions, and this is mainly consistent across land uses. This pattern is particularly evident in areas characterized by intensive agricultural activities, such as LA and LC (in the warmer C3 region). Ecoregion C3 stands out for its extended growing season and hosts the largest proportion of LA, with over 70 percent of the area comprising croplands and pastures. Numerous studies have established a clear link between water quality degradation and land-use type, corroborating technical documents that classify land use as a primary environmental stressor in the Great Lakes basin (State of the Great Lakes, 2022; Tang et al., 2011; Eimers et al., 2020; Ayele et al., 2023). As a result, ecoregion C3-A consistently exhibits the highest density of elevated sites for SRP and TP, particularly within croplands and pastures. Although elevated sites can also be found in ecoregion C3-C, this was not observed in other classified zones. Although P is elevated in LA in the other climate zones (C1, C2) relative to LB or LC in those zones, the contrast with C3-A is stark. Nitrate shows a slightly different pattern. It is highly elevated in the cropped and pastured landscapes in C3 (LA and LC) but not in other land uses. However, in C2-C, NO3 is elevated across this zone, irrespective of land use. This may reflect groundwater contamination and its movement throughout the extensive morainal till in this zone (Sharpe, 2022). In contrast, Dillon and Kirchner (1975) conducted a systemic review that found watersheds dominated by forested areas have lower P export levels than agriculture-dominant basins. Hence, ecoregions C1 and LB have the lowest supply of SRP, TP, and NO3 sources, reflecting their lower agricultural suitability compared to C3 and LA.

The established ecoregions also underscore variations in the timing and mode of nutrient transport across the Lower Great Lakes. Ecoregions C3-A and C3-C, characterized by high nutrient supply, contribute significantly to nutrient transport, albeit with differences in timing. In C3-A, concentrations of SRP and NO3 remain consistently high throughout the year, accompanied by elevated levels of suspended sediments across all seasons. This may reflect the more regular occurrence of hydrologic events throughout the seasons as described above but may also reflect significant legacy stores of nutrients in agricultural soils (Van Staden et al., 2022), as well as the fact that there is more tile drainage in the region which can enhance P mobilization in clay-rich agricultural soils (King et al., 2015).

Conversely, in ecoregion C3-C, concentrations of SRP and NO3 peak notably during the spring and winter months, which coincides with peak flow conditions and the prevalence of overland flow at this time of year due to surplus from snowmelt (Macrae et al., 2010; Van Esbroeck et al., 2017; Macrae et al., 2019; Macrae et al., 2021). Additionally, elevated turbidity levels are observed in C3-C during the fall season, which coincides with rainfall on bare soils, and C3-C is at greater risk for erosion given its topography (Van Staden et al., 2022). The same patterns are not observed in C3-A in autumn, possibly due to drier autumn weather (Macrae et al., 2021) or the lack of slope, which lessens the potential for erosion. This contrasts with Zhu et al. (2012), who observed peak dissolved P concentrations during the growing season and highest NO3 levels during the non-growing season in a headwater watershed.

5.3 Assessing Changes under Projected Future Climate Conditions Across Ecoregions

Under the assumption of constant geophysical characteristics such as soil texture, elevation, and landforms, the projected changes in climate conditions are expected to drive shifts in the patterns of climate ecoregions across the Lower Great Lakes region. These shifts are anticipated to impact precipitation and temperature differentially, with varying degrees of influence on streamflow dynamics and agricultural suitability across ecoregions (Eimers et al., 2020). As shown in the previous section, this variability contributes to differing nutrient loss risks across the Lower Great Lakes region (Lucas et al., 2023).

Future climate projections indicate that temperature rates will undergo significant changes, with the Great Lakes watershed experiencing average regional rates surpassing the global mean (IPCC, 2023).

Average minimum temperatures below freezing are predicted to vanish across all emission scenarios, including in the traditionally cooler region of C1 during winter and spring. Conversely, extreme temperatures exceeding 30 degrees Celsius are expected to rise exponentially across emission scenarios, with even low-emission scenarios projecting C1's future average to match contemporary C3 averages.

The IPCC (2023) projected an increase in future precipitation rates and extreme events across the Great Lakes basin. Despite variations across the three climate ecoregions, with C1 being the wettest and C2 the driest, all regions are expected to experience an overall increase in average yearly precipitation, ranging from over 50 mm/year in low-emission scenarios to more than 100 mm/year in high-emission scenarios. These changes are anticipated to be most pronounced during winter and spring, significantly impacting streamflow levels and nutrient loss from agricultural landscapes (Lucas et al., 2023).

5.3.1 Effects of Agricultural Suitability Shifts on Water Quality Risk

These temperature shifts will notably affect the duration of GDD across the study area, potentially transforming regions previously deemed unsuitable into viable agricultural areas. For example, while C1 and C2 historically have shorter GDD lengths than C3, future climate conditions may elevate their GDD levels to match or exceed contemporary C3 levels. This pattern could lead to forest-to-cropland conversions, mirroring findings by ECCC (2021), which documented over 800 km^2 of forest converted to agricultural land between 2010 and 2015 in Ontario and Quebec. Historically, ecoregion C3 has exhibited the highest levels of water quality degradation. However, regions boasting favourable future climate conditions (C1 and C2) and geophysical characteristics for agriculture (LA and LC) may emerge as focal points for water quality concerns.

Temperature fluctuations are pivotal in shaping precipitation patterns, potentially transitioning snowfall-dominant regions to rainfall dominance or leading to more sporadic snow cover during cooler months (Burnett et al., 2003; Reid et al., 2018). Spring snowmelts drive streamflow patterns in C1; however, with warmer winters, streamflow patterns may mirror those seen in C3, where stream discharge is elevated across multiple cool months. However, nutrient loss—whether through surface or sub-surface pathways—varies depending on the geophysical characteristics of the ecoregion (Plach et al., 2019; Macrae et al., 2021). In heavily tile-drained regions like LA, increased transport of SRP through tile drains following storm flow events is expected. It is unclear if and to what extent areas in

LB and LC will be affected. Currently, P losses in LC are associated with the surface overland flow (Van Esbroeck et al., 2017; Plach et al., 2019), which typically occurs during the peak snowmelt period (predominantly) each year (Jamieson et al., 2003; Macrae et al., 2007; Macrae et al., 2010; Van Esbroeck et al., 2017). The greater proportion of rainfall relative to snow melt anticipated under warmer climates will enhance the erosion of surface soils from bare fields in LC. Although this may also occur in LA, the lack of slope will prevent these areas from being at as great a risk as LC. However, the generally warmer winters and consequent lack of snow cover may reduce overland flow and lead to greater tile discharge and groundwater flow (Hanke, 2018), which will lessen erosion and the associated particulate losses and could instead lead to greater dissolved P losses (Singh et al., 2023) caused by chronic leaching into tile drains as soil sorption sites become saturated. Given this potential, conservation practices such as no-till, nutrient management and cover crops will become more critical under future climates.

The anticipated intermittent snow cover may lead to frozen ground conditions, hindering soil infiltration rates (Pittman et al., 2020) and increasing the likelihood of topsoil erosion into adjacent water bodies (Eimers et al., 2020). In light of this, cover crops will have to be used with caution and careful species selection to avoid winter P losses (Cober et al., 2018). Moreover, the intensification of freeze-thaw cycles, both in duration and frequency, is expected to have multifaceted impacts on P loss dynamics, including heightened runoff from tile drainage systems (Lucas et al., 2023; Eimers et al., 2020). Elevated evapotranspiration rates and reduced snowfall are anticipated to lower soil moisture levels, potentially facilitating deeper infiltration of P-enriched runoff into the soil matrix (Lucas et al., 2023), enhancing tile drainage losses over time. These processes will be most important in C1 relative to C2 or C3 in the short term but will likely not be a significant issue towards the end of the century as frosts will be minor.

Extended periods of extreme temperatures above 30°C elevate the risk of heat stress and drought, affecting crops and livestock in agricultural activities. Such conditions are anticipated to be most prevalent in the warmest ecoregion, C3; under a low-emission scenario, the number of days surpassing 30°C is projected to rise from 10 to 25, while under a high-emission scenario, it is expected to surge from 10 to 70. This, coupled with summer temperatures averaging 30°C, will hinder crop production in C3 by impacting plant growth at various stages and overall crop yields (Venkatesh et al., 2022; Porter & Gawith, 1999). For instance, wheat has an optimal temperature range of 17 to 23°C, but plant growth stops at and above 37°C (Porter & Gawith, 1999). Moreover,

summer precipitation is not expected to increase in this region, posing the risk of drought conditions in the warmer months. Consequently, the demand for irrigation systems will rise in the area and introduce new water quality risks beyond contemporary concerns. Without irrigation, it is unclear which crops will succeed in the C3 region, particularly C3-A, due to the high wilting points in clay soils, which may prevent the growth of many crops currently grown (i.e., soy, corn) due to moisture stress. However, if crop growth is sustained by irrigation, water quality issues may prevail due to the legacy nutrients in the region (Van Staden et al., 2022), coupled with the water inputs from irrigation. Indeed, Merchán et al. (2013) found that introducing irrigation systems increased output flow via drainage ditches by 23 percent and nitrate concentrations by 8 percent. As such, careful nutrient management will be essential in these regions.

Similarly, extreme temperatures increase the likelihood of heat stress for animals in pastures within ecoregion C3. Chronic heat stress impacts the animal's quality of life and the agricultural system's economic success (Polsky & Von Keyserlingk, 2017). The livestock industry in the US has experienced a $1.69 to 2.36 billion economic loss due to heat stress (St-Pierre et al., 2003). For instance, the dairy industry has lost $900 million due to decreased milk production, a rise in mortality rates and impaired reproduction (Polsky & Von Keyserlingk, 2017; St-Pierre et al., 2003). Cattle experience heat stress when temperatures reach and exceed 25℃, as their ability to cool down through evaporation becomes compromised under high thermal loads (Kadzere et al., 2002). This results in elevated body temperatures, which can become fatal if conditions persist over an extended period (Kadzere et al., 2002). At present, there is little pastureland in C3, but it is mainly present in C2 and C1. The warmer temperatures and increased GDD anticipated in C1 and C2 will permit the migration of crops such as corn and soy into C2 and C1, mainly if these crops cannot succeed as effectively in C3, which will displace livestock from the current pasture lands. This can potentially increase water quality issues in C1-C and C2-C, as such problems are already seen in C3-C. The displacement of livestock and pastures to LB is a plausible solution, as, despite the anticipated increase in air temperatures, the geophysical characteristics in LB are unsuitable for cropping. The LB region, mainly in C2, can easily support livestock production as farmers face fewer adverse effects of temperature rises induced by climate change. However, this shift may result in water quality concerns spreading into this region as natural areas (which currently do not have water quality issues) are displaced by agricultural livestock production. Given that many of these regions flow outside of

Lake Erie and instead into Lake Huron/Georgian Bay, Lake Ontario, and the St. Lawrence River, an increase in water quality issues in these lakes may occur.

5.4 Importance of Context-Dependent Agricultural Management Practice Recommendations

The preceding sections underscore the significant variations in dominant spatiotemporal and geophysical factors across the Lower Great Lakes region, which result in distinct risks associated with nutrient loss and water quality. Implementing agricultural management practices across these diverse ecoregions is particularly challenging, especially given the changing climate. The implications of these regional differences and the anticipated shifts in water quality risks necessitate tailored approaches to agricultural management practices (Kleinman et al., 2022; Tomer & Locke, 2011). Adapting these practices to changing climate conditions is crucial for sustainable agricultural management and preserving water quality in the Lower Great Lakes region.

Experts advocate for implementing BMPs in the Great Lakes region to mitigate nutrient loss from agricultural landscapes by focusing on managing nutrients, soils, and water (ECCC & MECP, 2018). Notably, ecoregions LA and LC harbour the highest farming activities and contribute the highest concentrations of nutrients to waterways. However, due to differences in geophysical characteristics, BMPs implemented within each region will vary to address unique nutrient loss mechanisms. For example, in ecoregion LA, which is characterized by flat, smooth surfaces with fine-textured soils, high adoption rates of tile drainage minimize soil compaction. Still, they can facilitate nutrient transport to subsurface pathways (OMFRA, 2008a). Consequently, preferential pathways that facilitate drainage also allow surface-applied nutrients to reach subsurface pathways. Initially, recommendations in 2002 to reduce soil erosion and PP loads in farms with tile drainage systems led to a 65% increase in SRP delivery (Jarvie et al., 2017). Consequently, experts have revised recommendations to include conservation tillage practices that disrupt macro pores and enhance nutrient sorption within the root zone, thereby preventing soluble nutrients from reaching subsurface pathways (OMFRA, 2011b). In contrast, ecoregion LC, characterized by steep, variable surfaces with coarse-textured soils, is highly susceptible to water erosion. Hence, no-till or minimum tillage practices are strongly encouraged to mitigate the risk of topsoil enrichment transported via surface runoff (OMFRA, 2011a).

The intersection with climate ecoregions further complicates BMP implementation across LA and LC. In ecoregion C1, where spring snowmelt intensifies runoff and nutrient transport, BMPs aimed at improving runoff water quality may prioritize snow management practices like snow fencing or snow capture structures to mitigate meltwater runoff volume and velocity (OMFRA, 2008b). Additionally, strategies must consider the potential for nutrient runoff during snowmelt events, necessitating adherence to the 4R principle—right source, right rate, right timing, and right placement of fertilizers and manure (GLWQA NAS, 2019). Research by Kast et al. (2021) suggests that focusing on subsurface placement reduces TP losses compared to green infrastructure like buffer strips. Adjusting nutrient application timing away from snowmelt periods, when soil saturation levels peak and runoff is likely, is crucial (GLWQA NAS, 2019). For example, within the Lake Erie watershed, subsurface application proves most effective in reducing TDP loads from March to July, whereas growing perennial cover crops and installing buffer strips efficiently reduces seasonal TP loads (Kalcic et al., 2016). In ecoregion C3, characterized by rainfall-dominant precipitation, BMP recommendations for LA may emphasize enhancing green infrastructure like vegetated buffer strips and constructed wetlands to manage runoff from frequent rain events (OMFRA, 2008b). In LC, BMPs for improving runoff water quality would likely focus on erosion control measures such as terracing, contour farming, or soil stability techniques such as cover crops (OMFRA, 2011a). However, Lemke et al. (2011) found that vegetated strips, riparian buffers, and strip tillage had no significant reduction in nutrient loss compared to base values, suggesting that field knowledge alone may not consistently achieve maximal environmental benefits (Kast et al., 2021).

Under a changing climate, agricultural management practices must adapt to shifts in hydrological cycles, including increased precipitation volumes and temperature surges (Muenich et al., 2016). For instance, projected drought conditions in C3 could worsen with the introduction of irrigation practices, exacerbating water management challenges (Van Staden et al., 2022). Intensified irrigation, coupled with extensive tile drainage systems, may increase soil moisture variability and runoff rates, necessitating careful planning of irrigation scheduling and drainage management to mitigate waterlogging and nutrient leaching risks (Van Staden et al., 2022; Lemke et al., 2011). As C1 transitions to conditions akin to C3, BMPs should shift from snow management to resilience-building against more frequent or intense precipitation events, adjusting to changes in runoff characteristics. In LC, preserving soil fertility amid shifting precipitation patterns and moisture dynamics requires adaptive soil management techniques. Green infrastructure measures must accommodate larger runoff

volumes and flow rates, with LC-specific adaptations to effectively manage sedimentation and pollutant loads (OMFRA, 2011a). Legacy P loads may worsen with greater spring precipitation or snowmelt, necessitating ongoing watershed management efforts despite BMP implementation (Muenich et al., 2016; Tomer & Locke, 2011).

Chapter 6
Conclusion

This study aimed to delineate broad ecoregions based on spatiotemporal characteristics across agricultural landscapes within the Great Lakes Basin. These regional classifications were then utilized to assess water quality risks across various LULC types, explore potential shifts under a changing climate, and discuss implications for agricultural management practice recommendations. The research has revealed that the Lower Great Lakes region comprises three distinct climate and geophysical ecoregions. Furthermore, the study has highlighted how these diverse ecoregions exert varying impacts on water quality due to different nutrient drivers. Specifically, the climatic ecoregions have shown that water quality concerns exhibit a latitude-dependent pattern, with degradation decreasing from south to north. Additionally, two geophysical ecoregions (LA and LC) have emerged as particularly significant regions for water quality issues despite exhibiting opposing modes of nutrient transport (i.e., LA is characterized by subsurface-dominant runoff, while LC is characterized by surface-dominant runoff).

Under a changing climate, all climatic ecoregions experienced increased precipitation and temperature, resulting in a northward shift in agricultural suitability. The coolest climate zone (C1) is projected to resemble contemporary conditions of the warmest zone (C3), as longer GDD will support farming activities, and rising winter temperatures will lead to a transition from snowfall to rainfall dominance. Conversely, conditions within C3 are anticipated to introduce drought conditions, necessitating the implementation of irrigation systems. Extreme temperatures are expected to rise to levels that can adversely affect the productivity of croplands and pastures. These shifting climate patterns underscore the need for context-dependent and adaptive agricultural management practices to address the anticipated changes in water quality risks. Moreover, the distinct characteristics of ecoregions LA and LC necessitate contrasting BMP recommendations. However, these recommendations may yield unintended consequences under a changing climate and depending on the overlap with climate ecoregions.

This research builds upon the findings of Macrae et al. (2021), which focused on the Lake Erie watershed, by extending the analysis to encompass the entirety of the Lower Great Lakes basin. The implications of these expanded findings are significant, offering valuable insights into watershed analysis across the region and enhancing our understanding of the challenges associated with

preserving water quality and implementing agricultural management practices. This research has significantly advanced our understanding of the complex interactions between ecoregional disparities, climate variability, and agricultural management practices in the Lower Great Lakes basin. By delineating distinct ecoregions based on spatiotemporal characteristics and analyzing their implications for water quality, this study has provided crucial insights into the challenges and opportunities for sustainable land use management in the region. These findings resonate with concerns raised by Jarvie et al. (2017), highlighting the consequences of implementing BMPs without tailoring them to specific regional contexts, which can result in increased nutrient loss. Additionally, Wilson et al. (2018) emphasize the importance of addressing historical failures and providing clear, practical BMP recommendations to improve adoption rates among farmers.

This study underscores the importance of adopting a context-dependent approach to agricultural management practices, particularly in light of projected shifts in climate patterns. Tailored strategies are essential to address the unique challenges posed by each ecoregion, which not only maximizes environmental benefits but also enhances BMP adoption rates. Furthermore, this research highlights the need for increased collaboration between researchers, policymakers, and stakeholders to develop and implement effective BMPs that consider local conditions and promote sustainable land management practices. Future research can further refine our understanding of complex dynamics and inform evidence-based policy decisions by integrating field-scale case studies and ongoing monitoring efforts. Ultimately, the success of efforts to preserve water quality and enhance agricultural sustainability in the Lower Great Lakes basin depends on our ability to adapt to changing environmental conditions.

References

AAFC. (2018a). *AAFC Semi-Decadal Land Use Time Series*. Government of Canada. https://open.canada.ca/data/en/ dataset/ba2645d5-4458-414d-b196-6303ac06c1c9

AAFC. (2018b). *Annual Crop Inventory*. Government of Canada. https://open.canada.ca/data/en/ dataset/ba2645d5-4458-414d-b196-6303ac06c1c9

AAFC. (2015). *Growing Degree Days*. Government of Canada. https://open.canada.ca/data/en/ dataset/c7b40829-bacb-4f67-a19b-e090b3d32992

Akpoti, K., Kabo-bah, A. T., & Zwart, S. J. (2019). Agricultural Land Suitability Analysis: State-of-the-art and outlooks for integration of climate change analysis. *Agricultural Systems*, *173*, 172–208. https://doi.org/10.1016/j.agsy.2019.02.013

Ayele, G. T., Yu, B., & Hamilton, D. P. (2023). Land use and climate change effects on streamflow and nutrient loads in a temperate catchment: A simulation study. *Land*, *12*(7), 1326. https://doi.org/10.3390/land12071326

Baker, D. B., Johnson, L. T., Confesor, R. B., Crumrine, J. P., Guo, T., & Manning, N. F. (2019). Needed: Early-term adjustments for Lake Erie phosphorus target loads to address western basin cyanobacterial blooms. *Journal of Great Lakes Research*, *45*(2), 203–211. https://doi.org/10.1016/j.jglr.2019.01.011

Beguería S, Vicente-Serrano SM (2023). *SPEI: Calculation of the Standardized Precipitation-Evapotranspiration Index*. R package version 1.8.1, https://CRAN.R-project.org/package=SPEI

Bennett, E. M., Carpenter, S. R., & Caraco, N. F. (2001). Human impact on erodable phosphorus and eutrophication: A global perspective. *BioScience*, *51*(3), 227–234. https://doi.org/10.1641/0006-3568(2001)051[0227:hioepa]2.0.co;2

Bezdek, J. C., Ehrlich, R., & Full, W. (1984). FCM: The fuzzy C-means clustering algorithm. *Computers & Geosciences*, *10*(2–3), 191–203. https://doi.org/10.1016/0098-3004(84)90020-7

Bunch, K. (2022, April 19). *The Great Lakes before the 1972 Water Quality Agreement*. International Joint Commission. https://ijc.org/en/great-lakes-1972-water-quality-agreement

Burnett, A. W., Kirby, M. E., Mullins, H. T., & Patterson, W. P. (2003). Increasing great lake–effect snowfall during the twentieth century: A regional response to global warming? *Journal of Climate*, *16*(21), 3535–3542. https://doi.org/10.1175/1520-0442(2003)016<3535:iglsdt>2.0.co;2

Byun, K., Chiu, C., & Hamlet, A. F. (2019). Effects of 21st century climate change on seasonal flow regimes and hydrologic extremes over the Midwest and Great Lakes region of the US. *Science of The Total Environment*, *650*, 1261-1277. https://doi.org/10.1016/j.scitotenv.2018.09.063

Cavalcante, H., Araújo, F., Noyma, N. P., & Becker, V. (2018). Phosphorus fractionation in sediments of tropical semiarid reservoirs. *Science of the Total Environment*, *619–620*, 1022–1029. https://doi.org/10.1016/j.scitotenv.2017.11.204

Choquette, A. F., Hirsch, R. M., Murphy, J. C., Johnson, L. T., & Confesor, R. B. (2019). Tracking changes in nutrient delivery to western Lake Erie: Approaches to compensate for variability and trends in streamflow. *Journal of Great Lakes Research*, *45*(1), 21–39. https://doi.org/10.1016/j.jglr.2018.11.012

Cober, J. R., Macrae, M. L., & Van Eerd, L. L. (2019). Winter Phosphorus Release from Cover Crops and Linkages with Runoff Chemistry. *Journal of Environmental Quality*, *48*(4), 907-914. https://doi.org/10.2134/jeq2018.08.0307

Condron, L. M., & Newman, S. (2011). Revisiting the fundamentals of phosphorus fractionation of sediments and soils. *Journal of Soils and Sediments*, *11*(5), 830–840. https://doi.org/10.1007/s11368-011-0363-2

Da-Peng, L., & Yong, H. (2010). Sedimentary phosphorus fractions and bioavailability as influenced by repeated sediment resuspension. *Ecological Engineering*, *36*(7), 958–962. https://doi.org/10.1016/j.ecoleng.2010.04.014

DePinto, J. V., Young, T. C., & Martin, S. C. (1981). Algal-Available Phosphorus in Suspended Sediments from Lower Great Lakes Tributaries. *Journal of Great Lakes Research*, *7*(3), 311–325. https://doi.org/10.1016/S0380-1330(81)72059-8

Demaria, E.M., Palmer, R.N. and Roundy, J.K., 2016. Regional climate change projections of streamflow characteristics in the Northeast and Midwest US. *Journal of Hydrology: Regional Studies, 5*, pp.309-323.

Dillon, P. J., & Kirchner, W. B. (1975). The effects of geology and land use on the export of phosphorus from watersheds. *Water Research*, *9*(2), 135–148. https://doi.org/10.1016/0043-1354(75)90002-0

Dinnes, D. L. (2004). Assessments of Practices to Reduce Nitrogen and Phosphorus Nonpoint Source Pollution of Iowa's Surface Waters*, USDA-ARS. 0034*(515), 380.

Dinov, I. D. (2018). *Data Science and Predictive Analytics: Biomedical and Health Applications using R* (Vol. 1). Springer Cham. https://doi.org/10.1007/978-3-319-72347-1

Dittrich, M., Chesnyuk, A., Gudimov, A., McCulloch, J., Quazi, S., Young, J., Winter, J., Stainsby, E., & Arhonditsis, G. (2013). Phosphorus retention in a mesotrophic lake under transient loading conditions: Insights from a sediment phosphorus binding form study. *Water Research*, *47*(3), 1433–1447. https://doi.org/10.1016/j.watres.2012.12.006

Dodds, W. K., & Whiles, M. R. (2020). *Freshwater Ecology* (3rd ed.). Academic Press. https://doi.org/10.1016/B978-0-12-813255-5.00013-2

Dolan, D. M., & Chapra, S. C. (2012). Great Lakes total phosphorus revisited: 1. Loading analysis and update (1994–2008). *Journal of Great Lakes Research*, *38*(4), 730-740. https://doi.org/10.1016/j.jglr.2012.10.001

Eastman, M., Gollamudi, A., Stämpfli, N., Madramootoo, C. A., & Sarangi, A. (2010). Comparative evaluation of phosphorus losses from subsurface and naturally drained agricultural fields in the Pike River watershed of Quebec, Canada. *Agricultural Water Management*, *97*(5), 596–604. https://doi.org/10.1016/j.agwat.2009.11.010

ECCC. (2023). *Statistically downscaled multi-model ensembles of precipitation*. Government of Canada. https://climate-change.canada.ca/climate-data/#/downscaled-data

ECCC, & MECP. (2018). *Canada-Ontario Lake Erie action plan: Partnering on Achieving Phosphorus Loading Reductions to Lake Erie from Canadian Sources* (Cat No. En164-54/2018E-PDF). ECCC. https://www.canada.ca/content/dam/eccc/documents/pdf/great-lakes-protection/dap/action_plan.pdf

Eimers, M. C., Liu, F., & Bontje, J. (2020). Land use, land cover, and climate change in Southern Ontario: Implications for nutrient delivery to the lower Great Lakes. *The Handbook of Environmental Chemistry*, *101*, 235–249. https://doi.org/10.1007/698_2020_519

Fan, H., Huang, D., Zhou, L., & Jia, Y. (2014). Effects of freeze-thaw cycles on phosphorus adsorption and desorption in the black soil of northeastern China. *Acta Agriculturae Scandinavica Section B: Soil and Plant Science*, *64*(1), 24–32. https://doi.org/10.1080/09064710.2014.882401

Fouli, Y., Cade-Menun, B. J., & Cutforth, H. W. (2013). Freeze-thaw cycles and soil water content effects on infiltration rate of three Saskatchewan soils. *Canadian Journal of Soil Science*, *93*(4), 485–496. https://doi.org/10.4141/CJSS2012-060

Gao, Y., Zhu, B., He, N., Yu, G., Wang, T., Chen, W., & Tian, J. (2014). Phosphorus and carbon competitive sorption–desorption and associated non-point loss respond to natural rainfall events. *Journal of Hydrology*, *517*, 447-457. https://doi.org/10.1016/j.jhydrol.2014.05.057

Geological Survey of Canada. (2015). *Surficial Geology*. Government of Canada. https://open.canada.ca/data/en/dataset/cebc283f-bae1-4eae-a91f-a26480cd4e4a

Great Lakes Water Quality Agreement Nutrients Annex Subcommittee (GLWQA NSA). (2019). *Lake Erie Binational Phosphorus Reduction Strategy.* https://binational.net/wp-content/uploads/2019/06/19-148_Lake_Erie_Strategy_E_accessible.pdf

Grunes, D. (1959). Effect of Nitrogen on the Availability of Soil and Fertilizer Phosphorus to Plants. *Advances in Agronomy*, *11*, 369-396. https://doi.org/10.1016/S0065-2113(08)60127-3

Habibiandehkordi, R., Reid, D. K., Goel, P. K., & Biswas, A. (2020). Phosphorus loss assessment tools: a review of underlying concepts and applicability in cold climates. *Environmental Science and Pollution Research*, *27*(4), 3794–3802. https://doi.org/10.1007/s11356-019-06800-9

Hanke, K. (2018). *Impacts of Climate Change and Controlled Tile Drainage on Water Quality and Quantity in Southern Ontario, Canada* [Master's thesis, University of Waterloo]. UWSpace.

Hastie, T., Friedman, J., & Tibshirani, R. (2001). *The Elements of Statistical Learning: Data Mining, Inference, and Prediction* (1st ed., Ser. Springer Series in Statistics). Springer New York. https://doi.org/10.1007/978-0-387-21606-5

Hengl, T. (2006). Finding the right pixel size. *Computers & Geosciences*, *32*(9), 1283-1298. https://doi.org/10.1016/j.cageo.2005.11.008

Hofmann, N., Filoso, G., & Schofield, M. (2005). *The loss of dependable agricultural land in Canada* (pp. 1-16). Statistics Canada, Agriculture Division.

Holtan, H., Kamp-Nielsen, L., & Stuanes, A. O. (1988). Phosphorus in soil, water and sediment: an overview. *Hydrobiologia*, *170*(1), 19–34. https://doi.org/10.1007/BF00024896

Intergovernmental Panel on Climate Change (IPCC). (2023). *Climate Change 2021 – The Physical Science Basis: Working Group I Contribution to the Sixth Assessment Report of the Intergovernmental Panel on Climate Change*. Cambridge: Cambridge University Press. doi:10.1017/9781009157896

Jamieson, A., Madramootoo, C. A., & Enright, P. (2003). Phosphorus losses in surface and subsurface runoff from a snowmelt event on an agricultural field in Quebec. *Canadian Biosystems Engineering, 45*, 1-1.

Jarvie, H. P., Johnson, L. T., Sharpley, A. N., Smith, D. R., Baker, D. B., Bruulsema, T. W., & Confesor, R. (2017). Increased Soluble Phosphorus Loads to Lake Erie: Unintended Consequences of Conservation Practices?. *Journal of environmental quality*, *46*(1), 123–132. https://doi.org/10.2134/jeq2016.07.0248

Jarvie, H. P., Sharpley, A. N., Withers, P. J. A., Scott, J. T., Haggard, B. E., & Neal, C. (2013). Phosphorus Mitigation to Control River Eutrophication: Murky Waters, Inconvenient Truths, and "Postnormal" Science. *Journal of Environmental Quality*, *42*(2), 295–304. https://doi.org/10.2134/jeq2012.0085

Kadzere, C. T., Murphy, M. R., Silanikove, N., & Maltz, E. (2002). Heat stress in lactating dairy cows: A Review. *Livestock Production Science*, *77*(1), 59–91. https://doi.org/10.1016/s0301-6226(01)00330-x

Kalcic, M. M., Kirchhoff, C., Bosch, N., Muenich, R. L., Murray, M., Griffith Gardner, J., & Scavia, D. (2016). Engaging Stakeholders To Define Feasible and Desirable Agricultural Conservation in Western Lake Erie Watersheds. *Environmental science & technology*, *50*(15), 8135–8145. https://doi.org/10.1021/acs.es

Kalcic, M. M., Muenich, R. L., Basile, S., Steiner, A. L., Kirchhoff, C., & Scavia, D. (2019). Climate change and nutrient loading in the western Lake Erie Basin: Warming can counteract a wetter future. *Environmental Science & Technology*, *53*(13), 7543–7550. https://doi.org/10.1021/acs.est.9b01274

Kaltenecker, G. (2020). *Provincial (Stream) Water Quality Monitoring Network (PWQMN*.Open Government Licence – Ontario. https://data.ontario.ca/dataset/provincial-stream-water- quality-monitoring-network

Karahan, G., & Erşahin, S. (2017). Relating Macropore Flow to Soil Parametric and Morphological Variables. *Soil Science Society of America Journal*, *81*(5), 1014–1024. https://doi.org/10.2136/sssaj2016.10.0327

Kast, J. B., Kalcic, M., Wilson, R., Jackson-Smith, D., Breyfogle, N., & Martin, J. (2021). Evaluating the efficacy of targeting options for conservation practice adoption on watershed-scale phosphorus reductions. *Water research*, *201*, 117375. https://doi.org/10.1016/j.watres.2021.117375

Keatley, B. E., Bennett, E. M., MacDonald, G. K., Taranu, Z. E., & Gregory-Eaves, I. (2011). Land-use legacies are important determinants of lake eutrophication in the anthropocene. *PLoS ONE*, *6*(1). https://doi.org/10.1371/journal.pone.0015913

King, K. W., Williams, M. R., Macrae, M. L., Fausey, N. R., Frankenberger, J., Smith, D. R., Kleinman, P. J. A., & Brown, L. C. (2015). Phosphorus Transport in Agricultural Subsurface Drainage: A Review. *Journal of Environmental Quality*, *44*(2), 467–485. https://doi.org/10.2134/jeq2014.04.0163

King, T., Schoenau, J., & Elliott, J. (2017). Relationship between Manure Management Application Practices and Phosphorus and Nitrogen Export in Snowmelt Run-off Water from a Black Chernozem Saskatchewan Soil. *Sustainable Agriculture Research*, *6*(2), 93. https://doi.org/10.5539/sar.v6n2p93

Kleinman, P. J., Osmond, D. L., Christianson, L. E., Flaten, D. N., Ippolito, J. A., Jarvie, H. P., Kaye, J. P., King, K. W., Leytem, A. B., McGrath, J. M., Nelson, N. O., Shober, A. L., Smith, D. R., Staver, K. W., & Sharpley, A. N. (2022). Addressing conservation practice limitations and trade-offs for reducing phosphorus loss from Agricultural Fields. *Agricultural & Environmental Letters*, *7*(2). https://doi.org/10.1002/ael2.20084

Kleinman, P. J. A., Sharpley, A. N., McDowell, R. W., Flaten, D. N., Buda, A. R., Tao, L., Bergstrom, L., & Zhu, Q. (2011). Managing agricultural phosphorus for water quality protection: Principles for progress. *Plant and Soil*, *349*(1–2), 169–182. https://doi.org/10.1007/s11104-011-0832-9

Kleinman, P. J. A., Sharpley, A. N., Withers, P. J. A., Bergström, L., Johnson, L. T., & Doody, D. G. (2015). Implementing agricultural phosphorus science and management to combat eutrophication. *Ambio*, *44*(2), 297–310. https://doi.org/10.1007/s13280-015-0631-2

Knoben, M. W. J., Woods, R. A., & Freer, J. E. (2018). A Quantitative Hydrological Climate Classification Evaluated With Independent Streamflow Data. *Water Resources Research*, *54*(7), 5088-5109. https://doi.org/10.1029/2018WR022913

Kværnø, S. H., & Øygarden, L. (2006). The influence of freeze-thaw cycles and soil moisture on aggregate stability of three soils in Norway. *Catena*, *67*(3), 175–182. https://doi.org/10.1016/j.catena.2006.03.011

LaZerte, S. E. & Albers, S. (2018). weathercan: Download and format weather data from Environment and Climate Change Canada. *The Journal of Open Source Software, 3*(22), 571. *https://joss.theoj.org/papers/10.21105/joss.00571*

Lee, R. C. T. (1981). Clustering Analysis and Its Applications. In J. T. Tou (Ed.), *Advances in Information Systems Science* (Vol. 8, pp. 169–292). essay, Springer. Retrieved from https://doi.org/10.1007/978-1-4613-9883-7_4.

Lemke, A. M., Kirkham, K. G., Lindenbaum, T. T., Herbert, M. E., Tear, T. H., Perry, W. L., & Herkert, J. R. (2011). Evaluating agricultural best management practices in tile-drained subwatersheds of the Mackinaw River, Illinois. *Journal of environmental quality*, *40*(4), 1215–1228. https://doi.org/10.2134/jeq2010.0119

Li, H., Ren, R., Zhang, H., Zhang, G., He, Q., Han, Z., Meng, S., Zhang, Y., & Zhang, X. (2023). Factors regulating interaction among inorganic nitrogen and phosphorus species, plant uptake, and relevant cycling genes in a weakly alkaline soil treated with biochar and inorganic fertilizer. *Science of The Total Environment*, *905*, 167280. https://doi.org/10.1016/j.scitotenv.2023.167280

Li, S., Elliott, J. A., Tiessen, K. H. D., Yarotski, J., Lobb, D. A., & Flaten, D. N. (2011). The Effects of Multiple Beneficial Management Practices on Hydrology and Nutrient Losses in a Small Watershed in the Canadian Prairies. *Journal of Environmental Quality*, *40*(5), 1627–1642. https://doi.org/10.2134/jeq2011.0054

Liu, K., Elliott, J. A., Lobb, D. A., Flaten, D. N., & Yarotski, J. (2013). Critical factors affecting field-scale losses of nitrogen and phosphorus in spring snowmelt runoff in the Canadian Prairies. *Journal of Environmental Quality*, *42*(2), 484–496. https://doi.org/10.2134/jeq2012.0385

Liu, J., Yang, J., Liang, X., Zhao, Y., Cade-Menun, B. J., & Hu, Y. (2014). Molecular Speciation of Phosphorus Present in Readily Dispersible Colloids from Agricultural Soils. *Soil Science Society of America Journal*, *78*(1), 47–53. https://doi.org/10.2136/sssaj2013.05.0159

Lucas, E., Kennedy, B., Roswall, T., Burgis, C., & Toor, G. S. (2023). Climate change effects on phosphorus loss from agricultural land to water: A Review. *Current Pollution Reports*, *9*(4), 623–645. https://doi.org/10.1007/s40726-023-00282-7

Maccoux, M. J., Dove, A., Backus, S. M., & Dolan, D. M. (2016). Total and soluble reactive phosphorus loadings to Lake Erie: A detailed accounting by year, basin, country, and tributary. *Journal of Great Lakes Research*, *42*(6), 1151-1165. https://doi.org/10.1016/j.jglr.2016.08.005

Macrae, M. L., Ali, G. A., King, K. W., Plach, J. M., Pluer, W. T., Williams, M., Morison, M. Q., & Tang, W. (2019). Evaluating hydrologic response in tile-drained landscapes: Implications for phosphorus transport. *Journal of Environmental Quality*, *48*(5), 1347–1355. https://doi.org/10.2134/jeq2019.02.0060

Macrae, M., English, M., Schiff, S., & Stone, M. (2007). Intra-annual variability in the contribution of tile drains to basin discharge and phosphorus export in a first-order agricultural catchment. *Agricultural Water Management*, *92*(3), 171-182. https://doi.org/10.1016/j.agwat.2007.05.015

Macrae, M., English, M., Schiff, S., & Stone, M. (2010). Influence of antecedent hydrologic conditions on patterns of hydrochemical export from a first-order agricultural watershed in Southern Ontario, Canada. *Journal of Hydrology*, *389*(1-2), 101-110. https://doi.org/10.1016/j.jhydrol.2010.05.034

Macrae, M., Jarvie, H., Brouwer, R., Gunn, G., Reid, K., Joosse, P., King, K., Kleinman, P., Smith, D., Williams, M., & Zwonitzer, M. (2021). One size does not fit all: Toward regional conservation practice guidance to reduce phosphorus loss risk in the Lake Erie watershed. *Journal of Environmental Quality*, *50*(3), 529–546. https://doi.org/10.1002/jeq2.20218

Mancuso, J.L., Weinke, A.D., Stone, I.P., Hamsher, S.E., Woller-Skar, M.M., Snyder, E.B. and Biddanda, B.A., 2021. Bloom and bust: Historical trends of harmful algal blooms in Muskegon Lake, Michigan, a Great Lakes estuary. *Freshwater Science, 40(3)*, pp.463-477.

McDonnell, J., & Woods, R. (2004). On the need for catchment classification. *Journal of Hydrology*, *299*(1–2), 2–3. https://doi.org/10.1016/j.jhydrol.2004.09.003

Mcdowell, R. W., Sharpley, A. N., Condron, L. M., Haygarth, P. M., & Brookes, P. C. (2001). Processes controlling soil phosphorus release to runoff and implications for agricultural management. *Nutrient Cycling in Agroecosystems*, *59*(3), 269–284. https://doi.org/10.1023/A:1014419206761

Merchán, D., Causapé, J., & Abrahão, R. (2013). Impact of irrigation implementation on hydrology and water quality in a small agricultural basin in Spain. *Hydrological Sciences Journal*, *58*(7), 1400–1413. https://doi.org/10.1080/02626667.2013.829576

MNRF. (2019a). *Land Information Ontario Data Description– Tile Drainage Area*. Queens Printer for Ontario. https://www.sdc.gov.on.ca/sites/MNRF-PublicDocs/EN/CMID/Tile%20Drainage%20Area%20-%20Data%20Description.pdf

MNRF. (2019b). *Ontario Integrated Hydrology (OIH) data.* Open Government Licence – Ontario. https://geohub.lio.gov.on.ca/maps/mnrf::ontario-integrated- hydrology-oih-data/about

MNRF. (2019c). *Provincial Digital Elevation Model (PDEM)*. Open Government Licence – Ontario. https://geohub.lio.gov.on.ca/maps/mnrf::provincial -digital-elevation-model-pdem/about

Muenich, R. L., Kalcic, M., & Scavia, D. (2016). Evaluating the Impact of Legacy P and Agricultural Conservation Practices on Nutrient Loads from the Maumee River Watershed. *Environmental science & technology*, *50*(15), 8146–8154. https://doi.org/10.1021/acs.est.6b01421

NRC. (2014). *Canada's Plant Hardiness Zones.* http://planthardiness.gc.ca/images/PHZ_2014_CFS_Map.pdf

OMFRA. (2008a). *Best Management Practices Series: Soil Management.* https://bmpbooks.com/publications/soil-management/

OMFRA. (2008b). *Best Management Practices Series: Water Management.* https://bmpbooks.com/publications/water-management/

OMFRA. (2011a). *Best Management Practices Series: Controlling Soil Erosion on the Farm.* https://bmpbooks.com/publications/controlling-soil-erosion-on-the-farm/

OMFRA. (2011b). *Best Management Practices Series: Cropland Drainage.* https://bmpbooks.com/publications/cropland-drainage/

OMFRA. (2011c). *Best Management Practices Series: Phosphorus Primer.* https://bmpbooks.com/publications/a-phosphorus-primer/

Pärn, J., Pinay, G., & Mander, Ü. (2012). Indicators of nutrients transport from agricultural catchments under temperate climate: A review. *Ecological Indicators*, *22*, 4–15. https://doi.org/10.1016/j.ecolind.2011.10.00

Pasek, M. A., Sampson, J. M., & Atlas, Z. (2014). Redox chemistry in the phosphorus biogeochemical cycle. *Proceedings of the National Academy of Sciences*, *111*(43), 15468–15473. https://doi.org/10.1073/pnas.1408134111

Pittman, F., Mohammed, A., & Cey, E. (2020). Effects of antecedent moisture and macroporosity on infiltration and water flow in frozen soil. Hydrological Processes, 34(3), pp.795-809.

Plach, J., Pluer, W., Macrae, M., Kompanizare, M., McKague, K., Carlow, R., & Brunke, R. (2019). Agricultural Edge-of-field phosphorus losses in Ontario, Canada: Importance of the nongrowing season in cold regions. *Journal of Environmental Quality*, *48*(4), 813–821. https://doi.org/10.2134/jeq2018.11.0418

Plach, J. M., Macrae, M. L., Ali, G. A., Brunke, R. R., English, M. C., Ferguson, G., Lam, W. V., Lozier, T. M., McKague, K., O'Halloran, I. P., Opolko, G., & Van Esbroeck, C. J. (2018a). Supply and Transport Limitations on Phosphorus Losses from Agricultural Fields in the Lower Great Lakes Region, Canada. *Journal of Environmental Quality*, *47*(1), 96–105. https://doi.org/10.2134/jeq2017.06.0234

Plach, J. M., Macrae, M. L., Williams, M. R., Lee, B. D., & King, K. W. (2018b). Dominant glacial landforms of the lower Great Lakes region exhibit different soil phosphorus chemistry and potential risk for phosphorus loss. *Journal of Great Lakes Research*, *44*(5), 1057-1067. https://doi.org/10.1016/j.jglr.2018.07.005

Plach, J., Pluer, W., Macrae, M., Kompanizare, M., McKague, K., Carlow, R., & Brunke, R. (2019). Agricultural Edge-of-field phosphorus losses in Ontario, Canada: Importance of the nongrowing

season in cold regions. *Journal of Environmental Quality*, *48*(4), 813–821. https://doi.org/10.2134/jeq2018.11.0418

Polsky, L., & Von Keyserlingk, M. A. G. (2017). Invited review: Effects of heat stress on Dairy Cattle Welfare. *Journal of Dairy Science*, *100*(11), 8645–8657. https://doi.org/10.3168/jds.2017-12651

Porter, J. R., & Gawith, M. (1999). Temperatures and the growth and development of wheat: A Review. *European Journal of Agronomy*, *10*(1), 23–36. https://doi.org/10.1016/s1161-0301(98)00047-1

Rattan, K. J., Blukacz-Richards, E. A., Yates, A. G., Culp, J. M., & Chambers, P. A. (2019). Hydrological variability affects particulate nitrogen and phosphorus in streams of the Northern Great Plains. *Journal of Hydrology: Regional Studies*, *21*(January), 110–125. https://doi.org/10.1016/j.ejrh.2018.12.008

Reid, D. K. (2011). A modified Ontario P index as a tool for on-farm phosphorus management. *Canadian Journal of Soil Science*, *91*(3), 455–466. https://doi.org/10.4141/cjss09088

Reid, K., Schneider, K., & McConkey, B. (2018). Components of Phosphorus Loss From Agricultural Landscapes, and How to Incorporate Them Into Risk Assessment Tools. *Frontiers in Earth Science*, *6*(September), 1–15. https://doi.org/10.3389/feart.2018.00135

Rittenburg, R. A., Squires, A. L., Boll, J., Brooks, E. S., Easton, Z. M., & Steenhuis, T. S. (2015). Agricultural BMP effectiveness and dominant hydrological flow paths: Concepts and a review. *Journal of the American Water Resources Association*, *51*(2), 305–329. https://doi.org/10.1111/1752-1688.12293

River, M., & Richardson, C. J. (2019). Dissolved Reactive Phosphorus Loads to Western Lake Erie: The Hidden Influence of Nanoparticles. *Journal of Environmental Quality*, *48*(3), 645–653. https://doi.org/10.2134/jeq2018.05.0178

Römkens, M., Helming, K., & Prasad, S. (2002). Soil erosion under different rainfall intensities, surface roughness, and soil water regimes. *CATENA, 46*(2-3), 103-123. https://doi.org/10.1016/S0341-8162(01)00161-8

Ross, C., Moslenko, L., Biagi, K., Oswald, C., Wellen, C., Thomas, J., Raby, M., & Sorichetti, R. (2022). Total and dissolved phosphorus losses from agricultural headwater streams during extreme runoff events. *Science of The Total Environment*, *848*, 157736. https://doi.org/10.1016/j.scitotenv.2022.157736

Serra-Burriel, M., & Ames, C. (2021). Machine Learning-Based Clustering Analysis: Foundational Concepts, Methods, and Applications. In V. E. Staartjes, L. Regli, & C. Serra (Eds.), *Machine Learning in Clinical Neuroscience: Foundations and Applications* (Vol. 134, Ser. Acta Neurochirurgica Supplement, pp. 91–100). essay, Springer Cham. Retrieved from https://doi.org/10.1007/978-3-030-85292-4_12.

Scavia, D., DePinto, J. V., & Bertani, I. (2016). A multi-model approach to evaluating target phosphorus loads for Lake Erie. *Journal of Great Lakes Research*, *42*(6), 1139-1150. https://doi.org/10.1016/j.jglr.2016.09.007

Schindler, D. W. (1977). Evolution of phosphorus limitation in Lakes. *Science*, *195*(4275), 260–262. https://doi.org/10.1126/science.195.4275.260

Schindler, D. W., Hecky, R. E., Findlay, D. L., Stainton, M. P., Parker, B. R., Paterson, M. J., Beaty, K. G., Lyng, M., & Kasian, S. E. (2008). Eutrophication of lakes cannot be controlled by reducing nitrogen input: Results of a 37-year whole-ecosystem experiment. *Proceedings of the National Academy of Sciences*, *105*(32), 11254–11258. https://doi.org/10.1073/pnas.0805108105

Schipanski, M. E., & Bennett, E. M. (2021). The Phosphorus Cycle. *Fundamentals of Ecosystem Science (Second Edition)*, 189-213. https://doi.org/10.1016/B978-0-12-812762-9.00009-5

Sharpley, A. N., Bergström, L., Aronsson, H., Bechmann, M., Bolster, C. H., Börling, K., Djodjic, F., Jarvie, H. P., Schoumans, O. F., Stamm, C., Tonderski, K. S., Ulén, B., Uusitalo, R., & Withers, P. J. A. (2015). Future agriculture with minimized phosphorus losses to waters: Research needs and direction. *Ambio*, *44*(2), 163–179. https://doi.org/10.1007/s13280-014-0612-x

Sharpley, A. N., Kleinman, P. J. A., Jordan, P., Bergström, L., & Allen, A. L. (2009). Evaluating the Success of Phosphorus Management from Field to Watershed. *Journal of Environmental Quality*, *38*(5), 1981–1988. https://doi.org/10.2134/jeq2008.0056

Sharpley, A. N., Mcdowell, R. W., & Kleinman, P. J. A. (2001). Phosphorus loss from land to water: Integrating agricultural and environmental management. *Plant and Soil*, *237*(2), 287–307. https://doi.org/10.1023/A:1013335814593

Sharpley, A. N., Troeger, W. W., & Smith, S. J. (1991). The Measurement of Bioavailable Phosphorus in Agricultural Runoff. *Journal of Environmental Quality*, *20*(1), 235–238. https://doi.org/10.2134/jeq1991.00472425002000010037x

Sharpe, D. R. (2022). Seven hydrogeological terrains characteristic of Southern Ontario. *Canadian Journal of Earth Sciences*, *59*(12), 1006–1030. https://doi.org/10.1139/cjes-2022-0035

Singh, N. K., Van Meter, K. J., & Basu, N. B. (2023). Widespread increases in soluble phosphorus concentrations in streams across the transboundary Great Lakes Basin. *Nature Geoscience*, *16*(10), 893-900. https://doi.org/10.1038/s41561-023-01257-5

Sloan, B. P., Basu, N. B., & Mantilla, R. (2016). Hydrologic impacts of subsurface drainage at the field scale: Climate, landscape and anthropogenic controls. *Agricultural Water Management*, *165*, 1–10. https://doi.org/10.1016/j.agwat.2015.10.008

Soil Landscapes of Canada Working Group. (2011). *Soil Landscapes of Canada version 3.2*. Agriculture and Agri-Food Canada. (digital map and database at 1:1 million scale).

Smith, D. R., King, K. W., Johnson, L., Francesconi, W., Richards, P., Baker, D., & Sharpley, A. N. (2015). Surface runoff and tile drainage transport of phosphorus in the midwestern United States. *Journal of Environmental Quality*, *44*(2), 495–502. https://doi.org/10.2134/jeq2014.04.0176

St-Pierre, N. R., Cobanov, B., & Schnitkey, G. (2003). Economic losses from heat stress by US Livestock Industries. *Journal of Dairy Science*, *86*. https://doi.org/10.3168/jds.s0022-0302(03)74040-5

State of the Great Lakes. (2022). *State of the Great Lakes 2022 Report: An overview of the status and trends of the Great Lakes ecosystem.* https://binational.net/wp-content/uploads/2022/07/State-of-the-Great-Lakes-2022-Report.pdf

Steffen, M. M., Belisle, B. S., Watson, S. B., Boyer, G. L., & Wilhelm, S. W. (2014). Status, causes and controls of cyanobacterial blooms in Lake Erie. *Journal of Great Lakes Research*, *40*(2), 215–225. https://doi.org/10.1016/j.jglr.2013.12.012

Tang, L., Yang, D., Hu, H., & Gao, B. (2011). Detecting the effect of land-use change on streamflow, sediment and nutrient losses by distributed hydrological simulation. *Journal of Hydrology*, *409*(1–2), 172–182. https://doi.org/10.1016/j.jhydrol.2011.08.015

Tomer, M. D., & Locke, M. A. (2011). The challenge of documenting water quality benefits of conservation practices: a review of USDA-ARS's conservation effects assessment project watershed studies. *Water science and technology : a journal of the International Association on Water Pollution Research*, *64*(1), 300–310. https://doi.org/10.2166/wst.2011.555

Van Esbroeck, C.J., Macrae, M.L., Brunke, R.R., & McKague, K., (2017). Surface and subsurface phosphorus export from agricultural fields during peak flow events over the nongrowing season in regions with cool, temperate climates. *Journal of Soil and Water Conservation*, *72*(1), pp.65-76.

Van Staden, T. L., Van Meter, K. J., Basu, N. B., Parsons, C. T., Akbarzadeh, Z., & Van Cappellen, P. (2022). Agricultural phosphorus surplus trajectories for Ontario, Canada (1961–2016), and erosional export risk. *Science of The Total Environment*, *818*, 151717. https://doi.org/10.1016/j.scitotenv.2021.151717

Venkatesh, K., Senthilkumar, K., Mamrutha, H., Singh, G., & Singh, G. (2022). High-temperature stress in wheat under climate change scenario, effects and mitigation strategies. *Climate Change and Crop Stress*, 209-229. https://doi.org/10.1016/B978-0-12-816091-6.00014-6

Vymazal, J. (2007). Removal of nutrients in various types of constructed wetlands. *Science of the Total Environment*, *380*(1–3), 48–65. https://doi.org/10.1016/j.scitotenv.2006.09.014

Wang, L., Flanagan, D. C., Wang, Z., & Cherkauer, K. A. (2018). Climate Change Impacts on Nutrient Losses of Two Watersheds in the Great Lakes Region. *Water*, *10*(4), 442. https://doi.org/10.3390/w10040442

Wang, Y. T., Zhang, T. Q., Hu, Q. C., Tan, C. S., Halloran, I. P. O., Drury, C. F., Reid, D. K., Ma, B. L., Ball-Coelho, B., Lauzon, J. D., Reynolds, W. D., & Welacky, T. (2010). Estimating Dissolved Reactive Phosphorus Concentration in Surface Runoff Water from Major Ontario Soils. *Journal of Environmental Quality*, *39*(5), 1771–1781. https://doi.org/10.2134/jeq2009.0504

Watson, S. B., Miller, C., Arhonditsis, G., Boyer, G. L., Carmichael, W., Charlton, M. N., Confesor, R., Depew, D. C., Höök, T. O., Ludsin, S. A., Matisoff, G., McElmurry, S. P., Murray, M. W., Peter Richards, R., Rao, Y. R., Steffen, M. M., & Wilhelm, S. W. (2016). The re-eutrophication of Lake Erie: Harmful algal blooms and hypoxia. *Harmful algae*, *56*, 44–66. https://doi.org/10.1016/j.hal.2016.04.010

Wilson, R. S., Beetstra, M. A., Reutter, J. M., Hesse, G., Fussell, K. M. D., Johnson, L. T., King, K. W., LaBarge, G. A., Martin, J. F., & Winslow, C. (2019). Commentary: Achieving phosphorus reduction targets for Lake Erie. *Journal of Great Lakes Research*, *45*(1), 4-11. https://doi.org/10.1016/j.jglr.2018.11.004

Wilson, R. S., Schlea, D. A., Boles, C. M., & Redder, T. M. (2018). Using models of farmer behavior to inform eutrophication policy in the Great Lakes. *Water Research*, *139*, 38-46. https://doi.org/10.1016/j.watres.2018.03.065

Wolfe, J. D., Shook, K. R., Spence, C., & Whitfield, C. J. (2019). A watershed classification approach that looks beyond hydrology: Application to a semi-arid, agricultural region in Canada. *Hydrology and Earth System Sciences*, *23*(9), 3945–3967. https://doi.org/10.5194/hess-23-3945-2019

WSC. (2021). *HYDAT*. Government of Canada. https://open.canada.ca/data/en/ dataset/c7b40829-bacb-4f67-a19b-e090b3d32992

Zheng, S., Xia, Y., Hu, Y., Chen, X., Rui, Y., Gunina, A., He, X., Ge, T., Wu, J., Su, Y., & Kuzyakov, Y. (2021). Stoichiometry of carbon, nitrogen, and phosphorus in soil: Effects of agricultural land use and climate at a continental scale. *Soil and Tillage Research*, *209*, 104903. https://doi.org/10.1016/j.still.2020.104903

Zhu, Q., Schmidt, J. P., & Bryant, R. B. (2012). Hot moments and hot spots of nutrient losses from a mixed land use watershed. *Journal of Hydrology*, *414–415*, 393–404. https://doi.org/10.1016/j.jhydrol.2011.11.011